Escola de Camins
Escola Tècnica Superior d'Enginyeria de Camins, Canals i Ports
UPC BARCELONATECH

TREBALL FINAL DE MÀSTER

Interpretació d'Assajos Slug en un Medi Heterogeni de Baixa Permeabilitat i amb Caràcter Anisòtrop

Treball realitzat per:
Jose A Bosch Llufriu

Dirigit per:
Xavier Sánchez-Vila

Màster en:
Enginyeria del Terreny

Barcelona, 1 de Juny de 2017

Departament d'Enginyeria Civil i Ambiental

UNIVERSITAT POLITECNICA DE CATALUNYA

On the Interpretation of Slug Tests in Low Permeability, Heterogeneous and Anisotropic Porous Media

Jose A Bosch Llufriu

supervisor
Xavier Sanchez-Vila

Master Thesis

Hydrogeology Group
Department of Civil and Environmental Engineering

June 2017

Abstract

Despite the wide use of slug tests to estimate hydraulic properties of geological media, interpreted parameters by its means are usually seen with scepticism. This is the case especially in heterogeneous fractured media where a high dispersion of results might be obtained in a single site. The lack of representativeness of such parameters has been mostly attributed to skin effects, support volume and partial penetration, while the effects of variations in small scale permeability have seldom been addressed. In an attempt to understand better this test, I perform Monte Carlo simulations of slug tests in a variety of synthetic heterogeneous fields and compare the drawdown curves to that of a homogeneous field. Radial and spherical flow is studied. For most radial flow cases, early and intermediate period responses are strongly affected by the structure of the field, whereas late time responses are practically independent on the structure and approaches that of the equivalent homogeneous field. On the contrary spherical flow shows a homogeneous behaviour. It follows the numerical study a field case of a fractured rock site in which some slug tests have resulted in anomalous curves. The insight gained from the Monte Carlo simulations is useful to make assumptions on the estimated conductivities. Because different flow configurations can arise in the same field and boundary conditions may be crucial, the importance of discrimination between interpretation models is also highlighted.

Resumen

A pesar de usarse en la mayoría de estudios hidrogeológicos de campo, los parámetros obtenidos mediante ensayos slug o de cuchareo se consideran poco representativos. En medios muy heterogéneos, como por ejemplo macizos rocosos fracturados, se suele obtener una gran dispersión de resultados en un mismo acuífero. La falta de representatividad de los parámetros interpretados se suele atribuir al efecto piel, al volumen de soporte y a geometrías mal definidas. Sin embargo la heterogeneidad a pequeña escala ha sido objeto de pocos estudios en la literatura. Para entender mejor como funciona este ensayo en formaciones no homogéneas, se ha realizado una serie de simulaciones con el método de Monte Carlo de ensayos slug en campos con permeabilidad heterogénea a pequeña escala. Se han realizado modelos de flujo radial y esférico. La mayoría de simulaciones en flujo radial resultan en curvas de recuperación que presentan anomalías a tiempos pequeños e intermedios mientras que a tiempo avanzado se obtienen respuestas independientes de la estructura y se aproximan al comportamiento del campo homogéneo con la media geométrica. Por el contrario el flujo esférico resulta en curvas con la misma forma que la respuesta homogénea pero con respuestas más rápidas, que se interpretan con conductividades mayores a la media geométrica. El trabajo se completa con la interpretación de una serie de ensayos que se han realizado en un medio fracturado muy heterogéneo que presenta una marcada anisotropía. Para ello se ha hecho uso de las observaciones sobre los modelos numéricos en los casos de respuestas anómalas. Se pone especial énfasis al proceso de discriminación entre modelos de interpretación a fin de evitar resultados no realistas.

Resum

A pesar d'utilitzar-se en la majoria d'estudis hidrogeològics de camp, els paràmetres obtinguts mitjançant assajos slug es consideren poc representatius. En medis molt heterogenis, com per exemple els massissos rocosos fracturats, es sol obtenir una gran dispersió de resultats en un mateix aqüífer. La falta de representativitat dels paràmetres interpretats s'atribueix normalment a l'efecte de pell, al volum de suport i a geometries mal definides, no obstant l'heterogeneïtat a petita escala ha estat objecte de pocs estudis a la literatura. Per entendre millor com funciona aquest assaig en formacions no homogènies, s'ha realitzat una sèrie de simulacions amb el mètode de Monte Carlo d' assajos slug en camps amb permeabilitat heterogènia a petita escala. S'han realitzat models de flux radial y esfèric. La majoria de simulacions en flux radial resulten en corbes de recuperació que presenten anomalies a temps petits e intermedis mentre que a temps avançat s'obtenen respostes independents de l'estructura i s'aproximen al comportament del camp homogeni amb la mitjana geomètrica. Pel contrari, el flux esfèric resulta en corbes amb la mateixa forma que la resposta homogènia però amb recuperacions més ràpides, que s'interpreten amb conductivitats majors a la mitjana geomètrica. El document conclou amb la interpretació d'una sèrie d'assajos que s'han realitzat en un medi fracturat molt heterogeni que presenta una marcada anisotropia. S'han utilitzat les observacions sobre els models numèrics per interpretar els casos de respostes no homogènies. Per evitar resultats poc realistes es posa èmfasi al procés de discriminació entre models d'interpretació.

Agraïments

S'agraeix el finançament rebut per part de ENRESA per realitzar el present treball.

Aquest treball culmina una etapa de la meva vida que considero especialment fructífera gràcies a un conjunt de persones que mereixen un reconeixement:

En primer lloc agrair al meu supervisor, Xavier Sánchez-Vila, per l'oportunitat que m'ha brindat de treballar amb el grup d'hidrologia subterrània, per donar-me una visió pràctica sobre el camp de les aigües subterrànies i per tots els consells que he rebut durant aquests mesos sobre infinitat de temes.

A totes les persones amb les que he coincidit al grup d'hidrologia subterrània per l'ambient, pel que m'han ajudat i per tot el que he après de cadascú durant la meva estada.

Al Jean Vaunat, per la seva orientació, suport i consells durant aquests dos anys de màster.

Als companys de màster pels moments compartits tant a dins com a fora de les aules.

Per últim, i més important, als meus pares: les paraules es queden curtes per tot el que m'heu ajudat a aconseguir.

Contents

List of Figures

List of Tables

Symbols

A	area of flow	$[L^2]$
b	aquifer thickness	$[L]$
C_w	wellbore storage	$[L^2]$
C_D	wellbore storage to formation storage ratio	$[-]$
G	filter function	
h	hydraulic head	$[L]$
h_w	head at the well	$[L]$
h_0	initial head at the well	$[L]$
J_0	Bessel function of the first kind, zeroth order	
J_1	Bessel function of the first kind, first order	
$\mathbf{K}$	tensor of hydraulic conductivity	$[LT^{-1}]$
K^{eff}	effective hydraulic conductivity	$[LT^{-1}]$
K^{eq}	equivalent hydraulic conductivity	$[LT^{-1}]$
K^{int}	interpreted hydraulic conductivity	$[LT^{-1}]$
K_G	geometric mean of hydraulic conductivity field	$[LT^{-1}]$
$\mathbf{q}$	Darcy flow vector	$[LT^{-1}]$
r	radius	$[L]$
r_c	casing radius	$[L]$
r_w	well radius	$[L]$
r_D	dimensionless radius	$[-]$
r_e	influence radius	$[L]$
S	storativity	$[-]$
S_s	specific storage	$[L^{-1}]$
t	time	$[T]$
t_D	dimensionless time	$[-]$
T	transmissivity	$[L^2T^{-1}]$
T^{int}	interpreted transmissivity	$[L^2T^{-1}]$
T^{eff}	effective transmissivity	$[L^2T^{-1}]$
T_A	aritmetic averaged transmissivity	$[L^2T^{-1}]$
T_G	geometric averaged transmissivity	$[L^2T^{-1}]$

T_H	harmonic averaged transmissivity	$[L^2T^{-1}]$
u	dummy variable	$[-]$
V	total volume of medium	$[L^3]$
V_w	volume of injected water	$[L^3]$
$\mathbf{x}$	vector location	$[L]$
Y	natural logarithm of hydraulic conductivity	$[L]$
Y_0	Bessel function of the second kind, zeroth order	
Y_1	Bessel function of the second kind, first order	
z	Depth from ground surface	$[L]$
κ	small scale permeability	$[L/T]$
λ	ratio of matrix to fracture permeability	
λ_x	correlation length in x direction	$[L]$
λ_y	correlation length in y direction	$[L]$
ω	power averaging parameter	
σ_b^2	variance of random variable b	
Ω	volume of tested medium	

Chapter 1

Introduction

A slug test consists on introducing or withdrawing a known volume of water into a well or borehole, that is screened along the formation of which we are interested, and measuring the drawdown with time with the objective of deriving the transmissibility/permeability and the storage/specific storage of the formation. Figure 1.1 shows a representation of both ways of conducting a slug test.

The slug test is currently one of the main methods used in groundwater hydrology in order to determine the hydraulic parameters of a geological formation. Among its main advantages are the low amount of equipment needed, due to its simplicity, the relatively small time for its completion and the fact that no water treatment is needed in contaminated sites. The disadvantages of such tests are mainly related to the relatively low volume of medium sampled and the ambiguity of the results - which are usually in disagreement with other tests and highly dependent on the interpretation technique. In

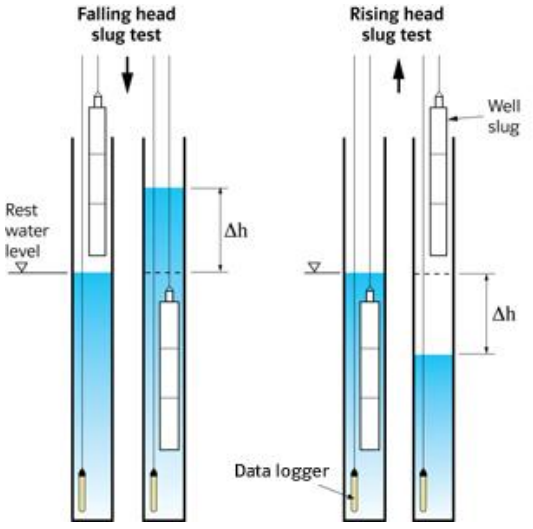

FIGURE 1.1: A sketch of the slug test procedure. The hydraulic level is suddenly increased (left) or decreased (right) creating a perturbation in the initial groundwater level. A pressure transducer is installed in order to monitor the changes in hydraulic pressure. Source: In situ Europe.

particular, in heterogeneous media, for instance fractured rock, is where having such disadvantages in mind is crucial to derive significant hydraulic parameters.

Despite the wide use of this test in all kinds of geological media, few studies have been made on the effects of heterogeneities in the results of these tests - unlike pumping tests, where heterogeneous fields have been studied both numerically and analytically. The closest studies of non-ideal systems are those of double porosity media [23], composite regimes [34], and radial flow in multi-Gaussian heterogeneous fields [8]. With this work we pretend to study the results of slug tests in correlated random fields of permeability with different interpretation methods, with the objective to advance on the understanding of this test and, more generally on hydraulic in situ testing[47].

The main question that we address is as simple as: what is the meaning of the interpreted parameters by slug tests? The complex nature of geological formations, in particular fractured rock mass, prevents us to derive a simple answer to this question.

The document is structured as follows.

In chapter two a comprehensive review of the relevant literature is done. We relate the work done by several authors, some of which is found to be very useful in well test analysis but barely used in practice for slug tests. Analytical solutions from different authors assuming different geometries and boundary conditions are presented together with the relationship between slug test and constant rate test. The results from both groundwater and petroleum engineering literature are reviewed in order to compare the different interpretation techniques and to unify results.

In chapter three the procedure and the results of a numerical study of the drawdown curves of slug test in heterogeneous media is presented. First a brief introduction of equivalent and interpreted parameters in radial flow is done, such studies are usually made to analyze pumping tests. The Monte Carlo methodology is used to generate multiple stochastic realizations of slug tests in two dimensional and three dimensional radial flow. The resulting drawdown curves are averaged and conclusions are derived from the results. Some singular curves obtained are also studied and interpreted.

In chapter four a set of slug tests performed in the safety area of El Cabril, in southern Spain, are interpreted. A short description of the site and the geological and hydrogeological features is done. The work flow of the interpretation procedure, which is derived from the conclusions of chapters two and three is presented. In particular three different formations in which slug tests have been performed, and which present signs of highly heterogeneous media are interpreted with different assumptions. A comparison with results of other tests is discussed and the need of complementary data for a consistent interpretation is highlighted.

Finally joint conclusions of the work are summarized in chapter five. The limitations of the study are also presented.

Throughout this work a porous medium at a representative elemental volume scale is always assumed. Since we are interested in low permeability media inertial effects in the wellbore will be neglected, thus we are only concerned with over damped responses.

Chapter 2

A review on the analysis of slug tests

The first studies of the interpretation of slug tests were those of Hvorslev (1951)[31] and Ferris & Knowles (1954)[24]. The Hvorlsev method, which due to its simplicity is still used nowadays, was derived from the assumption of a steady state flow - in other words, assumes the incompressibility of the medium. The hydraulic conductivity is estimated as

$$K^{int} = \frac{A}{F}\frac{1}{\Delta t}\ln\frac{h_1}{h_2} \tag{2.1}$$

Where the factor F depends on the aquifer and well geometry. The method can be accurate when the drawdown data forms a straight line with the logarithm of head. Otherwise the interpretation can be dubious and mostly inaccurate.

The same line was followed by Bower & Rice [10] who, assuming also steady state, derived an equation for the hydraulic conductivity where the well does not completely penetrate a non confined aquifer. Their solution is written as

$$K^{int} = \frac{r_c^2 \ln(r_e/r_w)}{2L}\frac{1}{\Delta t}\ln\frac{h_0}{h(\Delta t)} \tag{2.2}$$

It also provides satisfactory results when the conditions allow its application, namely when compressibility is negligible and the surrounding formation is homogeneous.

Although they can be of use for several boundary conditions, such as partially penetrating well or non-confined aquifers, these analysis have several limitations[16, 32]. Among other things, the linearity assumed in both solutions does not make them suitable when one intends to estimate parameters from non-uniform formations. This is why in this section, and this work in general, we will only focus on analytical solutions that consider transient flow.

2.1 Analytical solutions

2.1.1 Two dimensional flow

The Ferris & Knowles solution is based on the assumption that the well is acting as a line sink-source and does not take into account wellbore storage, which for early and mid-times is of considerable importance. An approximation of the line source solution for two dimensional flow is

$$h_{wD}(t) = \frac{h_w(t)}{h_0} = \frac{r_C^2}{4Tt} = \frac{1}{4t_D} \tag{2.3}$$

where the dimensionless time t_D is defined as $t_D = Tt/r_c^2$.

Cooper et al [18, 41] (from now on CBP model) presented an analytical solution to the problem of the slug test by analogy to the heat transfer problem. The analysis is based on a wellbore with storage and which is completely screened across the layer of a lateral infinite, isotropic and non-leaky aquifer, thus resulting in symmetric two dimensional radial flow. The partial differential equation and its associated boundary conditions governing this process are written as

$$\frac{\partial^2 h}{\partial r^2} + \frac{1}{r}\frac{\partial h}{\partial r} = \frac{S}{T}\frac{\partial h}{\partial t} \tag{2.4}$$

$$h(r_s + 0, t) = h(t) \qquad (t > 0) \tag{2.5}$$

$$h(\infty, t) = 0 \qquad (t > 0) \tag{2.6}$$

$$2\pi r_s T \frac{\partial h(r_s + 0, t)}{\partial r} = \pi r_c^2 \frac{h(t)}{\partial t}) \qquad (t > 0) \tag{2.7}$$

$$h(r, 0) = 0 \qquad (r > r_s) \tag{2.8}$$

$$h_0 = V_w/\pi r_c^2 \tag{2.9}$$

The solution is obtained by applying the Laplace transform, solving the resulting differential equation and taking the inverse Laplace transform. The water level h_{wD} at the well ($r_D = 1$) results

$$h_{wD}(t_D) = \frac{4C_D}{\pi^2} \int_0^\infty \frac{\exp(-u^2 t_D/S)}{u[f(u)]} du \tag{2.10}$$

where

$$f(u) = [uC_D J_0(u) - C_D J_1(u)]^2 + [uC_D Y_0(u) - C_D Y_1(u)]^2 \tag{2.11}$$

and the dimensionless storage or storage ratio C_D is defined as

$$C_D = \frac{2\pi r_w^2 S}{C_w} \tag{2.12}$$

where wellbore storage C_w is defined as $C_D = \pi r_c^2$.

The aspect of the obtained type curves are shown in Figure 2.1. For late times the CBP curves approach the asymtote given by the Ferris & Knowles approximation. This is due to the fact that wellbore effects are becoming less important once the head has dissipated and is relatively homogeneous along the formation. It can be seen that the transition between both solutions depends strongly on the storage of the formation. Actually a late time approximation of the CBP model was derived by [8] together with the late time approximation of a finite skin radius, obtained by Moench and Hsieh[38], showing that drawdown behavior at late time is mostly dependent on transmissivity whereas storage has a reduced effect. In [18] the difficulty in matching the storage coefficient for low values is highlighted due to the similarity of shapes.

In petroleum industry the slug test was studied by Ramey et al [44, 45] toghether with the drill stem test DST. They extended the analysis to a wellbore with skin effect deriving a new set of type curves. The results of their work were presented in a set of three different charts. The head response at the well was plotted in semilog (as in [18]), log log at early time and log log at late time. The skin effect was also studied by[38] who modified the CBP model to include a finite annulus with different hydraulic parameters from the rest of the reservoir, simulating a finite skin. Nonetheless the effects of a skin will not be considered in this work as its effects are relatively well understood.

Barker & Black[7] derived a model of a well intersecting various horizontal fractures. The type curves obtained are quite similar to those in the CBP model, but the estimated

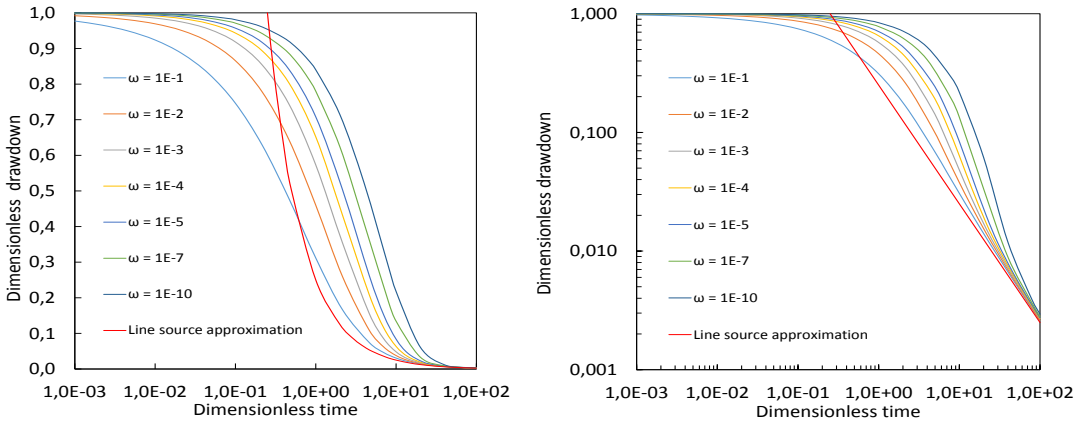

FIGURE 2.1: Left: Type curves obtained by Cooper et al (1967), the interpretation procedure consists in fitting the field data to one of the curves and derive from t_D the transmissivity. Also shown is the previous solution of Ferris and Knowles (1954) that is observed to be a good approximation for late time data. Right: The same type curves plotted in a log log axis. It shows that all type curves eventually collapse to the line source solution characterized by a unit slope. Here ω stands for the storage ratio C_D .

transmissivity in these cases will be an arithmetic average of the transmissivities of each fracture, reflecting the ambiguity of slug tests.

Sageev [48] derived approximations for early and late time responses of the slug test and studied the transient head evolution following Ramey et al, i.e. in three different plots to magnify the effects of different time periods. Early time behavior was therefore seen to be dependent mainly on wellbore skin. The determination of this parameter was suggested to be done on the basis of the slope at early time. In practice, however, initial head is not well defined [13] and thus, this does not seem to be a good way of fitting an analytical solution. He further showed that late time adjustment is satisfactory when the wellbore skin is negligible. His results for such approximations are consistent with those of Ferris & Knowles and Cooper et al, in the sense that for the limiting case of no wellbore storage, expression 2.3 gives the lower bound of the drawdown for a given permeability. When considering wellbore storage as in [18], the curve presents a transition between the initial head and the asymptotic behavior (see Figure 2.2) which depends on the relation between the wellbore storage and the storage of the formation and reaching the late time asymptotic slope in a log log plot. This slope is invariable as long as we have two dimensional radial flow and the straight line is shifted towards the right as skin effects are becoming important.

Late time approximations were also obtained by Beckie and Harvey [8] from the two annular zones model of [38]. They used this to justify how transmissivity field affects the estimation of storage by means of an equivalent homogeneous model, in this case the CBP. Indeed it was found that both models had the same late time structure with the interpreted homogeneous T being equivalent to exterior transmissivity T_2 and the

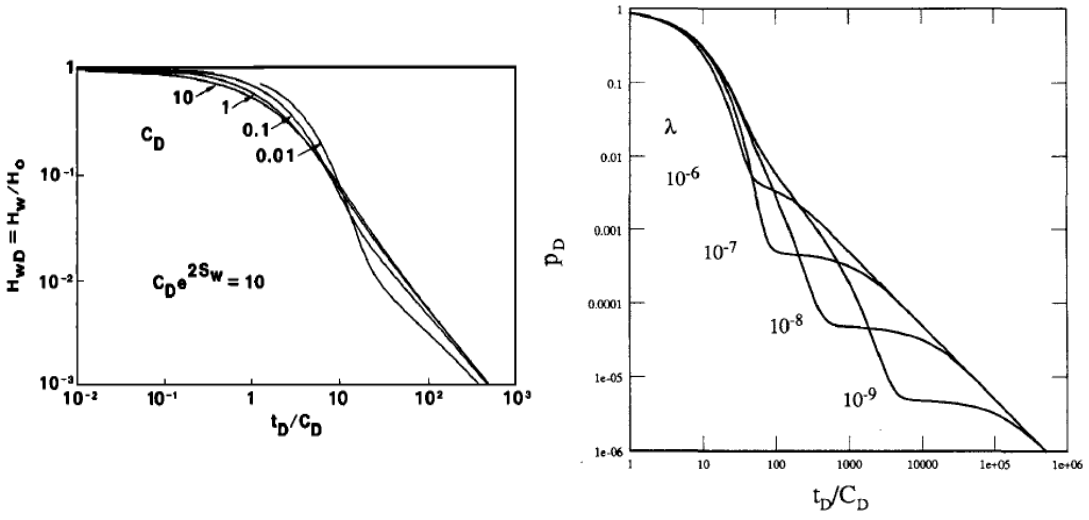

FIGURE 2.2: Left: (after Sageev [48]) Log-log late time plot of slug test response with skin effect. Right: (after Grader & Ramey [26]) Double porosity responses in log-log plot.

storage S being equivalent to $S(r'/r_w)^{(-2(T_2/T_1-1)}$.

An extension to the radial flow model was done by [23], who considered the medium to be a double porosity structure and the well screen generalized to non-completely penetrating cases. Grader & Ramey [26] analyzed the effects of the involved parameters in double porosity responses. Early time behavior is remarkably similar to that of an homogeneous reservoir with parameters equivalent to those of the fracture system. A transition period, characterized by a flattened response with constant head values is observed between the initial homogeneous period and the final slope, given once more by expression 2.3 (see Figure 2.2).

2.1.2 Type curves for general flow regimes

Karasaki et al [34], with the aim to interpret slug tests in fractured media, derived analytical solutions for various flow geometries and boundary conditions. In the following we present the solution for linear flow and spherical flow to complete the two dimensional flow solution of [18].

Linear flow may develop in those formations where a high conductivity fracture in vertical direction crosses the wellbore. Another possibility in fractured rock is the intersection with a high conductivity channel. The general solution for linear flow is

$$h_{wD} = \exp(C_{Dl}t_{Dl})erfc(C_{Dl}t_{Dl})^{1/2} \tag{2.13}$$

where $erfc$ stands for the complementary error function. The dimensionless parameters t_{Dl} and C_{Dl} in (2.13) are defined as

$$t_{Dl} = \frac{KAt}{r_w C_w} \tag{2.14}$$

$$C_{Dl} = \frac{Ar_w S_s}{C_w} \tag{2.15}$$

Note that this expression is only a function of the product $C_{Dl}t_{Dl}$ and therefore a unique match will prove difficult to obtain. For these cases complementary geological data such as fracture openning will be crucial for a correct interpretation. In petroleum engineering a single vertical fracture is usually considered to come from an hydraulic origin (e.g.[27]).

Spherical flow may develop basically when the well does not penetrate completely the formation of interest. Also in fractured media, where fractures in various directions intersect each other, a test may yield signs of spherical flow regime. The solution was derived from the analogy to heat conduction and it is expressed as

$$h_{wD} = \frac{2C_{Ds}}{\pi}\int_0^\infty \frac{\exp(-u^2 t_{Ds})u^2}{(u^2 - C_{Ds})^2 + C_{Ds}^2 u^2}du \tag{2.16}$$

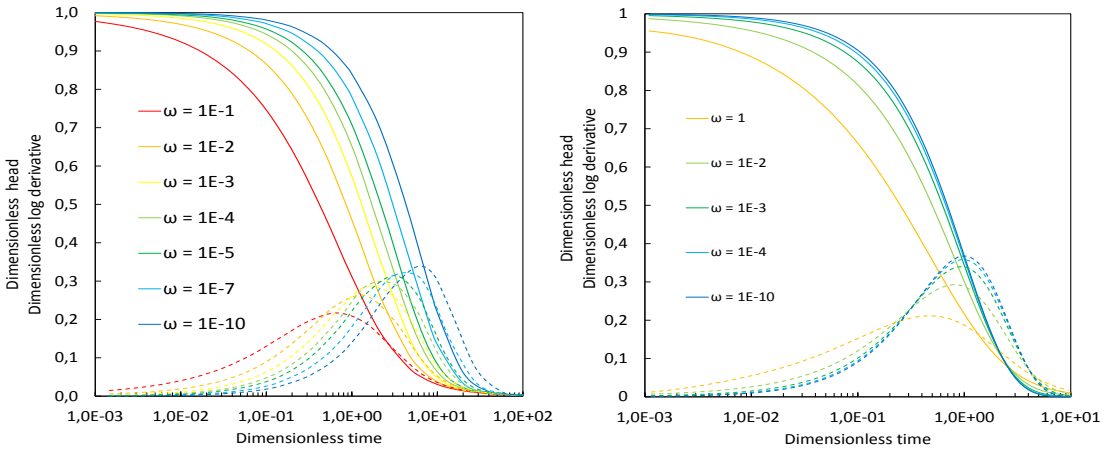

FIGURE 2.3: Left: The CBP type curves (continuous line) plotted together with its log-derivatives, showing that middle time drawdown is amplified and thus easing the fitting procedure in some cases. Right: Type curves for spherical flow derived by Karasaki et al (1988) and its derivatives.

The dimensionless parameters t_{Ds} and C_{Ds} for spherical flow are defined as

$$t_{Ds} = \frac{Kt}{r_w^2 S_s} \tag{2.17}$$

$$C_{Ds} = \frac{4\pi r_w^3 S_s}{C_w} \tag{2.18}$$

The wide range and sometimes similarity of their solutions exposes the ambiguity of such tests. One of the methods they proposed to reduce non-uniqueness is to match consistently both the drawdown data and the derivative of drawdown data with respect to the logarithm of time as proposed by Bourdet [9] for pumping tests in petroleum industry. Actually [36] noticed that the derivative plot respect to the logarithm of time is the sensitivity of drawdown to the formation's transmissivity, so that the higher is the peak of the derivative function, the more will affect transmissivity to the drawdown. Figure 2.3 shows the type curves derived by [34] in the case of spherical flow and its derivatives.

Most recent analytical studies are basically focused on the elimination of simplified hypothesis for the formulation of the analytical solution, for instance the generalization from fully confined to unconfined conditions, considering even non-saturated flow as in e.g. [54]. In practice the problem of non-uniqueness is still present as for its very nature the slug test (considering that none other but the slugged interval is monitored) is an ill posed "mathematical" problem [47]. During the nineties Butler and coworkers [12, 13, 32, 33, 36] did an extensive work on the analysis of slug tests. Among one of the results was the development of an analytical solution considering non penetrating well,

skin effect and anisotropy. This solution was used to compare the parameters resulting from the interpretation with classical methods such as Hvorslev, CBP and Bouwer & Rice in [33]. The results showed that none of the three methods was accurate for a general interpretation. In general the CBP analysis was the best for the cases in which two dimensional flow is developed. For the remaining cases the Hvorslev and Bower approximated the real parameters around the same order of magnitude.

2.2 Volume measured by the slug test

Despite what was found by [33], slug tests are still interpreted using the simplified methods of Hvorslev and Bouwer&Rice. This causes, among other things, a general trend where the interpreted values by means of slug tests are very different to those derived by pumping tests [52]. Nevertheless not only the interpretation procedure could be the cause to this variability. According to Ferris[24], slug tests are only representative of a small volume around the wellbore, while pumping tests can average larger volumes. The statement made by Ferris is not very rigorous as proved by several authors years later, for instance [34].

Guyonnet et al [28] from the work of [48] computed the maximum distances to which a specified head perturbation affected. The results, when plotted in a $r_D - t_D$ plot, showed that the perturbation reached a plateau at a given r_D. The value of maximum dimensionless radius r_{Dmax} affected by the slug perturbation is a function of the

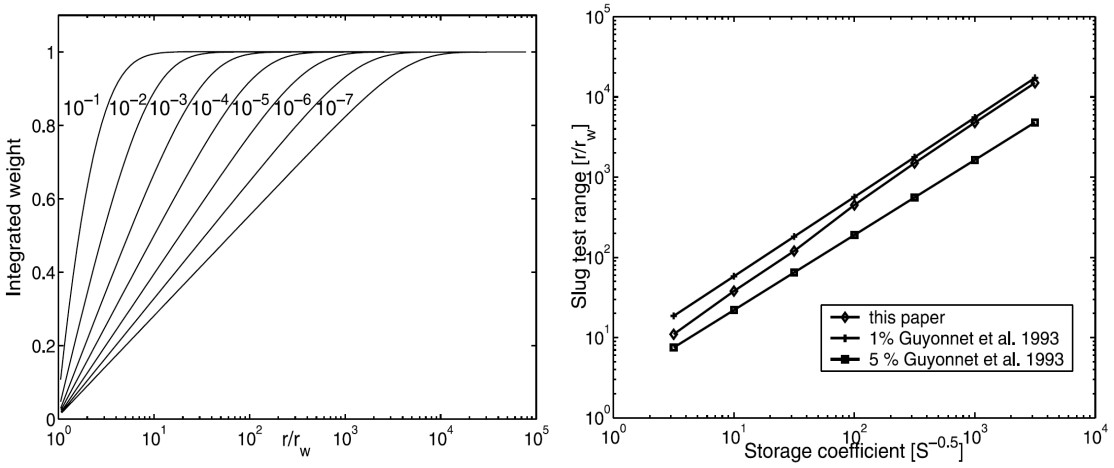

FIGURE 2.4: (From [8]) Left: Integrated weight of the contribution of transmissivities at small scale as a function of radial distance from the well and the storage of the formation. Here a value of 1 means that the transmissivities have no effects on the results of slug tests. Right: Maximum distance affected by a perturbation of 1 and 5% according to [28] and the radius to which a slug tests measures the transmissivity computed by [8].

dimensionless storage C_D and it is approximated by the relation

$$r_{Dmax} = \frac{8.37}{{C_D}^{0.495}} \tag{2.19}$$

when we track a dimensionless head of $h_D = 0.01$. This means that for a wellbore with the casing being of the same size of its radius and a formation with a storage of $S = 10^{-6}[-]$ the 1% head would travel a maximum radius of $8.37 \times (\pi r_w^2 / 2\pi r_w^2 S)^{0.495} = 8.37/(1/2{\times}10^{-6})^{0.495} = 5542 r_w$, considering a small wellbore radius of $0.05m$ this implies a maximum traveled radius of $277m$ which is fairly large. Note that the maximum volume is independent of the hydraulic conductivity.

Beckie & Harvey [8] by means of numerical simulations determined the approximate volume which is averaged by slug tests. This volume, provided that enough time for drawdown is available, is inversely dependent on the storage of the formation, such that for a low compressible medium a fairly large volume would be tested. Figure 2.4 shows the approximate results of [8]. Note that for storage of $S = 10^{-6}[-]$ the relation r_D approximates well the previous computation using (2.19). These were computed in heterogeneous domains of permeability, using a radial grid, showing that such volume is entirely dependent on the storage. Somehow these results are very useful in the sense that once a hypothesis on the formation storage is made the corresponding volume to the interpreted permeability can be assigned regardless of the structure of the permeability field. This is a feasible option as storage coefficient, unlike permeability, is not very variable throughout a certain geologic strata.

2.3 Converting slug test data to constant rate data

Due to the already mentioned similarity of drawdown curves in slug tests and the many interpretation possibilities, an alternative methodology was presented by [42] who noticed that the slug test solution given by Ramey et al [44] and that of Agarwal et al [1] for pumping tests at constant rate were related in the sense that the slug test is the derivative function of the constant rate divided by the wellbore storage.

The solution for a constant rate pumping test in a well with storage and skin is given by Agarwal et al [1] as

$$h_{wDc} = \frac{4}{\pi^2} \int_0^\infty \frac{1 - \exp(-u^2 t_D)}{u^3 f(u)} du \tag{2.20}$$

and the slug test solution is

$$h_{wD} = \frac{4C_D}{\pi^2} \int_0^\infty \frac{\exp(-u^2 t_D)}{u f(u)} du \tag{2.21}$$

Both expressions result from assuming a totally penetrating well in a confined non leaky aquifer. It is straightforward to see that

$$h_{wD} = C_D \frac{\partial h_{wDc}}{\partial t_D} \tag{2.22}$$

The relationship (2.22) was shown to be valid for any reservoir geometry. Fundamentally the method consists in integrating the pulse response of a slug test to obtain a constant rate response. Thus the resulting curve can be interpreted as a constant rate for which a wide set of solutions in the form of type curves exists (e.g. [46]). The results of the integration of spherical and radial flow are shown in Figure 2.5.

Constant rate test are characterized by an early time unit slope when the data is plotted in a log log plot. This is because of the wellbore storage effect, in other words while the unit slope persists the drawdown is only representative of the wellbore conditions and it does not give any information on the reservoir characteristics. This is in total agreement with the sensitivity analysis of McElwee [36], indeed the derivative plot of the slug test has a first interval characterized by very small values indicating that the transmissivity of the formation has no effect on the drawdown curve at that interval.

From Figure 2.5 it is seen that wellbore storage is dominating until $t_D = 0.1$ for almost all ratios of storage, and that this value increases as the ratio decreases, reaching $t_D = 0.5$ for ratios of $C_D < 10^{-7}$ which are representative of some fractured sites. Then in the case of two dimensional flow a transition period occurs whose length is proportional to the ratio C_D before reaching the constant slope in log log. A similar trend, but with different shapes, occurs in three dimensional flow cases. This means that in order to obtain meaningful results it is necessary to have drawdown data until late time and most certainly a duration longer than $t_D = 0.1$.

For the cases in which we are in a position to apply Jacob's method for the interpretation of constant rate tests, the interpreted transmissivity can be computed as (from [42])

$$T = \frac{1.151 C_w}{2\pi m} \tag{2.23}$$

being m the slope of the semi log plot of converted drawdown once reaches a straight line. Noticing that the semi log slope of the equivalent constant rate drawdown for any time is

$$m = \frac{\partial h_{wDC}}{\partial \ln t} = t \frac{\partial h_{wDC}}{\partial t} = h_{wD} t \tag{2.24}$$

the value of m is easily derived, requiring only that the value should persist for at least one log cycle [46]. Unfortunately the typical duration of a slug test will not allow us to reach the period in which m is practically constant. On top of that the straight line is developed for dimensionless drawdown less than around 1% (coinciding with the log log straight line of the CBP solution) and thus measurements will be of little precision. The

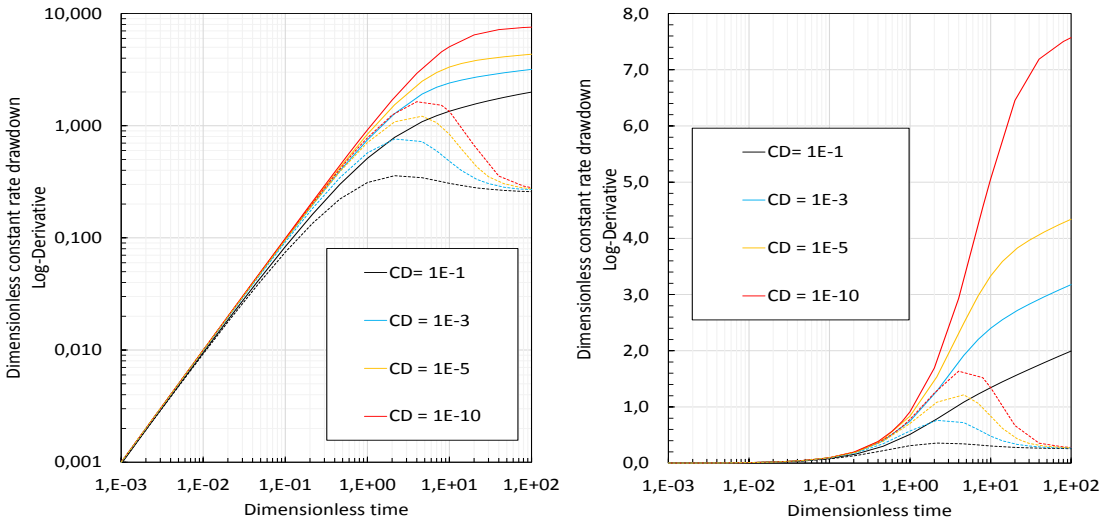

FIGURE 2.5: Results of the integration of the CBP type curves (in continuous line) as proposed in [42] and its log-derivative in dashed line. Left: log-log plot. Right: semi-log plot.

method was applied for instance in [15] apparently with satisfactory results, and after removing the wellbore storage effects.

2.4 Summary

The slug test since its inception, more than half a century ago, has proved to be an economical and relatively inexpensive means to assess the properties of a permeable formation. Nevertheless, the relevance of the interpreted parameters has been questioned since then and it is still an unresolved issue. Most relevant studies were made during between 1980's and 1990's mainly concerning analytical solutions and the suitability of these for practical problems.

It could probably be because of the complexity of such analytical solutions, which most of them are in Laplace space and require the use of numerical codes to solve them the reason why slug tests have been mostly interpreted using more simple expressions such as Hvorslev and Bouwer methods. The support volume of slug test has been proved to be larger than what some authors suggested by the interpreted conductivities are most conditioned to the immediately surrounding medium, being these one of the reasons why parameters must be viewed with special skepticism when skin effect is suspected.

A crucial question then arises: why heterogeneity has not been studied as it has been, for instance in pumping tests? A comprehensive study could reveal much of the problems that are inherent to the representativeness of interpreted parameters from slug tests.

Chapter 3

A numerical study of slug tests in heterogeneous media

In chapter two we have reviewed the current interpretation techniques that exist in order to analyze slug tests. All of them have in common that were derived from analytical solutions and that no effects of heterogeneous structures were considered. Indeed in some of them the authors introduce different boundary conditions and layered or composite structures with different properties, but all of them form relatively ideal systems.

To my knowledge the only relevant study of single well slug tests in heterogeneous fields is that by Beckie and Harvey[8]. In that paper the authors use a finite difference method in cylindrical coordinates to generate multiple realizations of slug tests which are interpreted with the CBP method. The interpreted transmissivity and storage are compared with the equivalent transmissivity of the field, which is averaged by a power law expression. The limitations of the study are the cylindrical mesh used which could result in fields that are not consistent along the radial direction and which do not permit certain structures like anisotropy and channeling to develop. Second, drawdown curves are interpreted automatically without visual check, therefore losing some qualitative interpretation.

In the following sections, with the aim of filling this gap, we present a numerical study using the Monte Carlo method of the effects of heterogeneities on the drawdown curves and its interpretation in slug tests.

3.1 Radial flow in heterogeneous media: Equivalent and interpreted parameters

It is well known that geological formations present heterogeneities at practically all scales of observations, from pore to formation scales. Hydraulic conductivity is by far the most affected parameter by such heterogeneity, varying sometimes various orders of

magnitude in a single site [25, 50]. This poses major challenges in well test analysis and reservoir modelling [43].

An approach to model such heterogeneity in a consistent manner is by means of stochastic techniques, where we acknowledge that several geological structures might be equally representative of the underlying formation (i.e. equally probable). Generally we assume that hydraulic conductivity follows a spatial random function SRF, which is correlated by means of a variogram function (see e.g. Dagan [20]). Since field observations evidence that hydraulic conductivity is generally log normally distributed, the variable used in geostatistical models is the natural logarithm of the hydraulic conductivity $Y(\mathbf{x}) = \ln K(\mathbf{x})$.

Values of hydraulic conductivity are often estimated from analysis of well tests at the site of interest. Well testing allows us to derive (normally) one set of transmissivity and storativity, which we will denote here as T^{int} and S^{int} respectively. Nevertheless, as we have mentioned, conductivity is not homogeneous throughout the volume sampled by the well test and therefore T^{int} and S^{int} represent a certain average of such volume.

In saturated flow, when Darcy's law applies, we define the equivalent conductivity $\mathbf{K}^{eq}$ as the tensor representative of the average flow in a heterogeneous domain i.e.

$$\overline{\mathbf{q}(\mathbf{x},t)} = \mathbf{K}^{eq}\overline{\nabla h(\mathbf{x},t)} \tag{3.1}$$

the over bar referring to spatial average i.e.

$$\overline{\mathbf{q}} = \frac{1}{V}\int_V \mathbf{q}dV \qquad \overline{\nabla h} = \frac{1}{V}\int_V \nabla h dV \tag{3.2}$$

Although $\mathbf{K}^{eq}$ in general is not isotropic, from single well testing we can only derive one value of K and hence, for convenience, we will assume that $\mathbf{K}^{eq}$ is isotropic and use it as a scalar value K^{eq}. Note that $\mathbf{K}^{eq}$ depends on the gradient field and hence on the flow configuration. Therefore, in general it is not the same for convergent and parallel flow. The interpreted conductivity is a case of equivalent parameter under convergent flow, though not exactly the same as its value also depends on the interpretation method [50]. The solution of K^{eq} for convergent flow is not straightforward as the gradient field is not uniform over radial distance.

Because of the importance in well testing, the averaging of expression (3.1) has been studied extensively over the years for convergent flow, particularly for pumping tests, e.g. [21, 40, 49, 51]. For instance Desbarats [22], by means of numerical analysis, found that an expression for this average process could be

$$K^{eq} = \left[\frac{1}{\Omega}\int_V \frac{\kappa^{\omega}(\mathbf{x})}{\mathbf{r}^2}dV\right]^{1/\omega} \tag{3.3}$$

resulting from steady state radial flow in three dimensional fields.

In order to see how small scale permeabilities are averaged by a slug test, Beckie and Harvey [8] computed numerically an averaging (or filter) function for the CBP model. Their filter function has the same structure as that of Desbarats i.e.

$$K^{eq}(\mathbf{x}) = \left[\int_V G(\mathbf{x} - \mathbf{x}')\kappa^{\omega}(\mathbf{x}')d\mathbf{x}' \right]^{1/\omega} \tag{3.4}$$

They observed that as storage coefficient shrinks, the filter approaches the behavior of expression (3.3), which is logical since Desbarats assumed steady state i.e. $S = 0$. The role of the power exponent ω is as follows: for $\omega = 0$ small scale parameters are averaged geometrically, for $\omega = -1$ harmonically and for $\omega = 1$ arithmetically. The optimal value of ω in [8], that approaches the CBP homogeneous parameters, was found to be dependent on the ratio between correlation scale and support volume (hence on the storage coefficient).

Since parameters derived from slug tests are obtained under convergent flow but used in the simulation of parallel flow, seldom is the case where T^{int} and S^{int} are representative for the same region at which this parameter has been obtained, resulting in discrepancies of the numerical model and the measured groundwater levels in ordinary aquifer conditions.

Meier et al. [37] using numerical simulations of pumping tests in various heterogeneous fields of conductivity found that T^{int} approximated well T^{eq} for parallel flow regardless of the distance between the pumping well and the observation well (as long as pumping time lasts enough to apply confidentially the Jacob's method). The same problem was addressed analytically by Sanchez-Vila et al.[51] using a small perturbations approach, deriving similar results.

From the results of [8] we expect that a slug test in a heterogeneous media will yield a transmissivity estimate that approaches T_G. Moreover bearing in mind the relationship between a slug test and a constant flow rate test, as shown by [42] and discussed in the previous chapter, we will expect the geometric average to be a good approximation for the slug test at late times.

3.2 Monte Carlo simulations

To derive the results mentioned in the previous section, Meier et al. [37] performed a series of numerical simulations in geostatistical fields of conductivity. The procedure used herein is pretty much based on the same philosophy.

We build two numerical models of a slug test in a well both completely and partially screened in a confined aquifer. The drawdown obtained from these setups is compared to the analytical solutions of CBP for radial flow and Karasaki et al. [34] for spherical

flow to validate both models respectively. Next using a simulator of geostatistical fields we change the permeability field of our setup sequentially. For each field a slug test is simulated and the obtained drawdown curve is registered. After at least 50 simulations for a given statistical set of parameters the drawdown curves are averaged and the resulting curve is interpreted. Singular curves that may appear within the ensemble are also interpreted separately.

Note that in reality an aquifer consists of a single realization. The averaging process described above would be the equivalent of averaging various slug tests performed throughout the formation and representative if the geospatial structure of the aquifer is stationary.

3.2.1 Numerical setup

We use the code Modflow from the USGS [30] which is based on the finite difference method to create a model of a slug test. Although radial flow is difficult to model with finite differences we use a discretization that proves to be adequate when compared to the analytical solutions. This discretization at the same time also allows to simulate geostatistical fields with correlation lengths comparable to the wellbore radius and whose structure, being the grill size constant, is independent of the radial distance to the well bore. To this end we use two superimposed grids of different discretization to ease the computation. The inner grid has a cell size of $0.25r_w$ and has an extension of $42r_w$ with r_w being the wellbore radius, whereas the outer region has a cell size of $0.8r_w$ and an extension of $84r_w$. The aspect of the numerical grid for the radial two dimensional flow is displayed in Figure 3.1. In depth the aquifer has a thickness of $8.33r_w$ and it is only discretized in one layer.

The size of the inner grid has been defined bearing in mind the results of Beckie and Harvey (Figure2.4) for a storage value of $10^{-3}[-]$ and checked with numerical simulations. This has been tested by assigning a different hydraulic conductivity to the outer grill, such that the interpreted conductivity is always consistent with the inner one and independent of the outer domain. The relatively high storage value used in this set up allows the model to be relatively small such that computing time is reasonable. Of course, this has limitations but since we are interested on the effects of heterogeneity we think that is of minor importance.

For the two dimensional case the governing equation is that presented by Cooper et al. [18]. Figure 3.2 shows the adjustment of the numerical model to their solution.

The three dimensional setup model consists of a grid cell of a size of $0.25r_w$ for the inner region which extends to $9r_w$. The outer region has a cell size of $2.4r_w$ and an extension of $42r_w$. The depth of the formation, unlike the two dimensional radial case, is discretized in the whole aquifer into 5 different zones, the central one being where

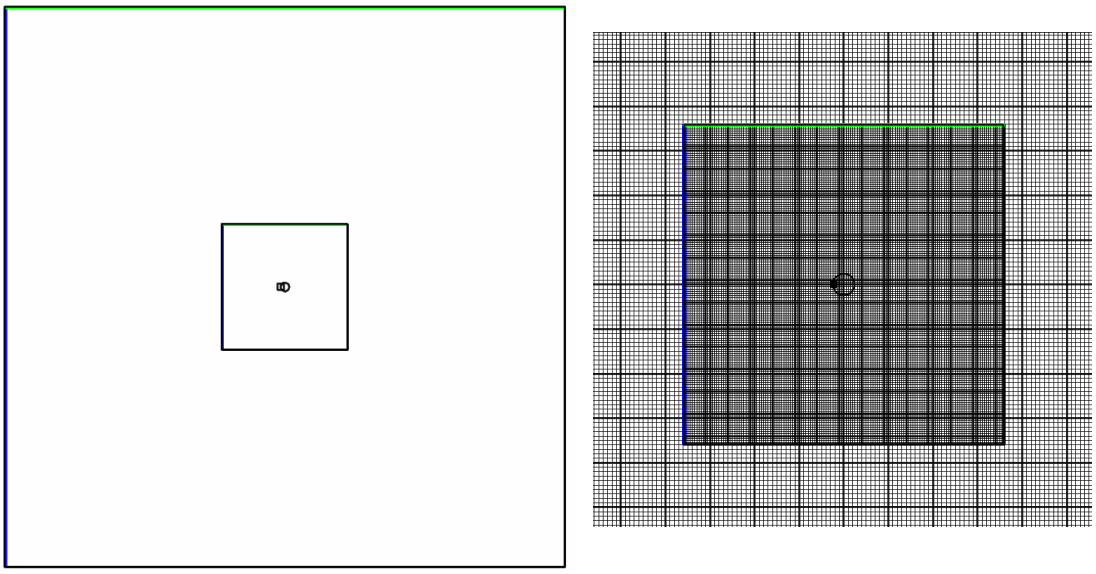

FIGURE 3.1: Left: The domain for the two dimensional set up of a slug test. This has an outer domain of 1500×1500 length units, an inner domain of 500×500 units and a wellbore of $r_w = 12$ units, where the monitoring point is situated in its perimeter. Right: Discretization of the inner and outer domain. The spherical setup is of the same structure with different size and with the aquifer discretized in 28 horizontal layers.

the well is screened. In addition the inner zone is discretized further into a total of 28 layers. The parameters used for its validation are a permeability of 1×10^{-3} [L/T] (arbitrary units) and a storage coefficient of 2.09 [1/L] which gives a dimensionless storage of $C_D = 1 \times 10^{-4}$. The performance of the model is checked against the solution for spherical flow from [34]. This is quite satisfactory as shown in Figure 3.2.

This model also serves to prove that the support volume of the slug test is not dependent on the flow dimension. We checked the suitability of the size of the inner grid by performing simulations where we maintained the inner conductivity while we increased the outer conductivity by 3 orders of magnitude. The results showed that when the inner grid was extended to $8r_w$, the curve was slightly affected at late time and the volume of the circumscribed sphere was approximated to that computed in [8] for radial flow.

3.2.2 Workflow algorithm

In Figure 3.3 we present the general algorithm that has been used to perform the aforementioned Monte Carlo procedure. First a certain set of statistical parameters is chosen. With this parameters geostatistical fields of log-hydraulic conductivity are generated using the software Visim [29]. This simulator allows to easiliy define any chosen pdf for the input of conductivities, although the size of the output matrix is restricted to around

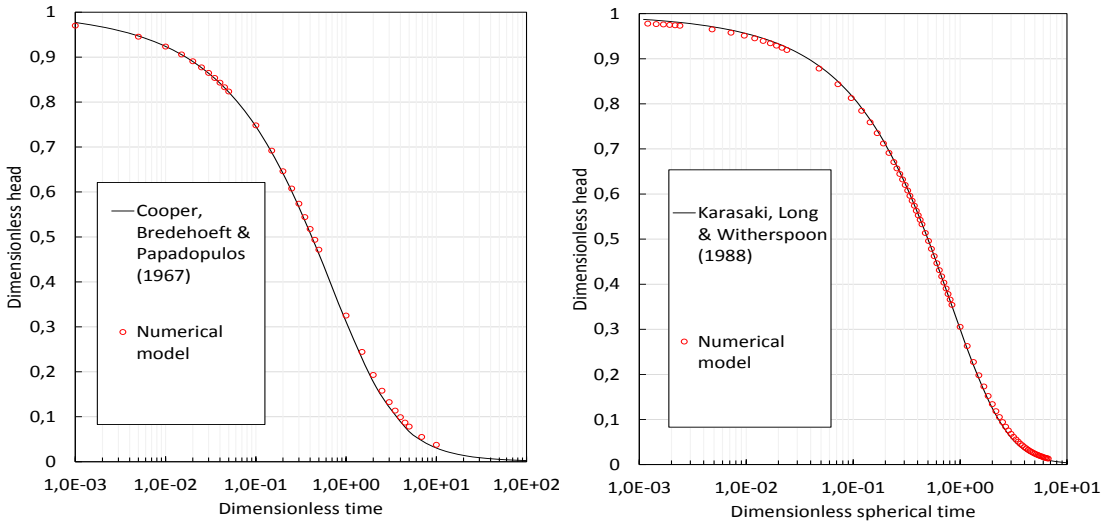

FIGURE 3.2: Left: Adjustment of the numerical model to the CBP solution for the case of two dimensional flow. Right Adjustment of the numerical model of 3D flow to the solution in [34].

200×200. Since our inner grid is smaller this is not a limitation. All fields are generated using a Gaussian variogram.

The resulting geostatistical field is converted to hydraulic conductivity and used to modify the input file .lfp of the inner grid (child grid as in Modflow notation) from Modflow. The conductivity assigned at the wellbore is equal to the maximum between the maximum conductivity of the field plus 1 log cycle or $K_w = 0.1$ i.e. $K_w = \max[\exp(\max(K_{ij}), 0.1]$. The outer grid is kept with a conductivity equal to K_G. To make sure that this does not interfere our results three simulations with a log-normal field of log-variance of 4 were performed increasing the size of the inner grid up to 200×200 and checking that the resulting drawdown was invariable.

Once the conductivity field is assigned to the numerical model the slug test is simulated and the resulting drawdown registered. The process is repeated again for another conductivity field with the same statistical parameters. The algorithm has been compiled in Matlab.

3.2.3 Results

In the following sections we present the drawdown curves obtained using the Monte Carlo procedure as exposed above.

25 different ensembles have been analyzed in radial flow, which is the regime that has been subjected to most of studies in literature, and 5 ensembles in spherical flow. The number of simulations for each ensemble has been determined analyzing the convergence of the average drawdown, such that when it stabilizes around 1% for 5 sequential simulations it is considered that it has already provided a meaningful set of results. If

we were to refine this results we would need an extra amount of simulations of the order of one logarithmic cycle [5].

The different sets of simulations which have been performed are summarized at the beginning of each section. Of particular interest are the effects of the variance of permeability and anisotropy in the fields. Two sets of simulations have also been done with bimodal PDFs with the aim of representing double permeability media such as fractured rock. The influence of the different geostatistical parameters, anisotropy, correlation length and block scale is studied with a relatively heterogeneous field of ${\sigma_{lnK}}^2 = 2$.

For spherical flow realizations the permeability fields are not correlated in depth. This is not an unrealistic assumption as generally stratification or fractures occur horizontally leading to different properties within layers. The curves are plotted against dimensionless time corresponding to the geometric average of the permeability field i.e.

$$t_{Dl} = \frac{T_G t}{r_c^2} \qquad t_{Ds} = \frac{K_G t}{r_c^2 S_s} \tag{3.5}$$

for linear and sperical flow respectively, in our model $r_c = r_w$.

All ensembles are compared to the homogeneous case of a field with $K(\mathbf{x}) = K_G = 10^{-3}$ arbitrary units. The interpretation is done with the best match to the curve of homogeneous conductivity. The fit obtained with the homogeneous curve is not always the best and it goes without saying that in practice the real storage is not known a priori. Nevertheless it allow us to provide consistent results and to compare the different ensembles.

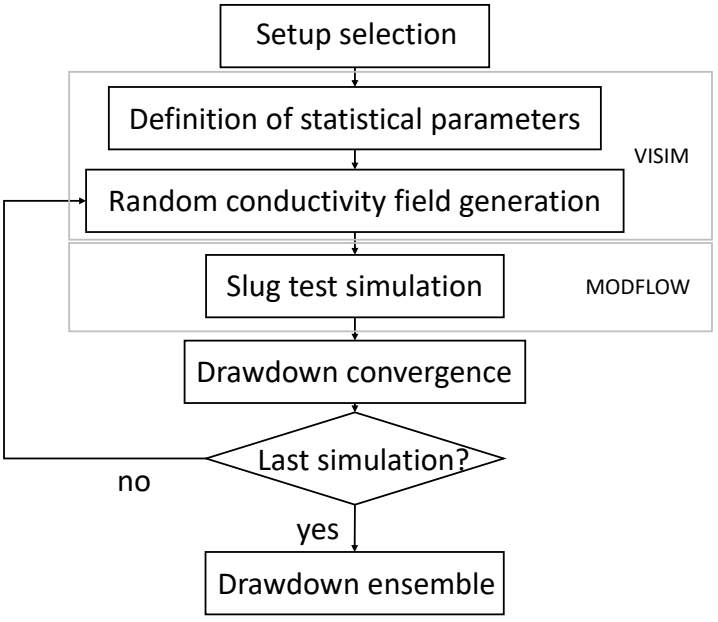

FIGURE 3.3: Workflow of the algorithm implemented in Matlab for the Monte Carlo simulations.

TABLE 3.1: Multigaussian ensembles simulated

Ensemble	${\sigma_{lnK}}^2$	λ_x	λ_y	Block scale	Simulations
1	0.1	r_w	r_w	$0.2r_w$	50
2	1	r_w	r_w	$0.2r_w$	50
3	2	r_w	r_w	$0.2r_w$	70
4	3	r_w	r_w	$0.2r_w$	70
5	4	r_w	r_w	$0.2r_w$	80

For radial flow a single simulation takes between 18 and 22 minutes to complete in a 2.7 GHz CPU. Therefore a complete ensemble of simulations can take around 17 hours to complete, and up to 25 hours for the ensembles comprising more than 70 simulations. For spherical flow the model is not only discretized in one plane but in three dimensions and thus the computing time increases considerably. Specifically, the homogeneous case needs a running time of 50 minutes in the same computer. In total, more than 28 days of computing time has been needed to complete all simulations.

3.2.3.1 Effects of variance on drawdown

The statistical parameters used for the first set of heterogeneous fields are summarized in Table 3.1. All fields are simulated using a Gaussian isotropic variogram and a log-normal PDF that yields a value of $K_G = 10^{-3}$. The only parameter that is shifted between ensembles is the log-variance ${\sigma^2}_{lnK}$, ranging from 0.1 to 4. According to the theory of composite conductive media [35], $K^{eff} = K_G$ (and therefore T^{eff} also). Thus we want to check if this relation also holds for K^{int} from a slug test. An arbitrary correlation length equal to r_w has been chosen for this case, the implications of such length will be studied in ensembles 23 and 24.

Figure 3.5 shows the results of the five ensembles. At first sight it is seen that the change of the variance in this conditions does not have a general trend. For instance increasing from 0.1 to 1 the average curve shifts towards right but from 1 to 4 the curve shifts towards left. This could be because of the different amount of Monte Carlo simulations needed to achieve convergence. Nevertheless the point here is that the ensembles tend towards the geometric mean of transmissivity field.

Figure 3.5 also shows the standard deviation for each ensemble from its expected drawdown. The effects of variance are clearly seen, increasing the range of possible drawdown curves for intermediate times as the variance of the field increases. Note that for late times all curves converge to the geometric mean curve.

This could be explained from the fact that slug test estimates depend, as it is logical, on the volume sampled along time. Once the perturbation has reached a distance of the order of various correlation lengths, the transmissivity estimates will approximate the geometric mean of the field. When this distance is covered, the radius of the volume will

be large enough to ensure that the sampled transmissivities at small scale comprise a population of such a size that yields a well-defined log-normal ensemble form there on. Since this involves the scale at which conductivities are defined (block scale), ensemble 20 will be devoted to study the effects of coarsening the field.

To visualize this process, Figure shows one realization with variance 2 and the evolution of the head perturbation, resulting from the slugged well in the center, for different dimensionless times. Note that the darkest zones (low permeability) are not perturbed until relatively advanced time.

The best match with the type curve of the homogeneous field is not completely satisfactory. The interval that best fits the shape in all cases is after a time of $t_D = 1$. In order to simplify matters we have not taken into account a possible fit with a curve of different storage. Figure 3.6 shows the interpreted conductivity of the fields by this means. It is seen that variance does not have a major effect on the average estimated conductivity but it does on the range of possible interpreted parameters. Thus it is possible in a multi-Gaussian field to have estimates either higher or lower than the geometric average. The most striking result here is that of the ensemble 1, which consists of a $\sigma^2_{lnK} = 0.1$, mainly because it is not expected that with such low variance it would yields results that different from a homogeneous field.

3.2.3.2 Effects of anisotropy on drawdown

This set of simulations has the aim of studying how anisotropy in horizontal direction is manifested in slug tests. Note that in this study anisotropy is modeled as a statistical variable instead of a local homogeneous anisotropy. This approach should be better for the cases in which we are modeling a fractured media with an equivalent continuum approach. Thus anisotropy is modeled by considering two different correlation lengths in the directions of maximum and minimum horizontal conductivity. Of course a certain amount of variance in the conductivity field must be considered for anisotropy to develop.

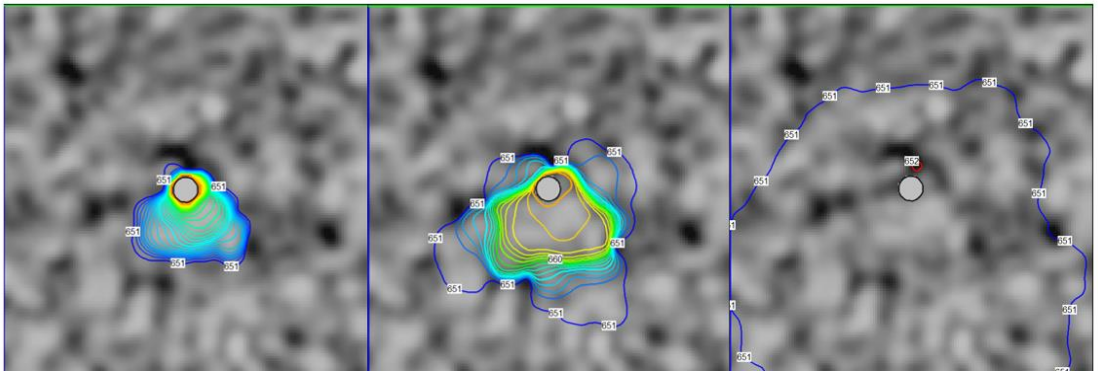

FIGURE 3.4: Head distibution in a multigaussian field of ${\sigma_{lnK}}^2 = 2$ for a t_D of (from left to right) 0,07; 0,75 and 11,6. The initial head at the wellbore was 700 and in the formation 650 length units.

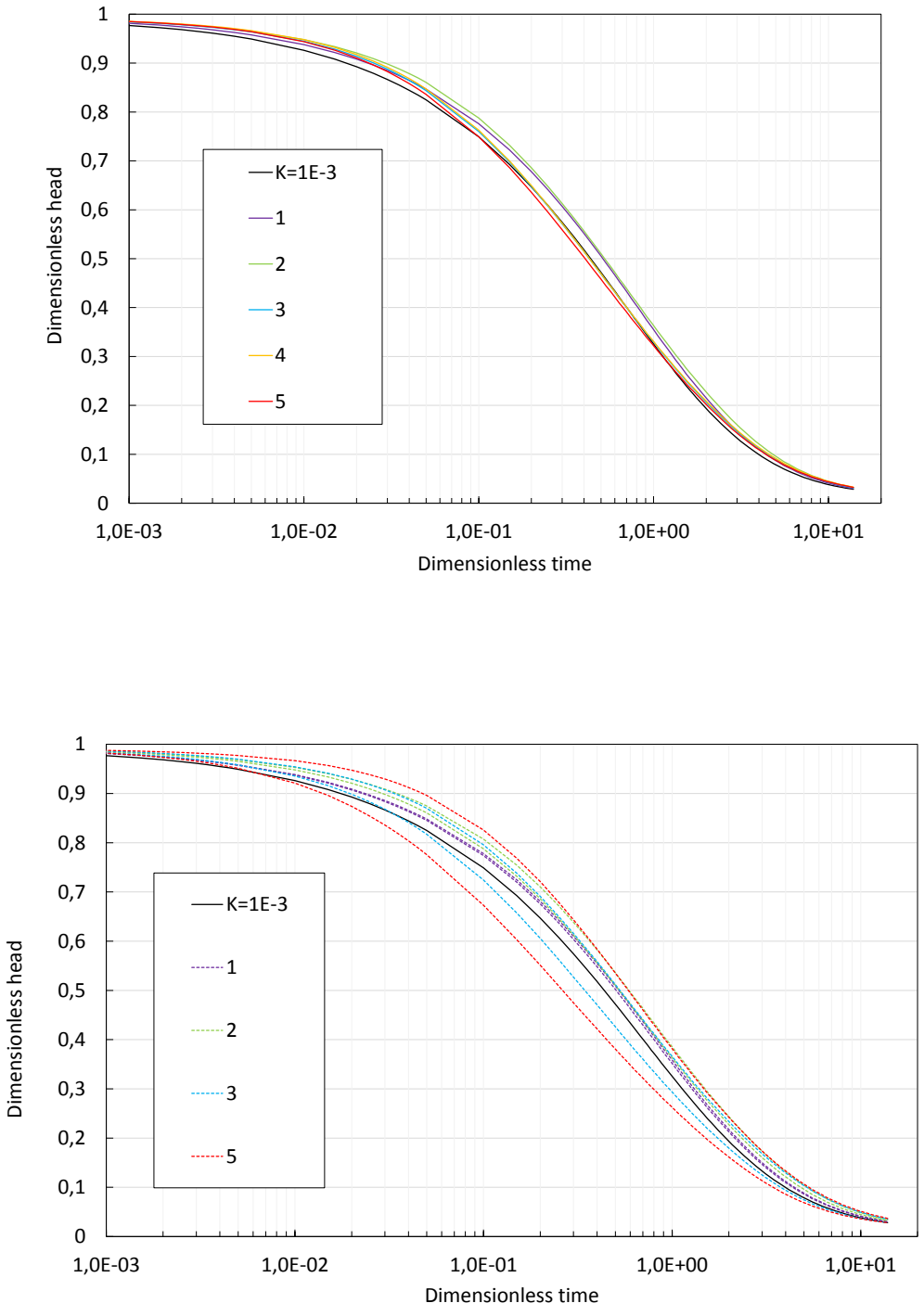

FIGURE 3.5: Resulting drawdown curves from the ensembles in multigaussian fields from table 3.1. Above: averaged drawdown of all simulations for each ensemble. Below: Range of standard deviation from the averaged drawdown.

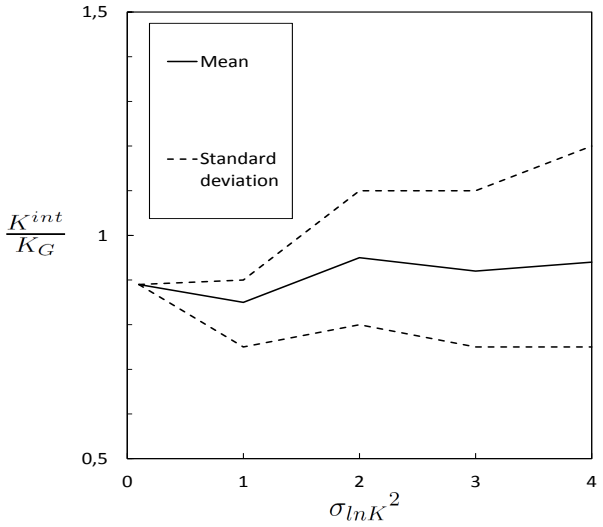

FIGURE 3.6: Interpreted conductivity normalized by the geometric average of the field in isotropic multi-Gaussian fields (ensembles 1-5), the matching point is $t_D = 1$.

TABLE 3.2: Parameters used to simulate anisotropic fields

Ensemble	σ^2_{lnK}	λ_x	λ_y	Block scale	Simulations
6	0.5	$0.25r_w$	r_w	$0.2r_w$	70
7	1	$0.25r_w$	r_w	$0.2r_w$	70
8	2	$0.25r_w$	r_w	$0.2r_w$	70
9	4	$0.25r_w$	r_w	$0.2r_w$	70
10	2	$0.25r_w$	$2r_w$	$0.2r_w$	70
11	2	$0.25r_w$	$4r_w$	$0.2r_w$	70
12	2	r_w	$4r_w$	$0.2r_w$	70

The parameters used for the generation of permeability fieds are summarized in Table 3.2.

From the above remarks it is deduced that anisotropy depends on the combinations of two statistical parameters, namely the correlation length ratio and the variance of the conductivity field. For this reason two different sets of Monte Carlo simulations have been performed, the first set (ensembles 6 to 9) consists on a series of ensembles for different values of the variance of the conductivity field whereas the second set (ensembles 10 to 12) is based on changing the correlation length ratio. The aspect of a field from the first set with variance 2 is depicted in Figure 3.8.

The results for the first set are shown in Figure 3.7. It is straightforward to see that the slope of the drawdown curve is smoothed as variance increases when compared to the homogeneous case, but still all of them continue to converge to the same curve for late time. This suggests that the derivative plot could be a good tool to analyze the behavior of drawdown. Hence we proceed computing the derivative plots.

Figure 3.8 shows the derivative plots of the homogeneous field with $T = T_G = 10^{-3}$

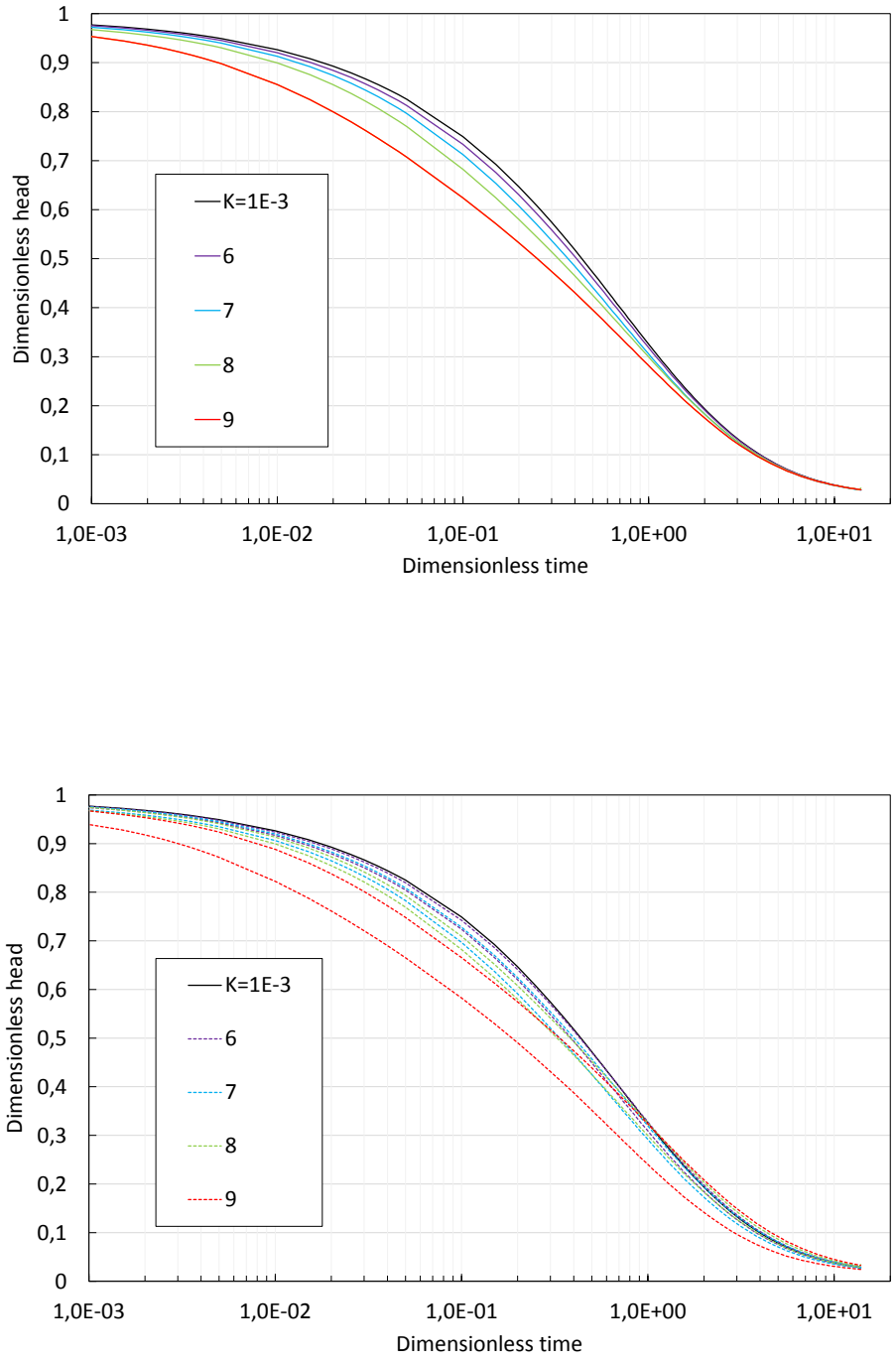

FIGURE 3.7: Resulting drawdown curves from the ensembles in multi-Gaussian fields with anisotropic ratio of 4 ($\lambda_x = 0.25 r_w$ and $\lambda_y = r_w$) from table 3.2. Above: averaged drawdown of all simulations for each ensemble. Below: Range of standard deviation from the averaged drawdown.

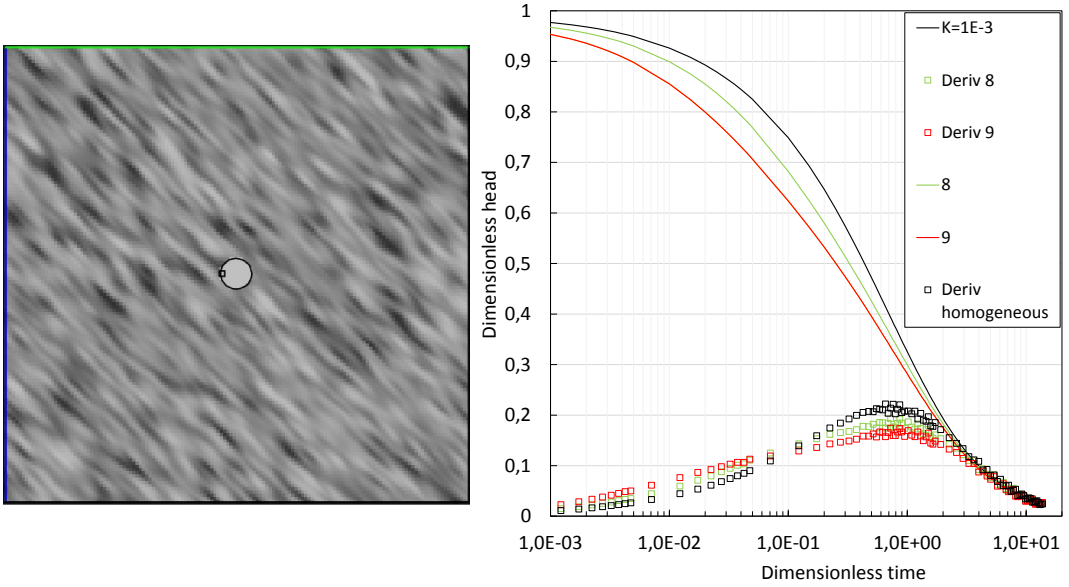

FIGURE 3.8: Left: Aspect of an anisotropic field generated with the parameters of the ensemble 8, where $\lambda_x = 0.25 r_w$ and $\lambda_y = r_w$. Right: Drawdown plots and log-derivative plots of the homogeneous field and the ensembles 7 ($\sigma^2_{lnK} = 2$) and 9 ($\sigma^2_{lnK} = 4$), which have an anisotropy ratio of 4.

and the derivatives of the ensembles 7 and 9 (see Table 3.2). Clearly as variance increases so does the plateau of the log derivative. To the authors knowledge no type curves exist in literature that present similar behavior. Therefore if deriving field data we obtain similar plots we can suspect anisotropic behavior. Of course, in fractured fields the low conductivity zones will occupy larger extends than the high conductivity zones and the ratio of permeabilities will be much higher (typically bimodal fields), thus it is expected that the plots will differ significantly from those of Figure 3.8 but with a similar trend. Furthermore it is observed that anisotropy (for small correlation lengths comparable to wellbore radius) still does not affect significantly late time slope, allowing to match with relative precision the geometric mean of transmissivity.

The second set of simulations aimed at the effects of correlation lengths in anisotropic fields. The interest of such results lies on the fact that in practice, high (or low) conductivity paths will be totally independent on the wellbore radius, as it is assumed in the previous set. Figure 3.9 shows the variability from a graphical point of view of such fields, note that although anisotropy ratios may be of the same magnitude, the aspect of the fields varies significantly at the same scale of observation.

The different ensembles resulting from the simulation of slug tests in such fields are presented in Figure 3.10. Because for large correlation lengths the early time behavior is delayed due to the low conductivity surrounding the well (this could be interpreted as a skin effect) different time scales have been used for the two cases where correlation

length of minimum conductivity is equal to the wellbore radius. This explains the different domains over time of the drawdown curves in Figure 3.10.

From Figure 3.10 it does not seem clear the effect of the anisotropy ratio on the drawdown. It rather seems that the main factor controlling the behavior of the test is the correlation length and its magnitude with respect to the wellbore radius. For large correlation lengths the skin effect appears to dominate the intermediate time behavior. If we were to match our semi-log curve, we would need either to use a transmissivity value lower than the geometric mean or to fit a non-real storage coefficient. From Figure 3.10 we see that even considering the higher drawdowns we would obtain lower transmissivity interpretations in such fields.

The interpreted conductivities are synthesized in the plots of Figure 3.11. It is seen that when keeping the correlation structure and increasing the variance the effects are very similar to those of isotropic fields, but obtaining slightly higher values. This increase could be explained if one observes the interpreted values as a function of the correlation structure (Figure 3.11 left). Recall that the anisotropy ratio is changed by increasing the largest correlation length, thus, the higher the correlation length the smaller the interpreted conductivity. In ensembles 6-8, what we have changed from the isotropic fields is one length towards a smaller value and this has resulted in higher interpreted conductivities.

Type curve match in this ensembles has been achieved from middle to late times. The effects of anisotropy in the curves, as seen in Figure 3.7 and 3.10 prevents us to obtain a good match until small drawdowns, which in practice are not always registered due to

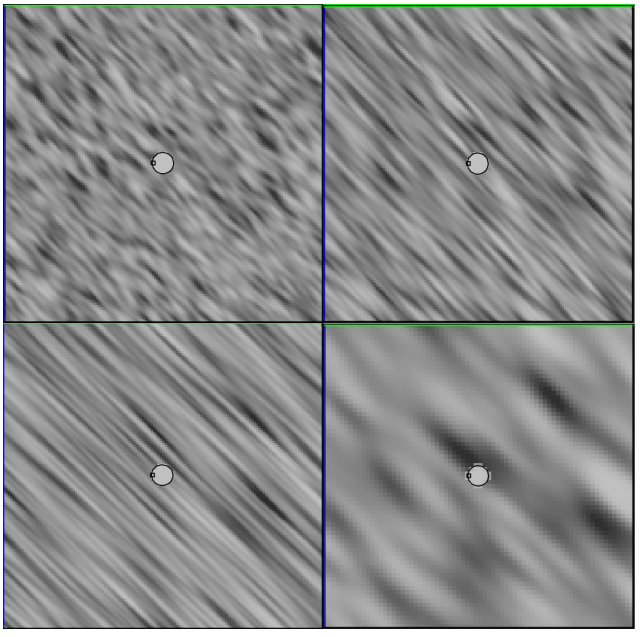

FIGURE 3.9: Aspect of the different anisotropic fields using the parameters of ensembles (from top to bottom and left to right respectively) 8, 10, 11 and 12.

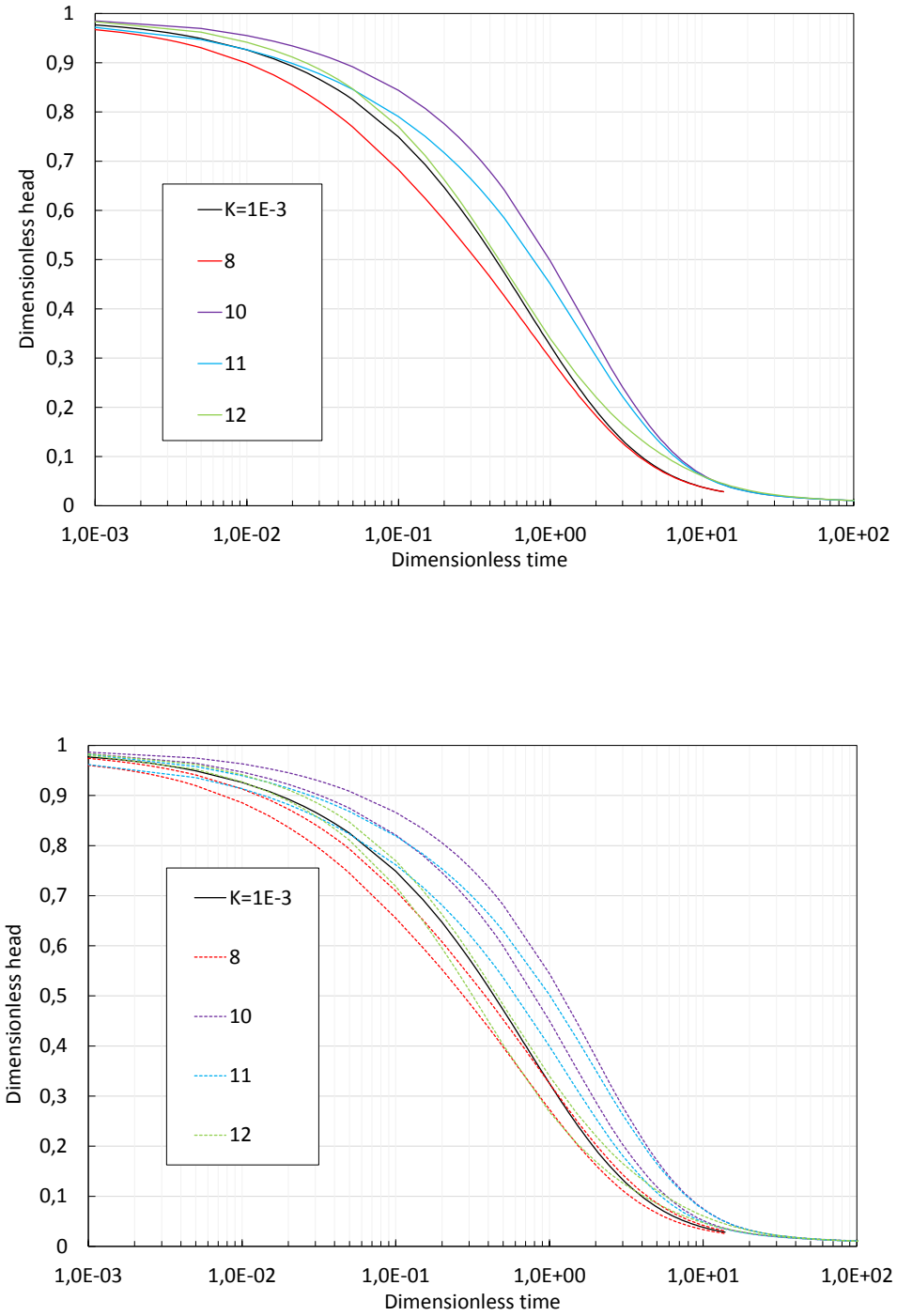

FIGURE 3.10: Resulting drawdown curves from the ensembles in anisotropic multi-Gaussian fields with various correlation lengths from table 3.2. Ensembles 8, 10 and 11 have a minimum correlation of $\lambda_x = 0.25r_w$ and anisotropy ratios of 4, 8 and 16 respectively. Ensemble 12 has a minimum correlation of $\lambda_x = r_w$ and a ratio of anisotropy of 4. Above: averaged drawdown of all simulations for each ensemble. Below: Range of standard deviation from the averaged drawdown.

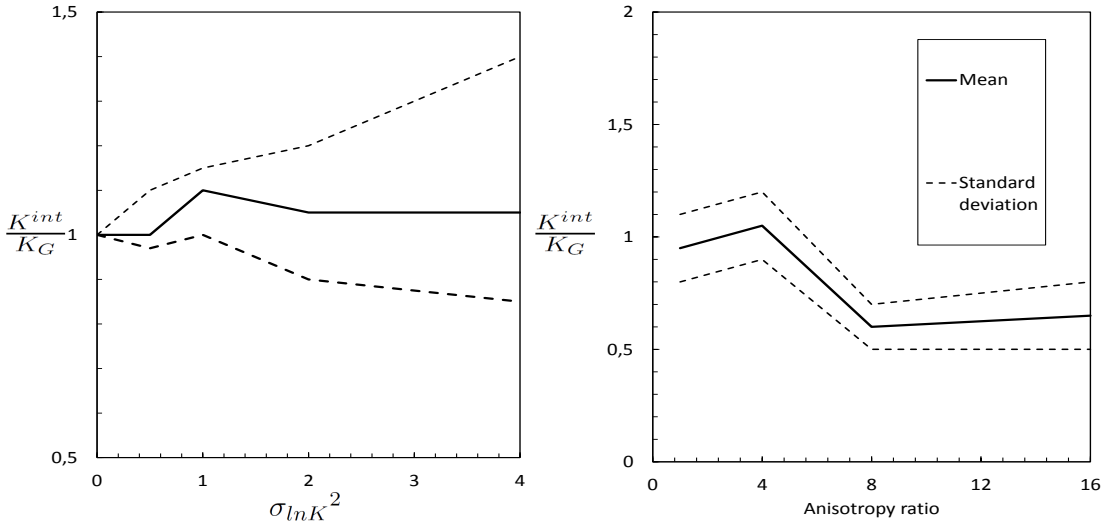

FIGURE 3.11: Left: Interpreted conductivities in anisotropic fields as a function of log variance (ensembles 6-9), the matching point is $t_D = 1$ for variance lower than 1 and $t_D = 3$ for higher variance. Right: dependence of the interpreted conductivity (normalized by the geometric average) in multi-Gaussian fields of the anisotropy ratio (ensembles 2, 8, 10, 11) with log variance=2, the matching point is $t_D = 4$.

operation constraints. The range of interpreted conductivities seems to be invariable to the anisotropy ratio, depending only on the variance value.

3.2.3.3 Radial flow in bimodal fields

It has been mentioned earlier that fractured media could be modeled with a continuum approach if a bimodal log-normal field is considered for hydraulic conductivity or transmissivity. Even though this is not exact, it is certainly better than a log-normal field [39]. The fields generated using bi-modal PDF are summarized in Table 3.3.

Logically, bimodal fields are dependent on a larger set of statistical parameters than log-normal fields. Therefore in order to synthesize better the effects of such parameters two different sets will be analyzed. The first set consists in varying the ratio of variances of both modes, resulting in three different ensembles, in that case the global variance is kept unchanged. The second set consists in varying the weight of both modes resulting in two more ensembles. The corresponding PDF consists of two different modes, but always with an average of $Y = -6.9$ (recall that $Y = \ln K$). Ensembles 14 and 15 have different averages for their modes in order to keep the geometric mean invariable, the averages of either modes are $Y_1(\mathbf{x}) = -5.05$ and $Y_2(\mathbf{x}) = -12.5$ for ensemble 14 and $Y_1(\mathbf{x}) = -1.3$ and $Y_2(\mathbf{x}) = -8.75$ for ensemble 15. For the ensembles 13, 16 and 17 the two averages of each modes, whose means are of $Y_1(\mathbf{x}) = -4.6$ and $Y_2(\mathbf{x}) = -9.2$, are invariant. Examples of generated histograms and fields are depicted in Figures 3.12 and 3.13 respectively.

TABLE 3.3: Parameters used to simulate bimodal fields

Ensemble	$\sigma^2_{lnK_1}$	$\sigma^2_{lnK_2}$	λ_x	λ_y	Density1	Density2	Simulations
13	1	1	r_w	r_w	0.5	0.5	50
14	1	1	r_w	r_w	0.75	0.25	50
15	1	1	r_w	r_w	0.25	0.75	50
16	2	1	r_w	r_w	0.5	0.5	50
17	1	2	r_w	r_w	0.5	0.5	50
18	1	1	$0.25r_w$	r_w	0.5	0.5	70
19	1	1	$0.25r_w$	r_w	0.75	0.25	70
20	1	1	$0.25r_w$	r_w	0.25	0.75	70
21	2	1	$0.25r_w$	r_w	0.5	0.5	70
22	1	2	$0.25r_w$	r_w	0.5	0.5	70

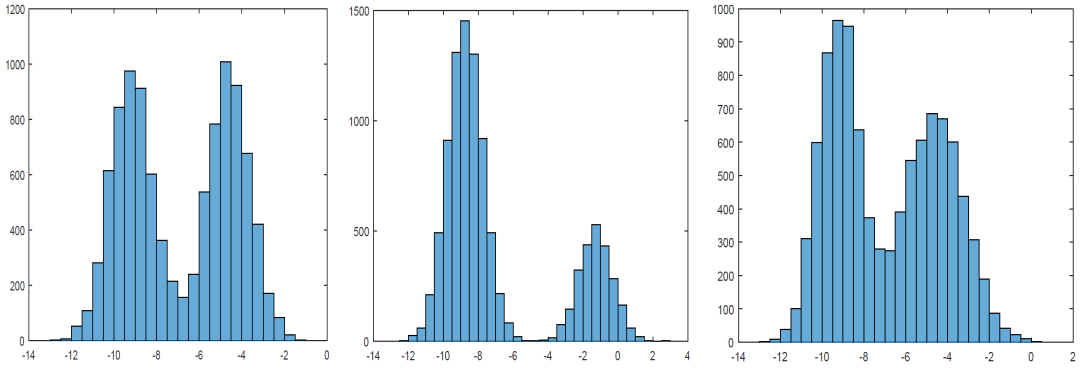

FIGURE 3.12: Some examples of historgams of $\ln K$ used in the simulations of bi-modal fields, corresponding to, from left to right: ensemble 13, ensemble 14 and ensemble 17. All of them have an average of $\ln K = -6.9$

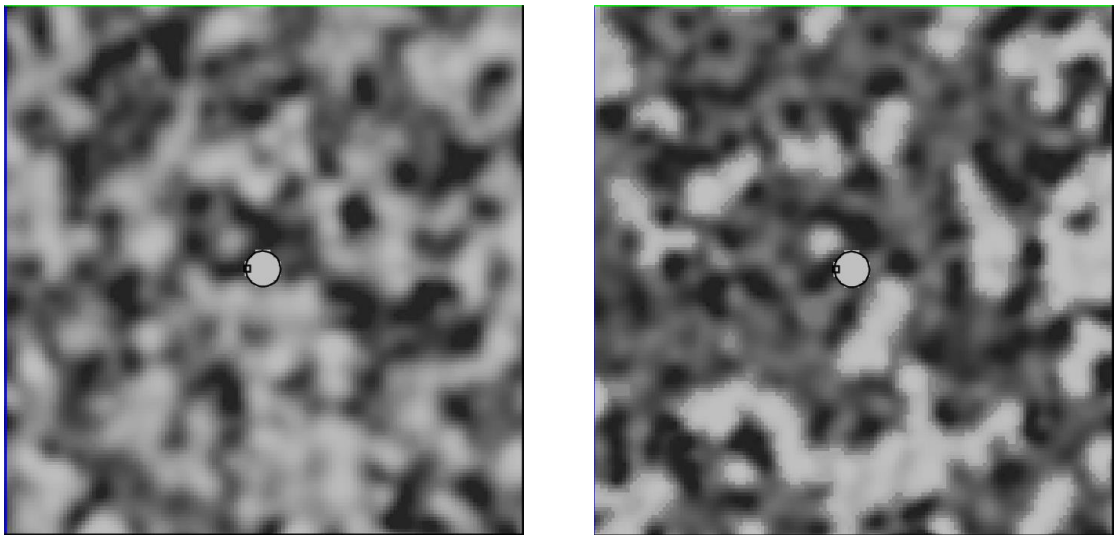

FIGURE 3.13: field from ensemble 13 and field of ensemble 17

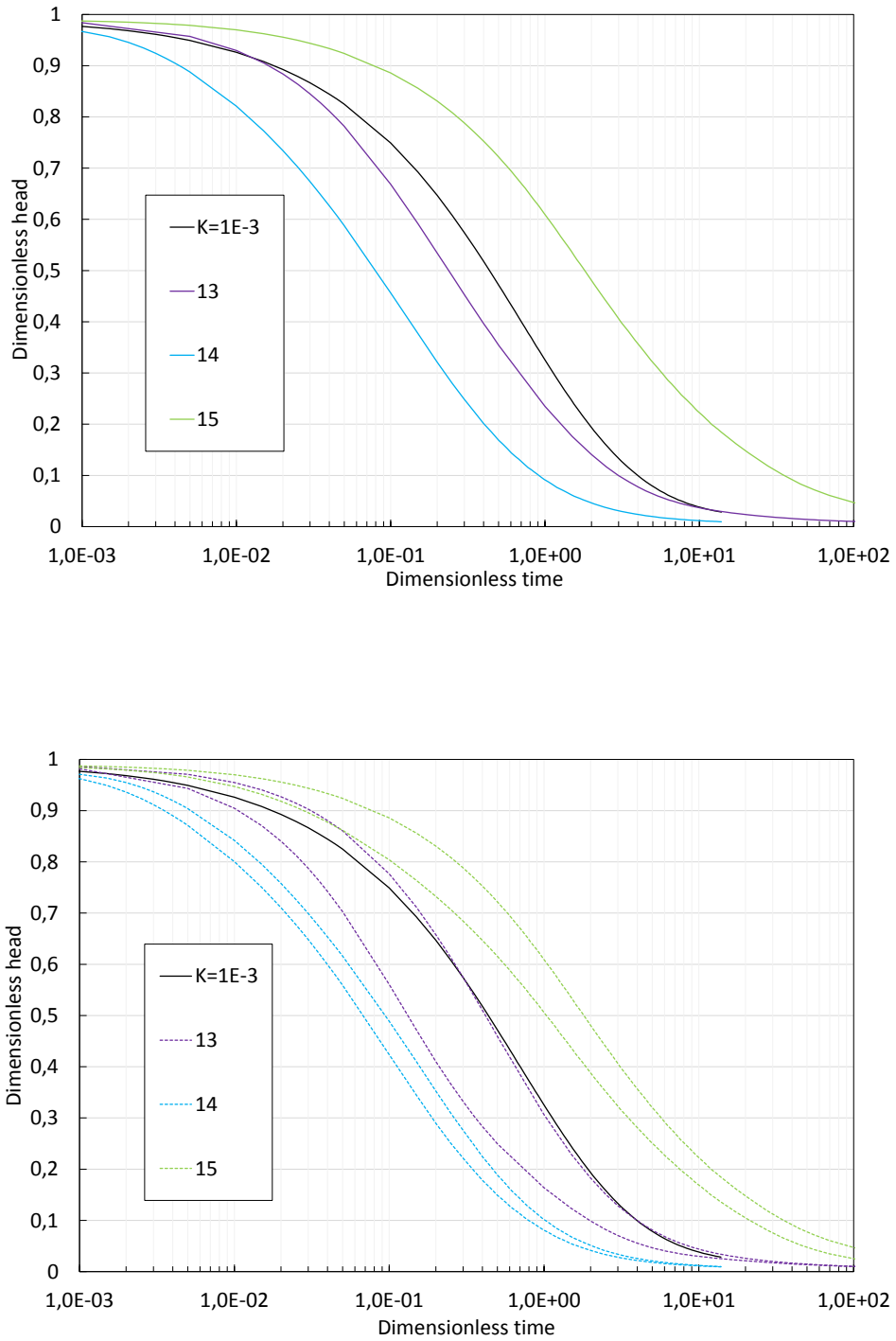

FIGURE 3.14: Resulting drawdown curves from the ensembles in bimodal Gaussian isotropic fields various weigths between modes from table 3.3. Above: averaged drawdown of all simulations for each ensemble. Below: Range of standard deviation from the averaged drawdown.

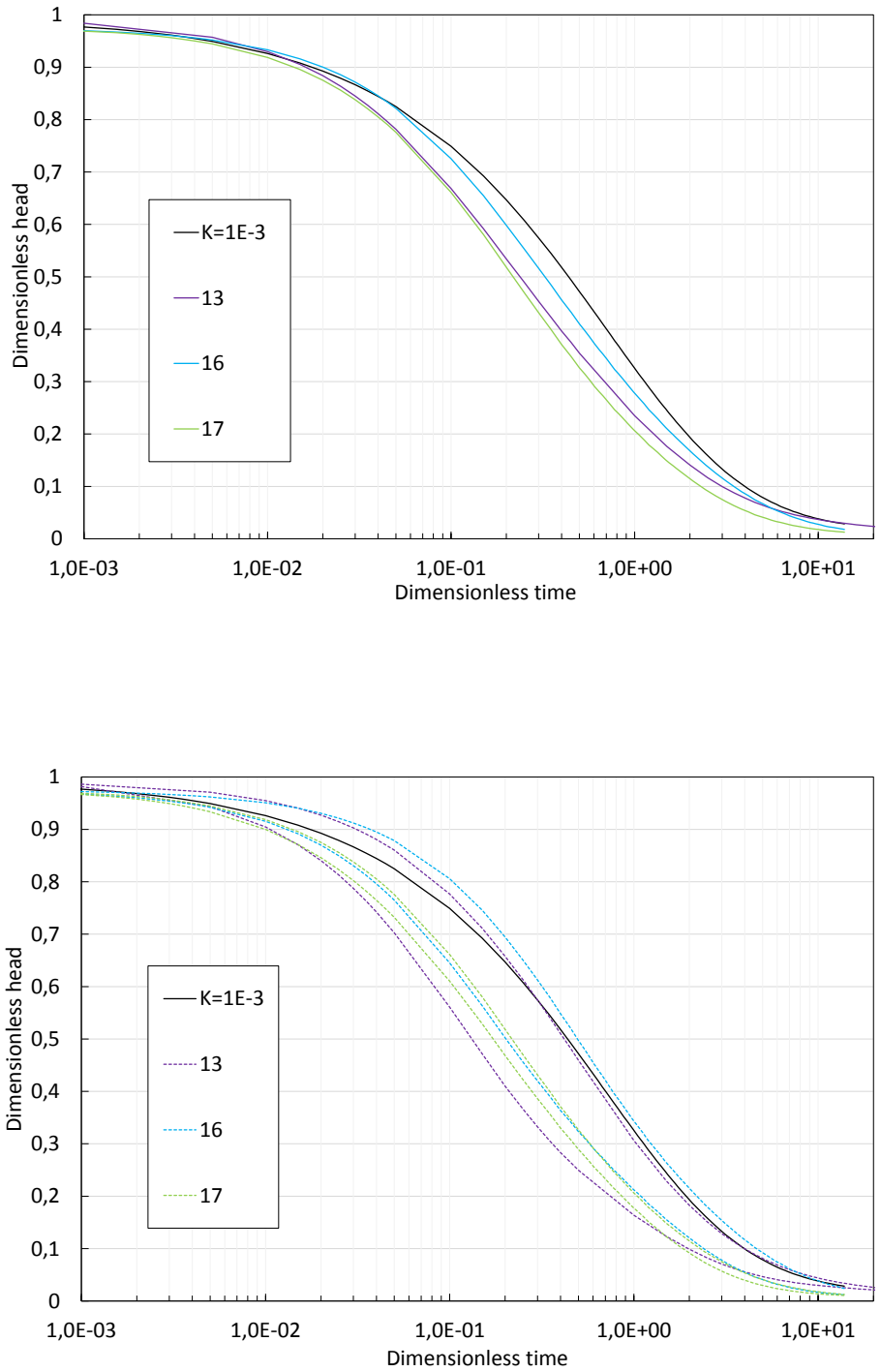

FIGURE 3.15: Resulting drawdown curves from the ensembles in bimodal Gaussian isotropic fields with with different log-variance ratios from table 3.3. Above: averaged drawdown of all simulations for each ensemble. Below: Range of standard deviation from the averaged drawdown.

The resulting drawdown curves, as with the other ensembles, have been averaged and presented in Figures 3.14 and 3.15. The first observations are related to the effects of changing the relative weights between both modes, which are clearly seen in Figure 3.14. As we increase the contribution of the high (ensemble 14) or low (ensemble 15) conductivity values, we are affecting the interpreted conductivity towards such high or low values respectively. This is so despite the fact that the averaged conductivity is the same for all of the simulations.

An interesting behavior of drawdown range is observed for the ensembles 16 and 17, which are the result of changing the variance between both modes. It is seen that when we increase the variance of the low permeability mode, the range of possible drawdown curves is significantly reduced compared to the cases of equal variances and variance towards the high permeability values. In that case interpreted conductivities are higher than the geometric average.

An important remark must be made regarding the representativeness of the averaged curves, this is the fact that the broad range of deviation may prevent us from observing the behavior that distinguishes a bi-modal field resulting from a single slug test. Indeed the drawdown curve in this cases is characterized by one initial curve that matches a homogeneous behavior. It follows that period a transition, with a relatively horizontal curve in log log plot that ends with another late time homogeneous behavior. The transition period, which appears in different dimensionless time depending on the field structure, is the responsible for the wide range during middle times of the ensemble.

Since we have mentioned two homogeneous periods for bi modal fields, it is natural that we try to derive two different conductivities and compare the resulting values with the corresponding averages of each mode. This has been done for two resulting drawdown curves belonging to ensemble 13 and represented in Figure 3.16. Note that the transition period in the simulation 25 is longer than the one in simulation 15, this means that even for a given statistical set of parameters, we may obtain significantly different results. Note also that the early time storativity has been matched to a value one order of magnitude lower.

Simulation 25 has yielded interpreted values significantly higher for both modes compared to the simulation 15. The geometric averages yielded by the two simulations i.e. the average of the two interpreted values, are 1.13×10^{-3} and 2.73×10^{-3} (arbitrary units) for the simulation 15 and 25 respectively, while the geometric average of the field is 10^{-3}. Therefore, a priori it seems that the longer the transition period the less representative of the geometric average are the interpreted conductivities.

Following the isotropic bimodal fields, we study the effects that a variable correlation length would have on the behavior of the slug test. We simulate five more ensembles with the same parameters as the previous ones but now all of them are performed considering

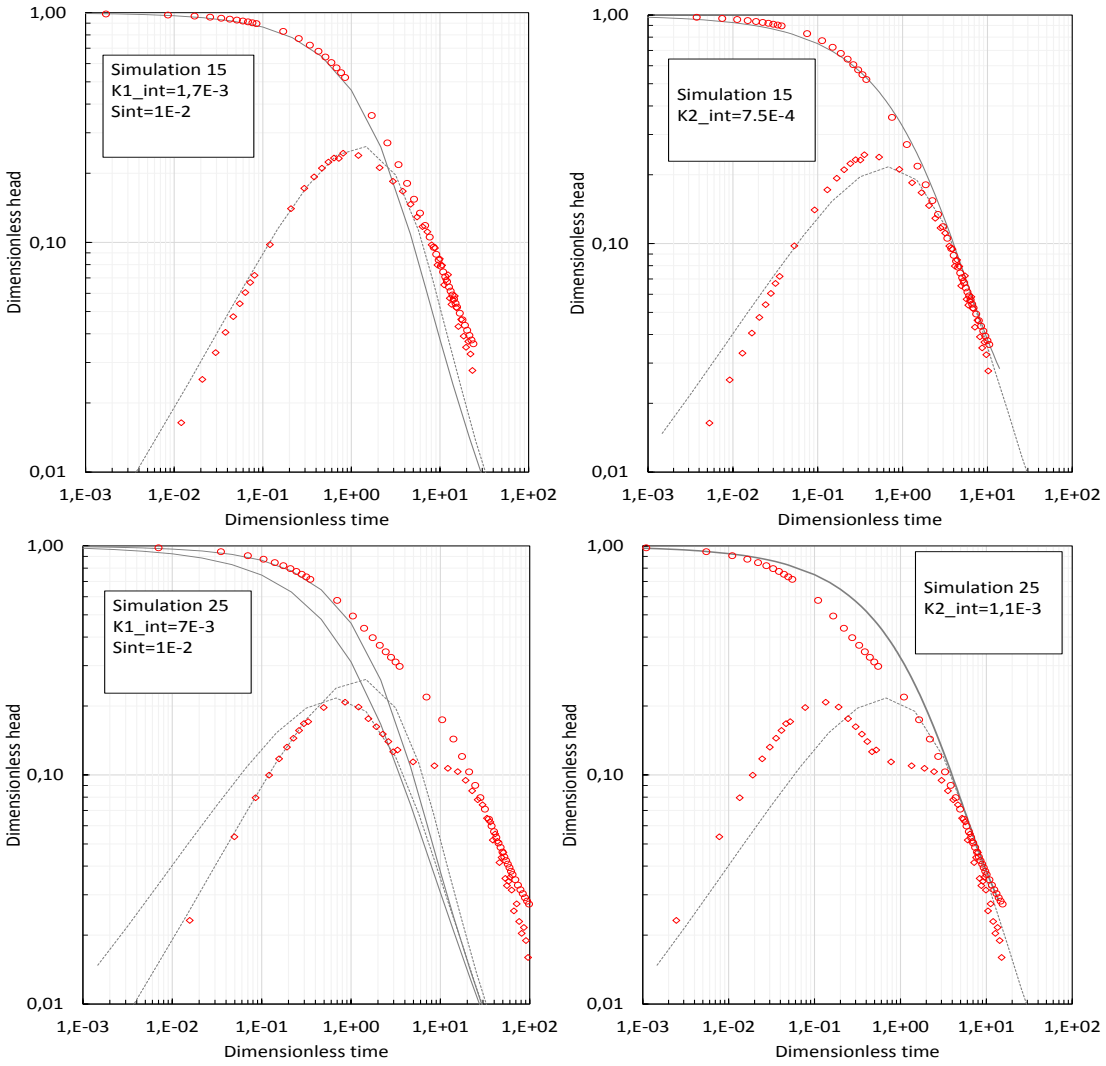

FIGURE 3.16: Interpretation of two different simulations from the ensemble 13, which present two different possible matches for early and late times. Log-log scale is used toghether with the log-derivative.

an anisotropy ratio of 4, with a maximum correlation length of r_w. Table 3.3 summarizes the used parameters.

The drawdown curves of the ensembles 18 to 22 are plotted in Figures 3.17 and 3.18 respectively.

Observing the average of drawdown of the first set, plotted in Figure 3.17, which represents the effects of the weight ratio on the drawdown, it appears that when the weight is shifted towards the low permeability the drawdown is smoother. When the high permeability zone is increased (ensemble 19) the drawdown curve gets steeper, as if the storage field was lower.

Thus, once again it seems that the derivative plot could be a good tool to compare such behaviors. Figure 3.19 shows the computed derivatives for both sets of ensembles.

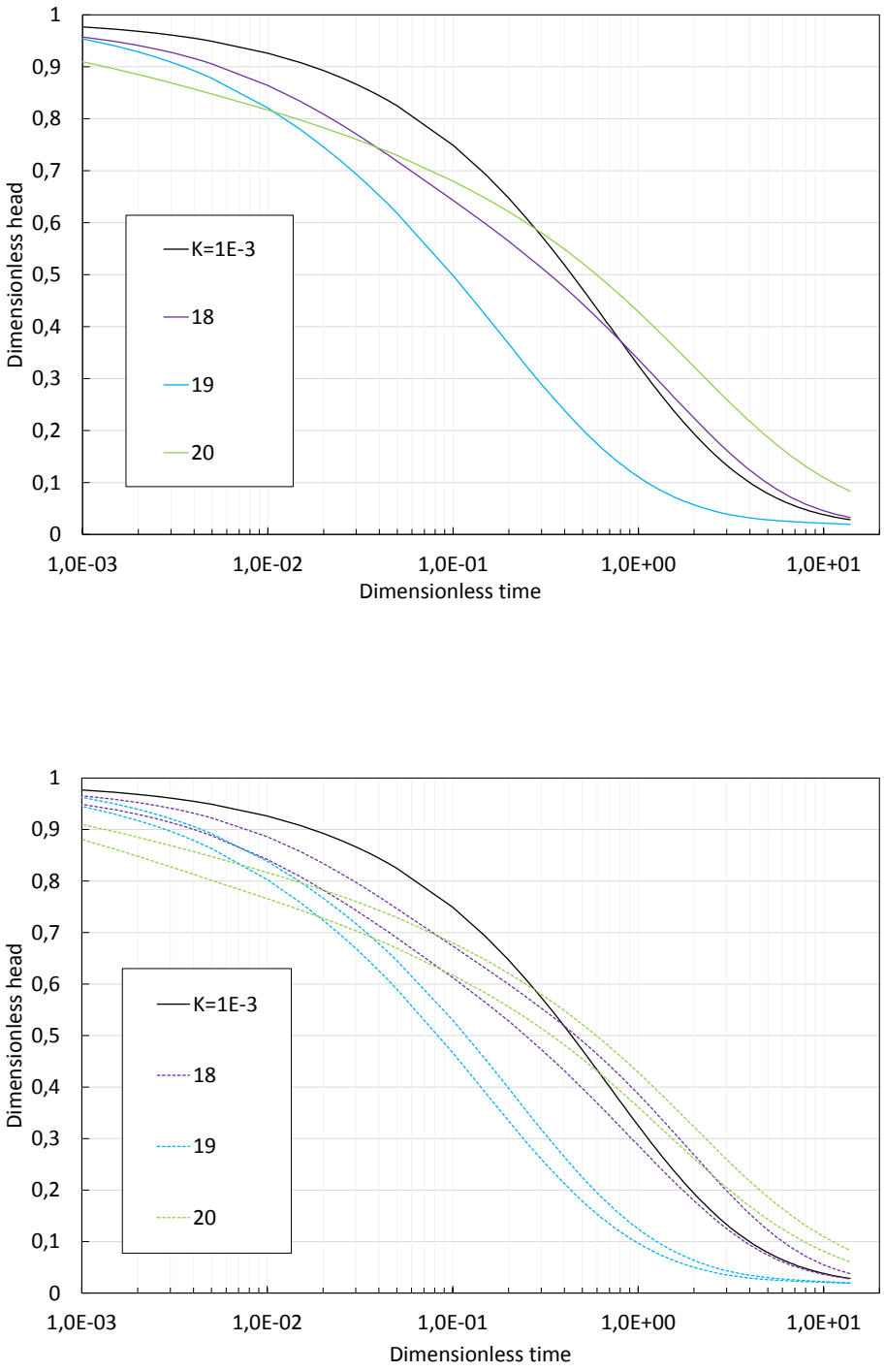

FIGURE 3.17: Resulting drawdown curves from the ensembles in anisotropic bi-modal fields with different weights ratio from table 3.3. Above: averaged drawdown of all simulations for each ensemble. Below: Range of standard deviation from the averaged drawdown.

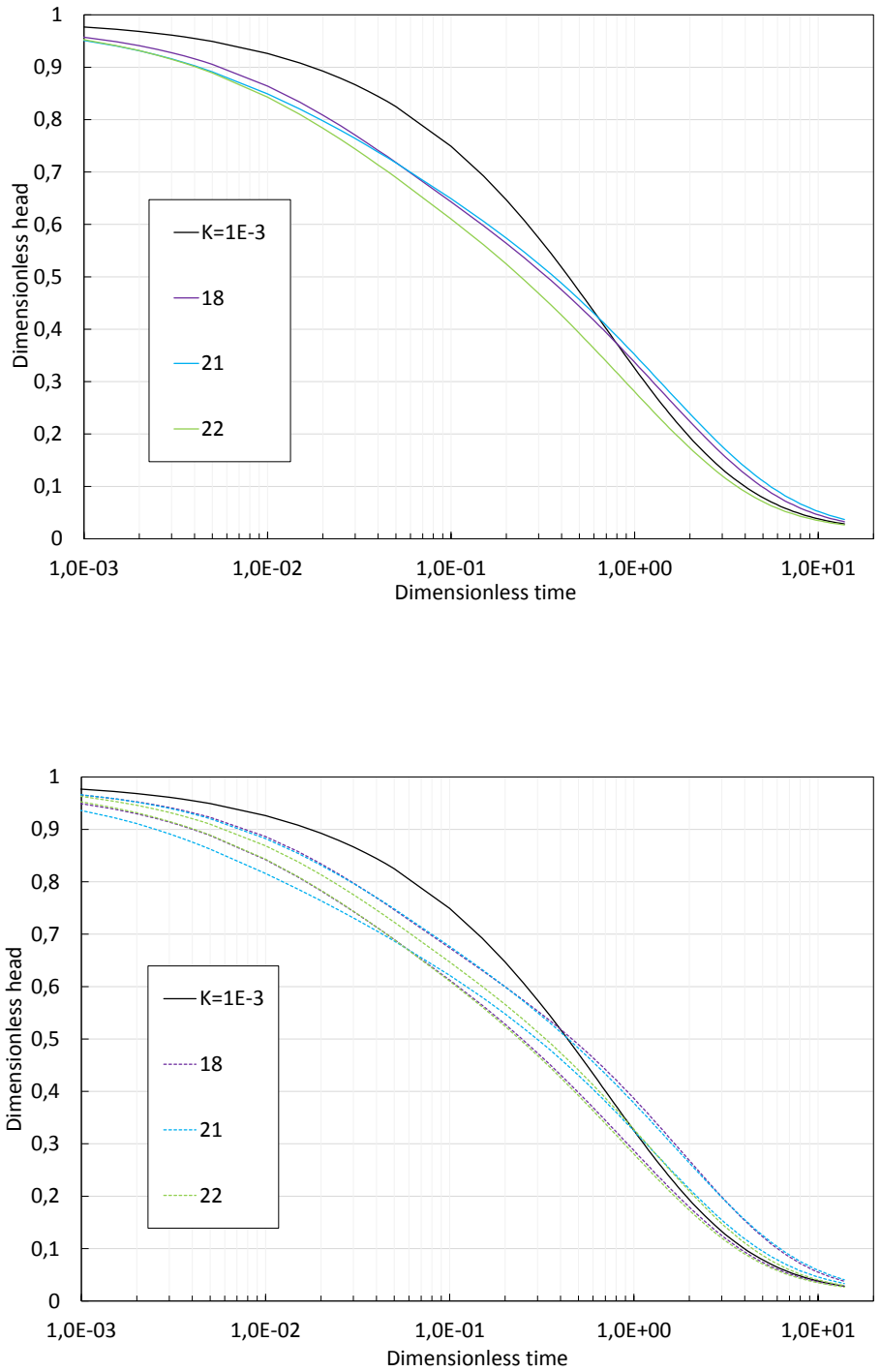

FIGURE 3.18: Resulting drawdown curves from the ensembles in anisotropic bi-modal fields with different variance ratios from table 3.3. Above: averaged drawdown of all simulations for each ensemble. Below: Range of standard deviation from the averaged drawdown.

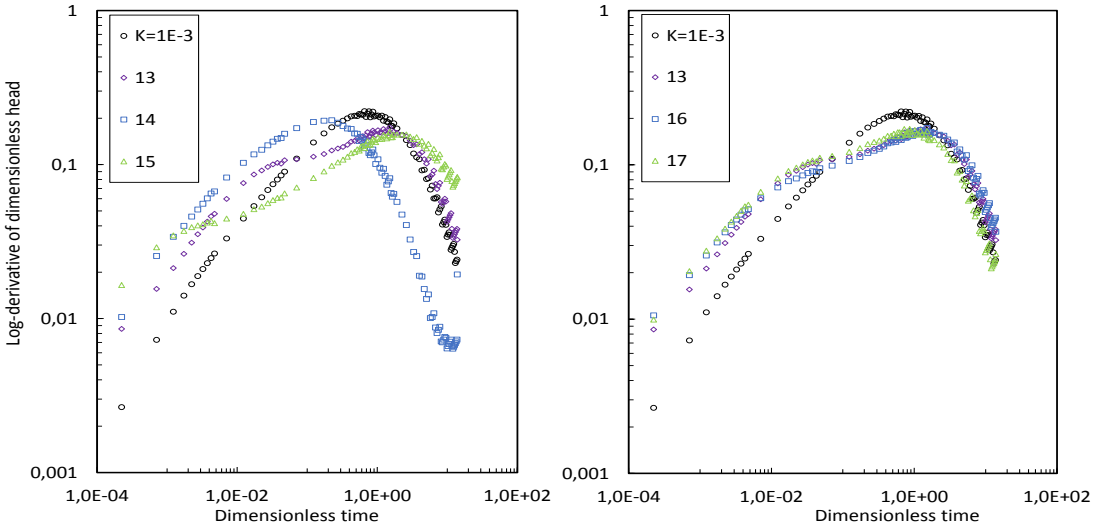

FIGURE 3.19: Log-derivatives computed over the averaged curves of bi-modal fields in log-log plots.

It is clear that the main factor controlling its shape is the relative weight between the modes of the PDF, while the variance ratio is not that determinant.

When the PDF is weighted towards the high permeability zones (ensemble nr 19) the derivative plot does not change its shape very much but is shifted towards the left. This causes that an interpreted conductivity would be lower than the geometric one, but since its shape would allow a good match it would provide a confident type curve fit. If the PDF is weighted towards the low permeability zone the shape of the derivative curve changes considerably, and it does not match any of the homogeneous behavior.

The effects of variance ratio are studied with ensembles 21 and 22, plotted in Figure 3.18. We clearly see that drawdown curves will be more variable for early-mid times if the variance is higher for low permeability mode and, conversely, the drawdown curve will have more variability on its shape for intermediate-late times if the variance is higher for the high permeability mode. In other words, in a semi-log plot, high conductivity zones dominate the early time behavior while the late time is influenced mainly by the low conductivity.

An interesting result is that the deviation range of the ensemble 18 matches the upper bound of ensemble 21 and the lower bound of ensemble 22. To observe better this behavior, the early and late time log log plots are depicted in Figure 3.20. This could be because the conductivity field involves two different time scales that are related to the low and high conductivity zones respectively. The distinctive feature here from the other log-normal fields is that the derivative shows two different peaks (actually, as seen in Figure 3.19 the first is not exactly a peak but a plateau zone). Ensemble 19 does not show this behavior because the high permeability is the prevailing mode and thus early

and intermediate time is influenced by such mode and it is not until late time that an anomalous behavior is observed corresponding to the low permeability zone.

In a geological media is expected that a sand formation with small inclusions of clay will present a behavior similar to that of ensemble 19 whereas fractured media will present a behavior more similar to that of ensemble 20.

The interpretation of the curves is quite ambiguous, particularly those resulting from ensemble 15, whose parameters yields curves that differ substantially from the homogeneous case. The interpreted values have been determining from log-log plot analysis, which consists in matching the slope at late time. Therefore the behavior at early-mid times has not been considered. Observing Figure 3.20, the use of derivative plots could be an alternative way of defining the interpreted parameters.

In Figure 3.21 we show the plots of the interpreted conductivity as the function of the two variables considered, namely the relative weight and variance between both modes of the PDF. First observation is that the results of the relative weight are quite logical. Recall that the geometric average of the field is kept invariable for all fields studied. Thus the PDF from ensembles 19 and 20 have the same shape but they are mirrored from each other being the geometric mean its axis of anti-symmetry. When we plot the interpreted parameters we see that this relation also holds in a semi-log axis, being $\log(K^{int}/K_G) = 0.33$ and 3.3 depending on whether the weight is mostly on lower or higher conductivity respectively.

From the interpretation of the other ensembles (Figure 3.21 right), which are differentiated by their variance between modes (the mean value of each mode is preserved), we see that if one of the modes has a higher variance then the interpreted conductivity will be shifted towards such mode. Nonetheless we have to bear in mind that in this case

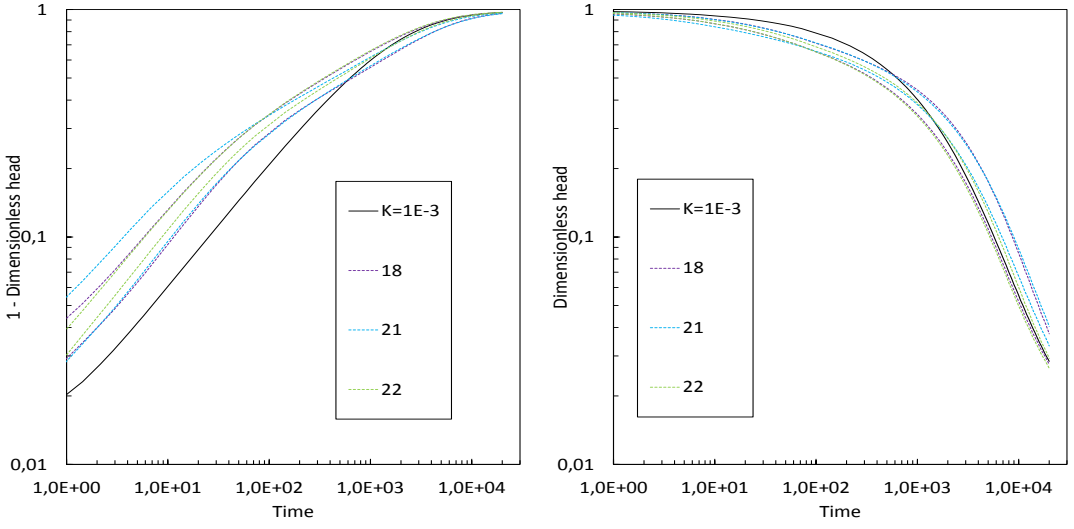

FIGURE 3.20: Log-log plots of early (left) and late times (right) of the standard deviation ranges of the bi-modal ensembles 18, 21 and 22.

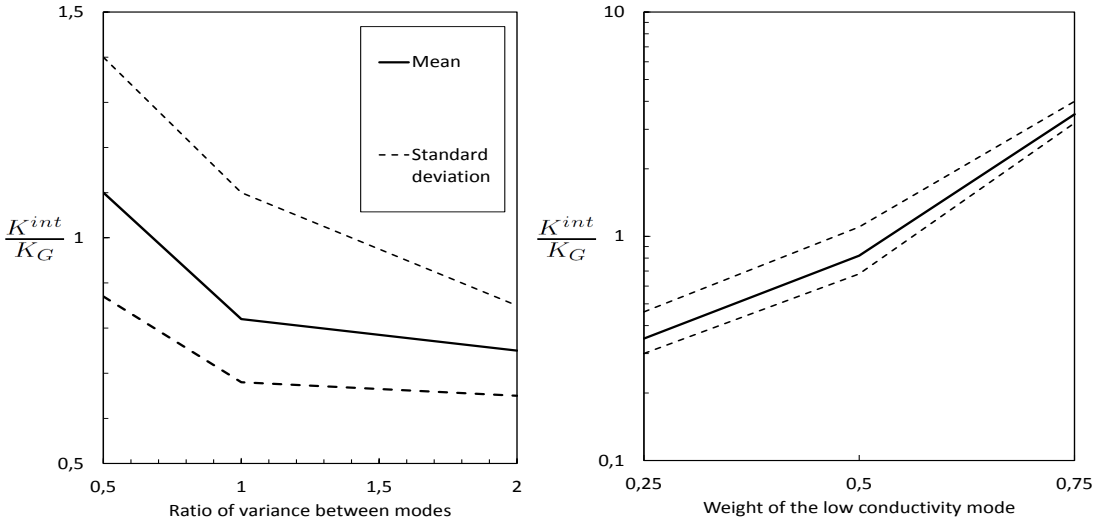

FIGURE 3.21: Left: Interpreted conductivity in anisotropic bi-modal fields as a function of the variance ratio $\sigma^2_{lnK1}/\sigma^2_{lnK2}$ between both modes, obtained from the ensembles 18, 21 and 22. Right: Increase of interpreted K as the weight of the PDF function moves towards the low permeability mode, maintaining the geometric average constant.

TABLE 3.4: Parameters used to study the effects of correlation lenght

Ensemble	${\sigma_{lnK}}^2$	λ_x	λ_y	Block scale	Simulations
23	2	$2r_w$	$2r_w$	$0.2r_w$	50
24	2	$4r_w$	$4r_w$	$0.2r_w$	50

we are assuming that both modes have the same weight and thus, to extrapolate this results in real bi-modal geological media such as fractured rock, is not straightforward. Fractured rock may have higher variance in high conductivity paths but the weight is likely to be higher on the low conductivity mode (rock matrix).

3.2.3.4 Effects of correlation length

Two ensembles have been performed in order to study the possible effects that the considered correlation length can have when we study heterogeneous fields by means of geostatistical techniques. Indeed in reality, even though geological media are not well represented by geostatistical fields, the correlation length is independent of the wellbore radius and hence we could derive conclusions from our numerical simulations that would not necessarily be representative of real geological media. Thus in ensembles 23 and 24 we consider the sensitivity of drawdown to the correlation length. The considered statistical parameters are shown in Table 3.4.

The results, as shown in Figure3.23, indicate a clear decrease on the interpreted conductivity as the correlation length increases. The precise cause of this is not clear but it could be that the well is usually surrounded by a low conductivity zone, affecting

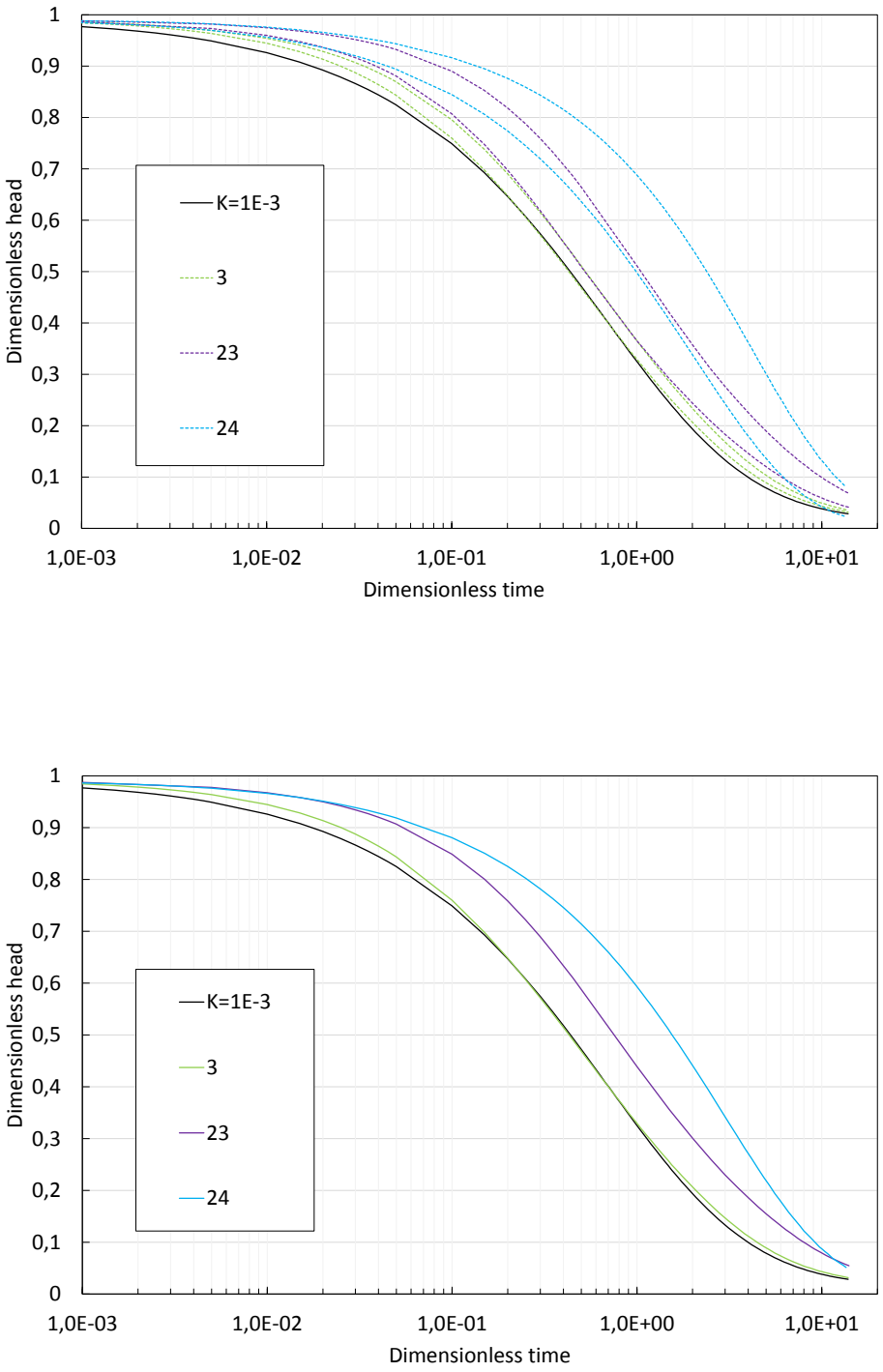

FIGURE 3.22: A comparison of the resulting drawdown curves from ensembles 3, 23 and 24, showing the effects of increasing correlation length. Above: averaged drawdown of all simulations for each ensemble. Below: Range of standard deviation from the averaged drawdown.

TABLE 3.5: Parameters used to study the effects of up-scaling the permeability fields

Ensemble	$\sigma_{lnK}{}^2$	λ_x	λ_y	Block scale	Simulations
25	2	r_w	r_w	$0.4r_w$	50

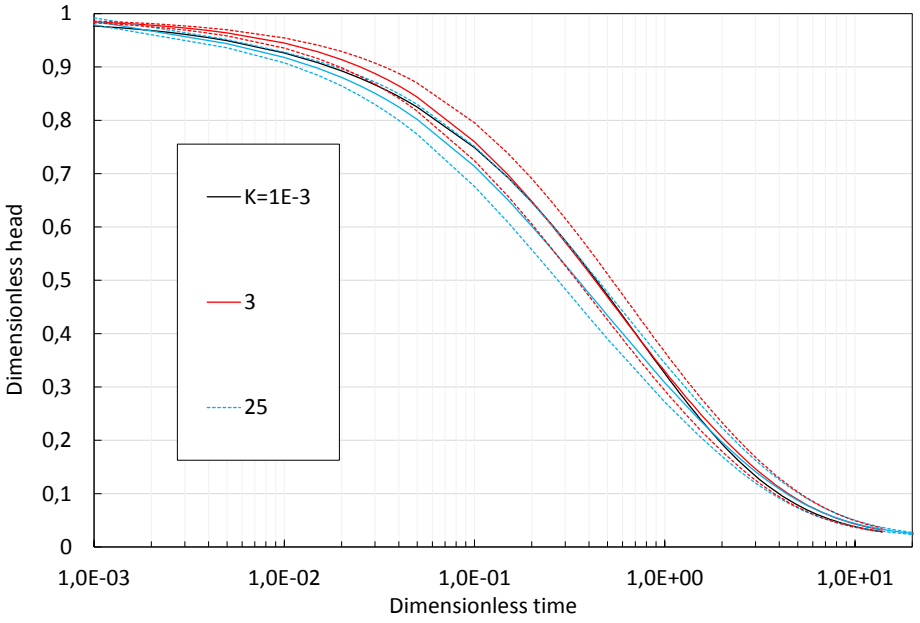

FIGURE 3.23: A comparison of the resulting drawdown curves from ensembles 3 and 25, showing the effects of coarsening the permeability field. Continuous lines represent the averaged drawdowns and dotted line the standard deviation range.

the results towards low conductivity. If the well turns out to be situated in the middle of a high conductivity zone, the drawdown will reflect a high conductivity zone at early time and then it will decrease.

3.2.3.5 Block scale dependence on the results

A last ensemble of simulations is performed to assess the convenience of the chosen cell size for the conductivity field. We use the same computational grid but we upscale the conductivity field to a block scale of $r_w/2.5$. The results are plotted in Figure 3.23. The curves obtained from the coarse fields seems to differ slightly from the finer ones at early times but then they converge at late times. This seems to indicate that if we were to refine the fields even more we would approach the homogeneous behavior curve. The range of standard deviation does not seem to change much.

TABLE 3.6: Parameters used for the three dimensional conductivity fields for spherical flow

Ensemble	$\sigma_{lnK}{}^2$	λ_x	λ_y	Block scale	Simulations
1	1	r_w	r_w	$0.2r_w$	50
2	2	r_w	r_w	$0.2r_w$	50
3	4	r_w	r_w	$0.2r_w$	50
4	2	$0.25r_w$	r_w	$0.2r_w$	50
5	2	$0.25r_w$	$2r_w$	$0.2r_w$	50

3.2.3.6 Spherical flow in heterogeneous media

The heterogeneous fields in the spherical simulations are set such that correlation exists only in horizontal direction. According to the discretization in depth, 28 different fields, all with the same geostatistical structure are assigned to each level. The effects of different values of log-variance in multi-Gaussian fields are studied and also the effects of anisotropic variograms. The different ensembles simulated are summarized in Table 3.6.

The results of the first three ensembles, as shown in Figure 3.24, indicate an increase of the interpreted permeability against the geometric average as the log-variance increases. A quite surprising result is that the range of standard deviation does not seem to be as wide as in any of the previous ensembles in radial flow. The shape of the drawdown curve presents a homogeneous behavior and thus a good match with a type curve can be obtained. From a practical point of view the problem would be that the interpreted conductivity is, for similar fields, larger than the geometric average even though a satisfactory match to a type curve is obtained.

The effects of anisotropy can be seen in Figure 3.25 where the results of the other two ensembles are plotted. Again we see that anisotropy does not change considerably the shape of the curve and that a good match is possible to obtain, but yielding a larger interpreted permeability to the geometric mean.

Interpreted conductivity in spherical flow is shown in Figure 3.26. The difference from the radial flow cases is easily noticed: while radial flow yielded quite constant interpreted values, spherical flow results in values that increase linearly with log-variance. A regression over the mean line yields the following equation

$$K^{int} = K_G\left(1 + \frac{\sigma^2_{lnK}}{2.5}\right) \tag{3.6}$$

Anisotropy ratio has also the same effect but the increase is not as sharp as with variance.

Therefore, two main issues are to be considered when slug tests yield spherical flow: first the interpreted conductivity is shown to be higher than the geometric average.

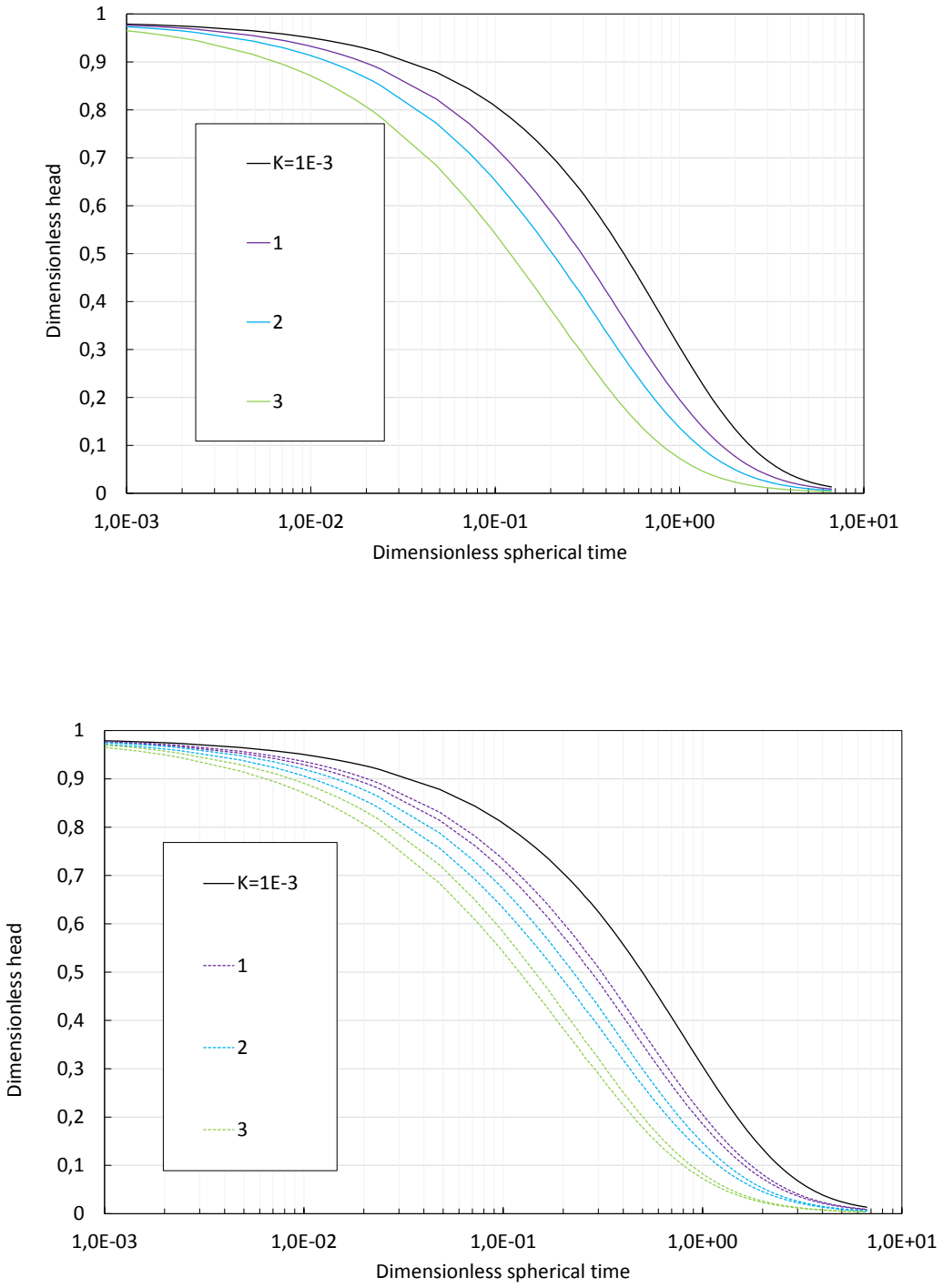

FIGURE 3.24: Resulting drawdown curves from the ensembles 1, 2 and 3 from table 3.6 in three-dimensional fields under spherical flow, showing the effects of increasing variance. Above: averaged drawdown of all simulations for each ensemble. Below: Range of standard deviation from the averaged drawdown.

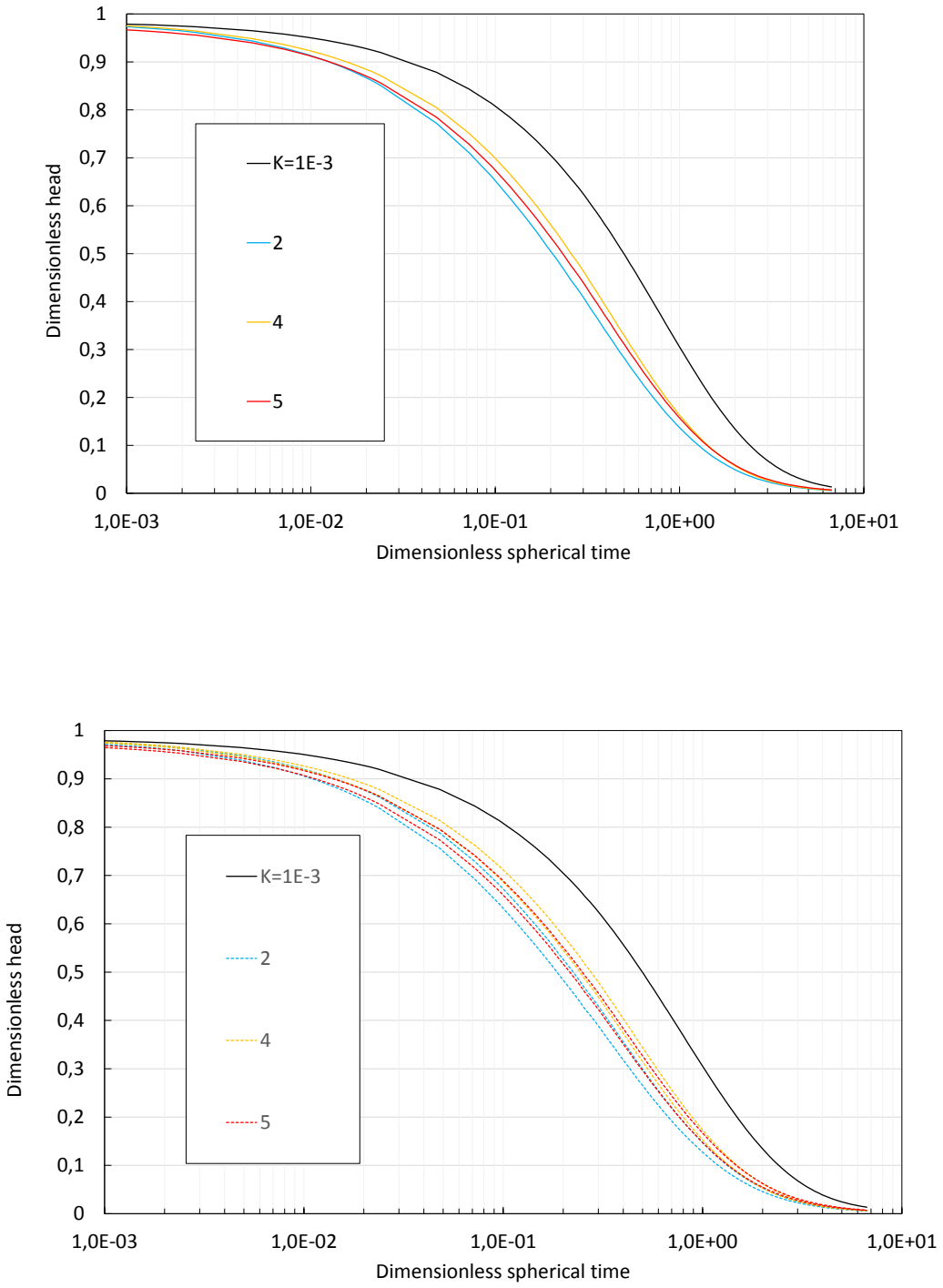

FIGURE 3.25: Resulting drawdown curves from the ensembles 2, 4 and 5 in three-dimensional fields under spherical flow with different anisotropy ratios as in 3.6. Above: averaged drawdown of all simulations for each ensemble. Below: Range of standard deviation from the averaged drawdown.

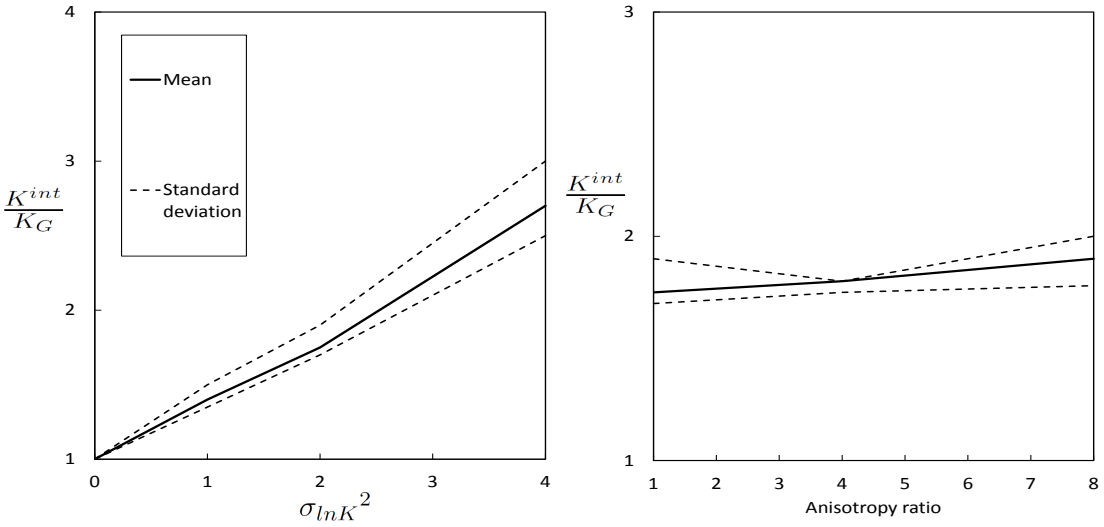

FIGURE 3.26: Left: The interpreted conductivity and the standard deviation range of slug tests yielding spherical flow in multi-Gaussian fields non correlated in depth (ensembles 1, 2 and 3). Right: Dependence of anisotropy ratio on interpreted conductivity in spherical flow. All fields have $\sigma^2_{lnK} = 2$ (ensembles 2, 4 and 5).

Second, although the volume of porous medium investigated is the same as in radial flow, the radius of investigation is smaller, and in that case the derived properties are representative of a small region.

A last consideration would be the mistake of actually matching spherical flow to radial flow. As an example consider our numerical set up of spherical flow. Figure 3.27 shows the error that would be introduced if we match our model to a radial flow type curve, despite the fact that no exact match can be obtained, as it is logical, it would result in an estimate of conductivity that would be around 3 times higher than the real

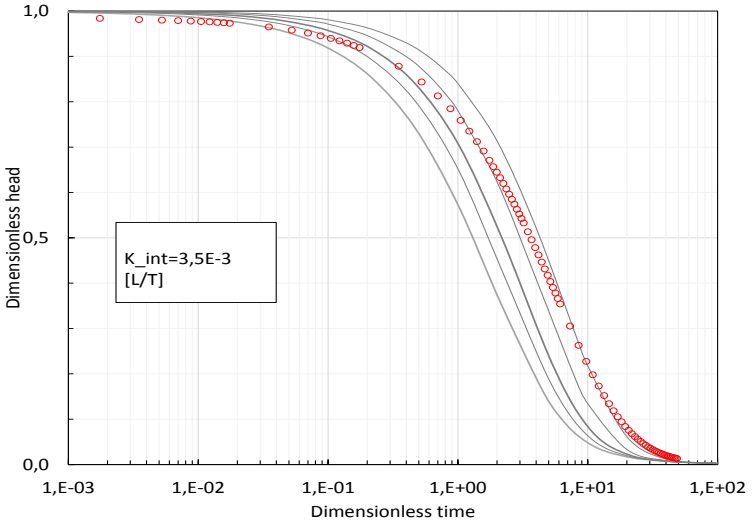

FIGURE 3.27: An example of the error which is induced when the flow dimension is miss matched. Here the real conductivity is of 1E-3 arbitrary units.

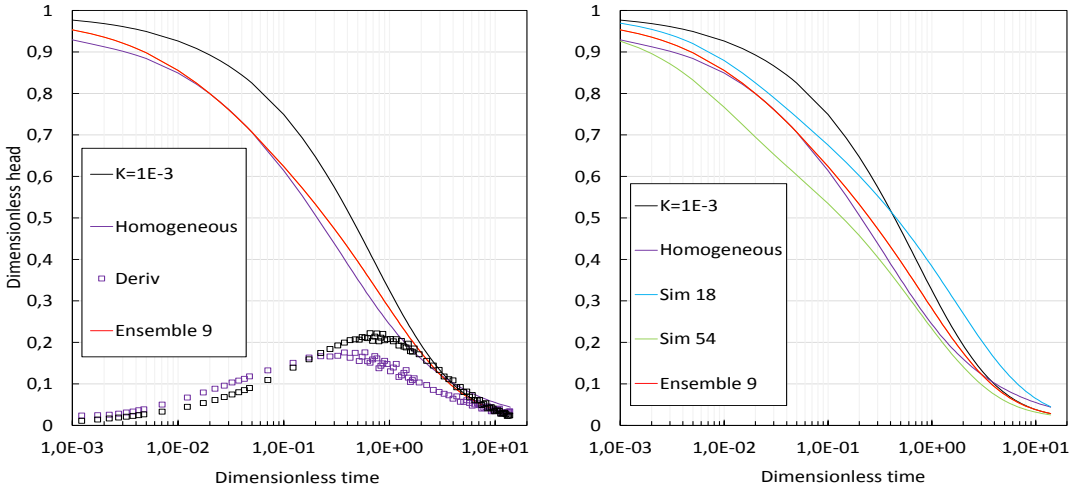

FIGURE 3.28: Drawdown curve obtained from the slug test simulated in the homogeneous anisotropic field, compared to the ensemble 9 in radial flow.

one. Hence caution must be taken and if possible before selecting a type curve, the two flow regimes should be considered to avoid this sort of mistake.

3.3 Singular fields

In the following we discuss numerical simulations in non geostatistical heterogeneous fields that could give us an extra insight into the drawdown behavior.

3.3.1 Homogeneous anisotropic formation

To compare the previous results where we simulated anisotropic fields with locally (cell scale) isotropic conductivity, we simulate a slug test in which the anisotropy ratio of the field is $K_x/K_y = 100$ being $K_x = 0.01$ (arbitrary units). The resulting curve, and its derivative, is compared to the ensemble 9 average curve and the isotropic case in Figure 3.28.

The first thing that differentiates the homogeneous case is the similarity in shape to the isotropic case unlike the statistical one. The early time similarity to the heterogeneous field could be circumstantial. Instead of starting the diversion at early time and then converge to the geometric response at late time, as those curves at Figure 3.28, it separates from it at the beginning and then it follows a relatively parallel path until for $t_D > 1.0$ starts to converge. Two "extreme" curves extracted from the Monte Carlo simulations are also compared to the homogeneous field curve. It shows that the homogeneous curve is comprised between the margins delimited by both simulations and it would come as no surprise if one of the simulations within the ensemble matches the homogeneous curve.

3.3.2 Homogeneous field with high conductivity channels

This example consists of a field of homogeneous hydraulic conductivity with vertical (parallel to the wellbore axis) channels separated by a distance of r_w parallel to each other and that have higher conductivity than the surrounding formation. The width of such channels is equal to the cell size ($0.2r_w$). The geometric mean of the field, channels included, is the same as the previous fields.

An interesting behavior of the obtained curve, as shown in Figure 3.29, lies on the fact that for early times follows that of the ensemble 9, though this could be casual. We have tried to match this behavior to one of the simulations within the ensemble but none followed such pattern.

3.4 Discussion

3.4.1 On type curve matching

Based on our numerical results we share the opinion of other authors [8, 34, 36, 41] regarding the impracticality of estimating the storage coefficient by means of slug tests exclusively. Actually our results indicate that in general it is not possible to derive this

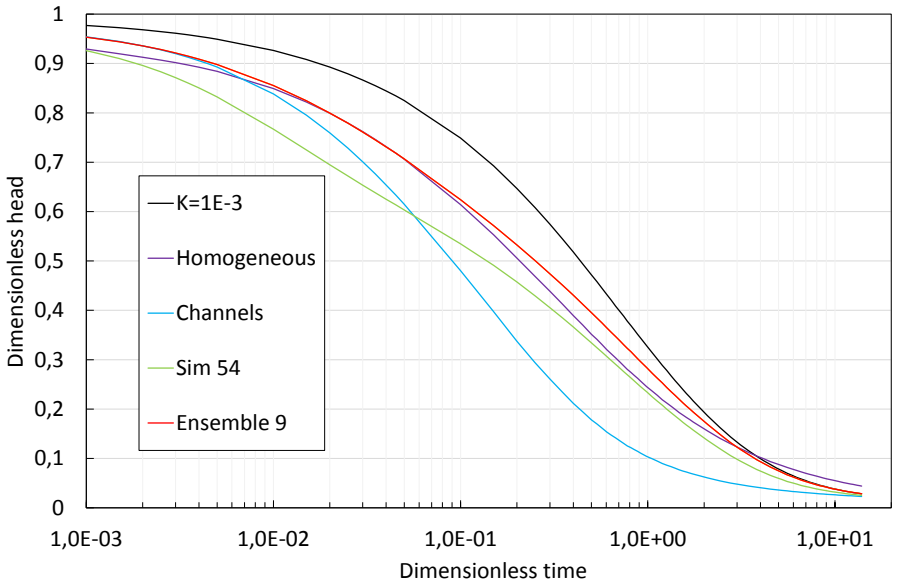

FIGURE 3.29: Drawdown curve obtained from the slug test simulated in the field of vertical channels, compared to the homogeneous anisotropic field, the ensemble 9 in radial flow and a drawdown curve that exhibited the maximum drawdown within ensemble 9.

parameter by type curve matching. Since it is the curve of the transition period the only reference to the storage value in a homogeneous formation, in heterogeneous media this curve is totally altered because of the structure and hence any reference to storage is apparently lost.

Nonetheless some of the statistical parameters have proved to yield consistent trends when they were shifted, mainly variance and its relation with anisotropy. The correlation length has a relatively unclear effect. The obtained curves from the Monte Carlo simulations can be helpful for the analysis of slug tests, as they provide a set of typical behaviors that one may encounter in heterogeneous media such as fissured rock.

Therefore, in highly heterogeneous fields, for which no analytical solutions exists, type curve matching by regression techniques seems to be not a very good idea, since any coincidence between a regression curve and the actual curve might be merely circumstantial, and from our results, only late time data and qualitative analysis can be helpful to derive a fairly representative conductivity of the formation. In the cases where homogeneous behavior is observed, it is recommended to dwell into the possibility of heterogeneity, since its effects on the interpreted conductivity can be of importance, as seen for instance in spherical flow.

3.4.2 Significance of the estimated parameters

Even though in practice slug tests may yield homogeneous behavior, as we will see for instance in Chapter four for the case of a tight fractured rock, our results show that this is not an assurance of homogeneous field. The isotropic multi-Gaussian fields under radial flow and the spherical flow simulations yielded quite homogeneous responses that would likely fit a type curve. Note that this implies estimating a conductivity that could be significantly different from the geometric average or the equivalent for parallel flow.

The support scale of the slug test is entirely dependent on the specific storage (provided that enough time has elapsed). If one wishes to determine the actual extend of the scale at which the parameter has been estimated, the flow regime developed should be taken into account, since for instance, in spherical flow the radius of investigation is smaller than in radial flow.

3.4.3 On the duration of slug tests

Our results show that heterogeneities are manifested during early and middle times on the drawdown curves. The smaller the storage coefficient the larger this period will be. After this anomalous period ceases, a straight line in a log log plot is observed which it seems to be totally independent on the structure of the medium and influenced only by the flow regime or boundary conditions. Constant rate type curves for infinite acting radial flow, which are the result of integrating the CBP curves, allow to understand this

process with the interpretation method of Cooper & Jacob [17]. Indeed transmissivity from constant rate tests can be derived with confidence only if pumping has last enough to achieve the infinite radial acting regime. Unfortunately, slug tests only reach this period after large drawdown, especially in sites with small storage. On top of that, data can be of little precision when we are measuring head perturbations smaller than 1%.

An important issue, based on this observations, arises when in practice slug test data is limited due to time constraints. This is the case for low conductivity media. If our test does not last enough to yield a straight line on a log log plot, the significance of the data will be dubious because of the large amount of different curves that can be obtained in heterogeneous media.

3.4.4 Limitations of the study

Even though we argue that storage coefficient has an important role on the results of slug tests, we have not studied its implications in our numerical models. This is a point that should be overcome in future studies.

Because we wanted to study small scale effects of permeability, lower storages would have increase exponentially computing time and would have limited the amount of results obtained in short term. The alternative would have been to use a variable grid size as in [8]. However the support scale grows exponentially as storage decreases and thus small reductions have important consequences on the required grid. This would have make the process of extracting consistent conclusions a bit complicated because of computational issues.

For instance, we have seen that correlation length has an important role on the interpreted parameters. Unfortunately the computational grid limits the efficiency of small correlation lengths. Also, for a Monte Carlo analysis is impractical to have to use several grids.

Chapter 4

A case study: El Cabril, Spain

4.1 The disposal area of El Cabril

El Cabril, located about 50 km from the city of Cordoba, Spain, is where the low and medium level radioactive waste generated in Spain is stored. It is in operation since 1992 and since then various extensions, including a separated storage site for very low level waste have been build.

Geologically speaking El Cabril is located in a quite particular site. It is situated above an anticlinal zone, where the underlying formations are metamorphic rocks, mainly gneisses and meta arkoses with a high degree of ductile deformation, with almost vertically dipping strata. The rock mass is highly fractured but with a considerably low permeability, which makes it a good candidate as a geological barrier to an eventual radionuclide escape. Fractures are present at all scales of observation, from faults to microfissures in a fractal but heterogeneous way. The stratification and fracture planes are anisotropic and generally parallel to the hydraulic gradient. This results in a regional groundwater that instead of following the direction of maximum hydraulic gradient, as in an isotropic medium, it goes perpendicular to it. A view of the geology map can be seen in Figure 4.1. To make an idea of the degree of heterogeneity, Figure 4.2 shows a photo taken at a slope excavated for the construction and operation of the Celda 29. The geological formation that forms the rock mass at the spot belongs to the so called transition gneisses. These have several inclusions of different minerals, though this is a feature present at all formations throughout the site.

Three main geological formations are present in the site: the Sierra Albarana quartzite, the Albariza schist and the Cabril formation, which is separated in four different members. The topography is quite sharp, resulting in a series of water streams that have an important role on the regional groundwater flow. In fact, because of the already mentioned flow direction, perpendicular to the gradient (both hydraulic and topographic) these water streams are the main path of water to exit the watershed.

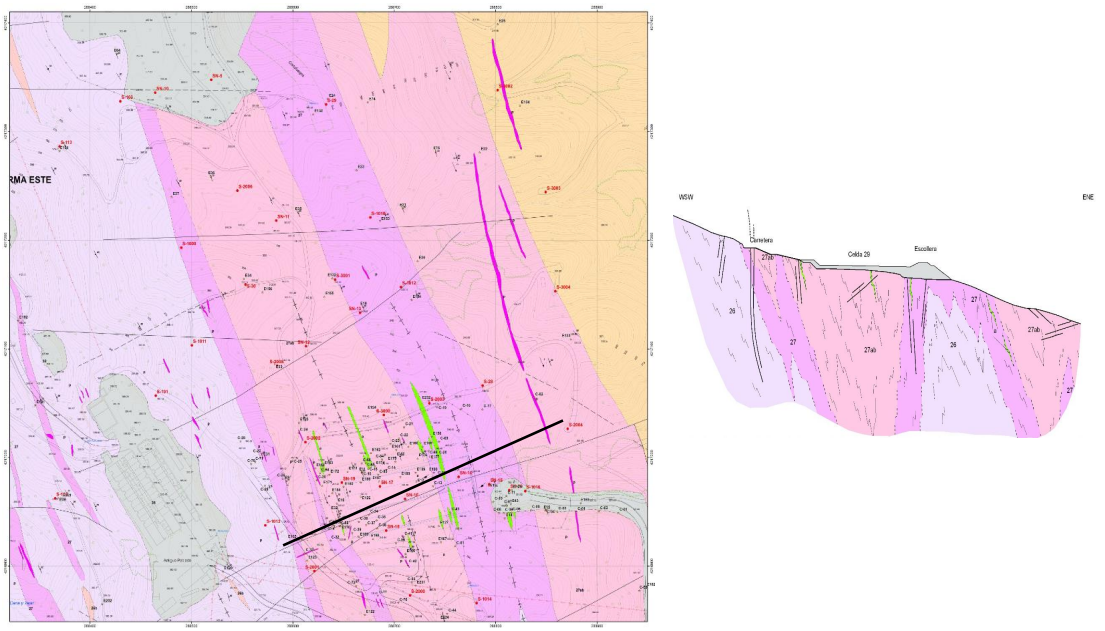

FIGURE 4.1: Geological structure of El Cabril site. Where the three main formations can be distinguished, together with the thin bands of inclusions in El Cabril formation.

Groundwater levels, measured in several piezometers throughout the site, show an important relation with precipitation records. Precipitation is highly irregular along the year, mainly concentrated in September and October. Some measurement points may increase its hydraulic level up to 4 meters after a single precipitation event. Three hydrographs, corresponding to three boreholes situated at a distance of around 50 meters within each other are represented in Figure 4.3 as an example of this heterogeneity. As a result, local hydrogeology is not only spatially heterogeneous but also temporally.

An important input in risk analysis is based on a good numerical model of the regional groundwater flow and transport. Hence a proper characterization of the hydraulic

FIGURE 4.2: A visible example of the heterogeneity and the vertical disposition of the geological facies of El Cabril. The picture is taken just from the borehole S2000 looking towards the Celda 29, which appears behind.

parameters such as hydraulic conductivity and storage coefficient is of paramount importance. In particular the numerical model of the site has been calibrated extensively over the years against a large set of data coming from the already mentioned extensive network of monitoring piezometers. Nevertheless, due to the highly heterogeneous nature of the fractured rock mass, a good match between simulations and monitored data proves to be difficult to obtain.

Needless to say, good estimates of hydraulic parameters from in-situ hydraulic tests are a crucial start for the calibration of the groundwater model. If we fail to match the parameters by back analysis to a set that is not representative of the actual one, most probably we will have high discrepancies when we try to model future scenarios or calibrating with new drilled piezometers.

It is precisely the aim of this chapter to interpret some of the slug tests that have been performed previously in El Cabril. To this end, we expect that the insight obtained from chapters two and three will be of practical use. The large amount of slug tests that have been performed at El Cabril, combined with the strong heterogeneity and anisotropy present at this site, constitutes a great example to put into field practice the previous concepts.

4.2 In situ hydraulic tests and previous analysis

4.2.1 Regional studies

Since late 1980's several hydraulic tests, namely Lugeon, pumping, pulse and slug tests, have been performed in El Cabril with the aim of improving hydrogeological description.

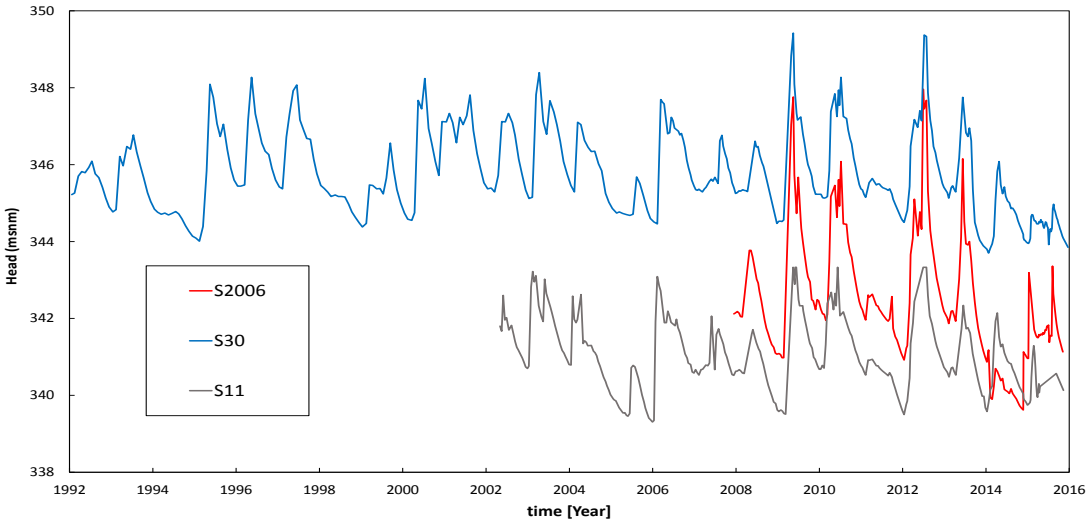

FIGURE 4.3: Three different hydrographs corresponding to three boreholes situated at a distance of 50 meters within each other, showing the spatial and temporal variability of head levels at El Cabril.

The results are mainly characterized by the dispersion of results, not only between the data from different kind of testing but also from that of different points. For a given borehole at different depths very dispersive results are obtained, the main reason being the irregular and anisotropic fractured structure.

The most affected parameters by such heterogeneity are those obtained from pulse and slug tests, this was already mentioned in the first studies where a dispersion of five orders of magnitude in interpreted transmissivity was reported [55]. It is worth to mention that tested intervals reached depths of 300 meters and interpreted values turned out to be in general independent of depth, though dispersion of results is higher in shallow intervals. Values between $K^{int} = 10^{-4}m/s$ and $10^{-9}m/s$ were interpreted from these tests.

Interpreted transmissivities by slug and pulse tests did not correlate very well with those obtained by the use of Lugeon test. Different support scales of both tests, in conjunction with the strong heterogeneity and anisotropy, could be an explanation of this phenomena. Conversely, good correlation coefficients were obtained when the Lugeon values were correlated to the geological formation at which these were obtained, especially when the intervals tested where separated in two main populations, based on the degree of meteorization. This is a very important fact that we will keep in mind. The Albariza formation thus, proved to be lest permeable of all the region, with interpreted transmissivities of the order of $T^{int} = 10^{-8}m^2/s$ and intervals with zero injection rate. On the contrary, El Cabril formation yielded the highest transmissivity values, reaching $T^{int} = 10^{-6}m^2/s$. It is highlighted, however, that the results of Lugeon tests were very dependent on the company that performed the tests and therefore, the results should be viewed with skepticism, being only relevant of the order of magnitude [55].

A pumping interference test performed at El Cabril was one of the cases that brought Meier et al. to the already mentioned paper [37] in which they investigated Jacob's method for heterogeneous fields. They reported the results obtained at the surrounding boreholes of the S33, which is situated on the Cabril formation at the intersection with meta arkoses, showing that transmissivities were very similar, ranging from $T^{int} = 0.38$ to $0.52m^2/d$.

4.2.2 Studies on the very low disposal area

Prior to the construction of the very low disposal facilities, several hydraulic tests were performed to improve on hydrogeological description of the local area. These started during early 2000's, specifically during the years 2002, 2003, 2005, 2009 and 2012 [2–4].

Three constant rate pumping tests of short term plus three of medium term were performed in 2002 on the surroundings of the medium level waste facilities. Interpretation of such tests yielded transmissivity values quite constant all throughout the tested

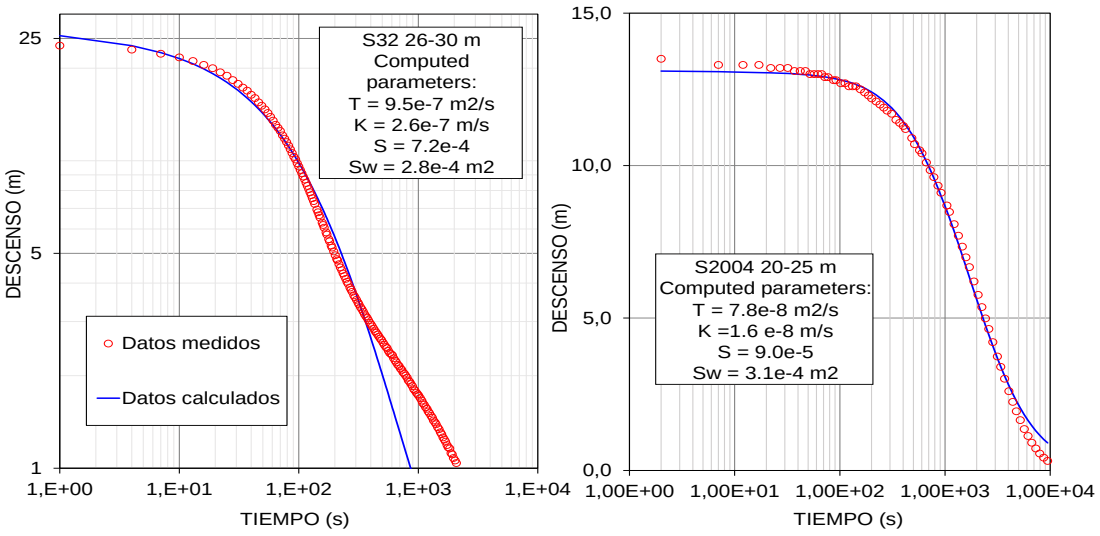

FIGURE 4.4: Two examples of interpretation plots obtained by back analysis using the MariaJ-IV code. The homogeneous response assumed by the model presents issues in heterogeneous media.

wells of $T^{int} = 10^{-6} m^2/s$. Monitored points where drawdown was observed allowed to interfere a storativity value of around $S^{int} = 10^{-4}[-]$.

Several slug tests were performed during 2003 in more than 20 boreholes. These were interpreted by back analysis using the code MariaJ [14], which uses a general flow model for the regression. Because of the difficulty in determining the storage of the rock mass, the analysis was done by assuming a known arbitrary storage. One of the main conclusions drawn from chapter three was precisely the difficulty of matching a certain storage in heterogeneous conductivity fields, and this is the case in El Cabril. Therefore, we think that the interpretation by back analysis, which assumes an isotropic homogeneous formation, does not provide a reliable mean to infer the hydraulic parameters from such tests.

Two examples of misleading regression curves are shown in Figure 4.4. The main reason to believe that they are not representative of the medium is that they do not match the response at late time, which based on the results of chapter three, is the only time period not affected by the heterogeneities at small scale. Furthermore, fixing the storage coefficient, makes the interpretation highly dependent on such hypothesis, especially knowing that conductivity is strongly coupled with this coefficient as shown in [8].

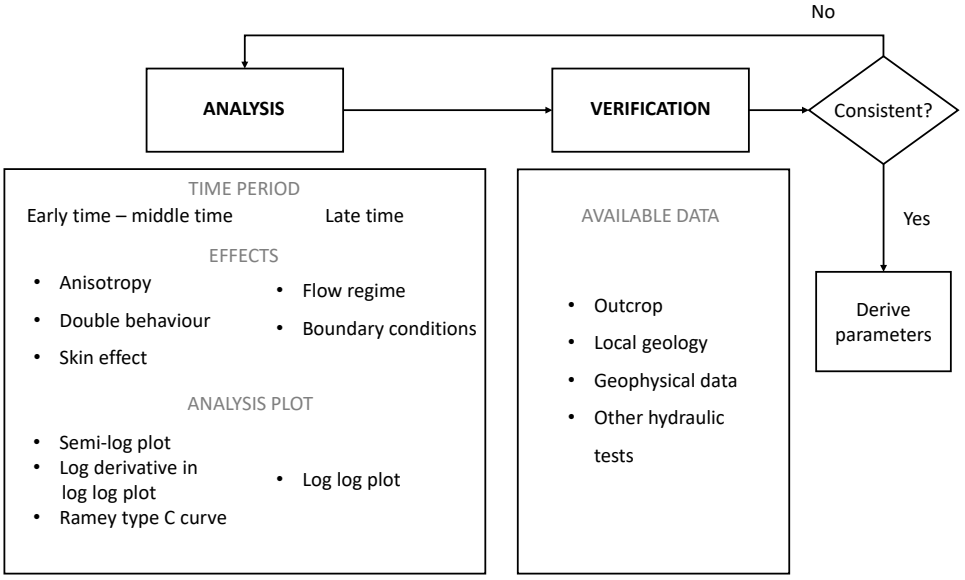

FIGURE 4.5: General workflow of the procedure followed for the interpretation of slug tests.

4.3 Re-interpretation of slug tests

4.3.1 Methodology

The interpretation procedure that has been followed is based on the one proposed by Gringarten [27], adapted for slug tests after the information gathered in chapter two and after the conclusions drawn from chapter three. A schematic view of this procedure is shown in Figure 4.5.

The slug tests will be interpreted using type curve match at different time periods, mainly for those tests which yield anomalous responses. First the derivative of the drawdown with respect to the logarithm of time is computed. This, as already mentioned in chapter two, is helpful when trying to fit the type curve of interest. Since field data is usually noisy the straight computation of the derivative gives highly perturbed results. Different derivation schemes exists to smooth the results and avoid the noise [46, 53]. Here the derivative is computed as

$$\left.\frac{\partial h_D}{\partial \ln t}\right|_{t_1} = \left|\frac{h_D(t_2) - h_D(t_0)}{\ln(t_2/t_0)}\right| \tag{4.1}$$

where $t_1 = \sqrt{t_0 t_2}$ and t_0 and t_2 are separated by at least 0.3 log cycles i.e. $\log(t_2/t_0) > 0.3$.

The data is then plotted in three different plots: head vs log time, log head vs time and log head vs log time. The fist plot is used to match the typical solutions existent. The second plot is used to assess the feasibility of considering steady state

i.e. the application of Hvorslev and Bouwer& Rice techniques. The last one is useful to identify flow regimes and, as seen in chapter three, gives information on the averaged conductivity, thus is used in parallel with the first plot.

When a suitable type curve has been identified, the plausibility of flow regime is checked against geological information such as boreholes, intersecting fractures and piezometric levels before the hydraulic test. For instance if two dimensional regime is suspected from the drawdown curve, a set of horizontal fractures could be evidence of such flow characteristics.

The type curves used are the CBP model for two dimensional flow and the spherical solution from Karasaki et al [34]. An important remark here is that the curve match will be done in a qualitative manner, such that storage curves will be approximated to the logarithm base 10.

We will bear in mind the results and curves obtained in chapter three to draw conclusions. Given the uncertainty of the real representative parameters from single well testing noticed in previous chapters and studies, from the set of interpreted parameters we will take the relevant statistics. The data for this purpose will be divided in three main groups, each corresponding to its geological formation. Previous field studies evidence correlation in such cases and so we expect [55]. Provided that stationarity holds, values of mean and variance could provide additional information into the structure of the formation and furthermore, we could invoque the relations between variance and interpreted conductivity with relation to the geometric average, which have been obtained numerically in the previous chapter.

Although support volume of slug test seems to be properly defined, it should be noticed that the actual shape of its extend is highly dependent on anisotropy of the surrounding formation and, on top of that a prematurely terminated test, lets say with $t < t_D = 10$ would complicate a precise determination of the actual extend of the support volume. Most important, the storage coefficient governs such volume and storage coefficient is not reliable when obtained from slug tests even in homogeneous responses. Given that we have obtained homogeneous responses only in relatively isotropic fields with the exception of spherical flow regimes, from the aspect of the drawdown curve one could decide whether it is feasible to make assumptions on the support volume, always assuming a representative storage coefficient.

Originally, the geology of El Cabril was divided in three different members, namely C, D and E. Since the 2009 studies this was redefined into the names according to the rock mass that composes each formation [19]. Because we are in possession of such valuable information it is natural that we also try to separate our interpreted parameters into the same divisions. Specifically three different materials will be considered, in principle without distinction regarding the fracture degree.

Therefore we divide the work in two phases: interpretation and integration of results. If properly done, and if our assumptions are correct, the results should yield similarities with those that one would obtain using other hydraulic testing such as pumping tests, and should provide a solid base for a conceptual model ready to incorporate geostatistical data.

In the following sections the results of the slug tests for each formation are discussed. The location of the slugs analyzed is shown in Figure 4.6. In Appendix A we present the fits that have been used to derive our parameters of hydraulic conductivity K^{int}. In those cases in which an anomalous behavior (neither radial nor spherical flow) is obtained the drawdown curve is also presented in order to justify the analysis.

4.3.2 Mica schistes of Albariza

From all boreholes in which slug tests were performed (see Figure 4.6) four, namely S3002, S3003, S3004 and S3005, were drilled in 2012 with the aim of improve the description of the schistes of sierra Albariza. These are situated eastwards of the VLLW disposal site at the intersection with the gneisses of El Cabril formation.

An outcrop example from the borehole S3003 in the interval of 12 to 15 meters depth is shown in Figure 4.7. The two main features of it, which can be extended all around El Cabril, are the density of fractures and the heterogeneity regarding its orientation. On top of that most of the outcrops present inclusions of different minerals such as biotite and pegmatite. Some of the intervals that consist of a relatively thick intrusion of a rock different than the meta schistes, generally result in a slug test that yields a remarkable double permeability drawdown curve. As an example we show in Figure 4.8 two slug tests that fairly match a radial curve during the early times but at middle time start to diverge. Although it seems that this behavior should come when the head has encountered a low permeability boundary. Both curves present a roughly similar slope of transition between this homogeneous period and a, not measured, interval representative of both media.

What complicates matters is that the interpreted conductivities in both cases are within the order of magnitude of the other intervals. Therefore if we assume that this is only representative of the most permeable medium, this means that the inclusion is the lest permeable. Another working assumption is to think of the interval as two different set of fractures or even as a double porosity medium. Indeed although the obtained curves in chapter three are not very similar, in the literature we can find examples such as that of Grader and Ramey [26] of analytical solutions for double porosity reservoirs. These curves are similar to those in Figure 4.8.

Table 4.1 summarizes the interpreted values, separating those obtained under the assumption of radial and spherical flow. Without distinguishing those intervals at which

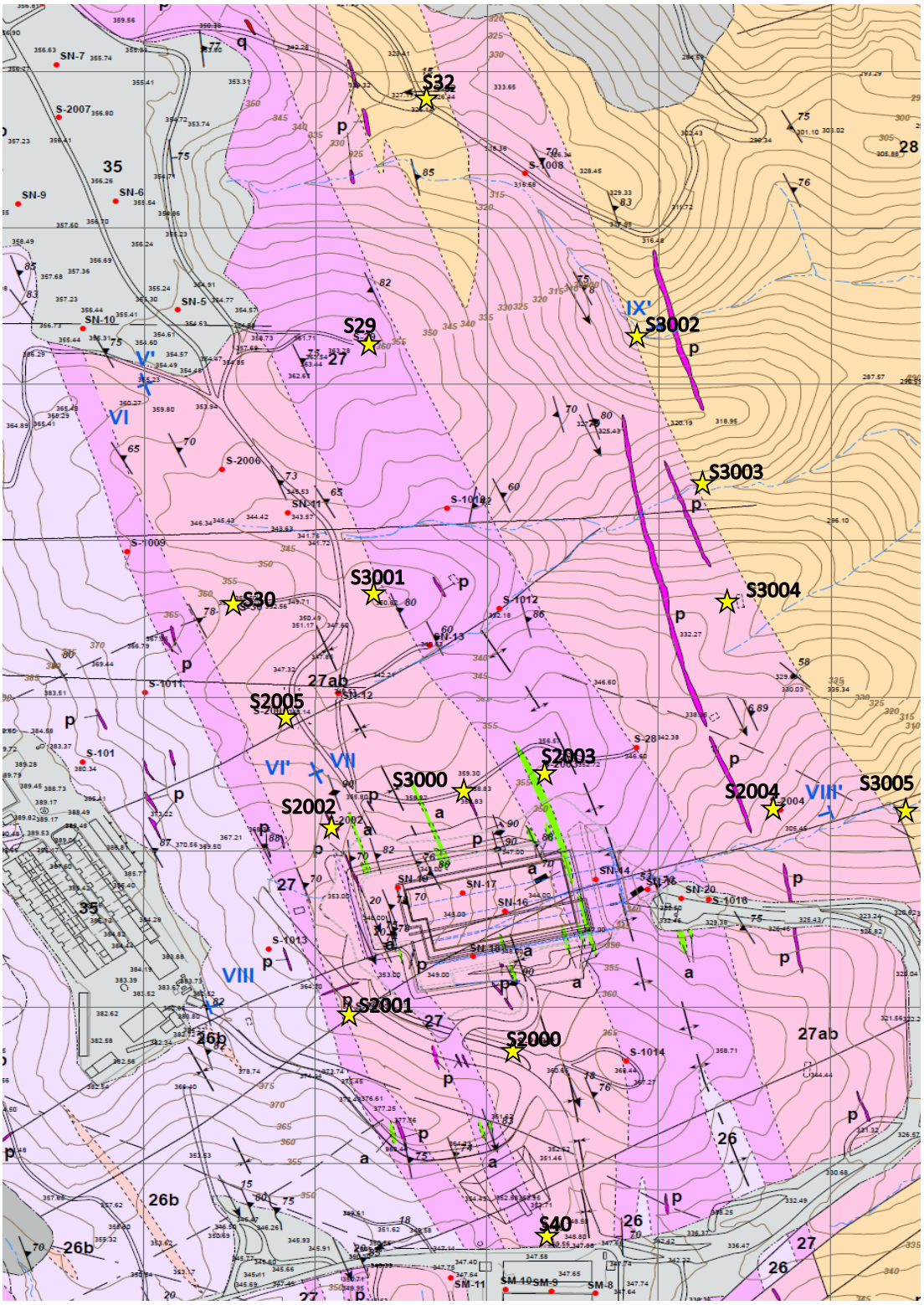

FIGURE 4.6: Geological location of the boreholes in which slug tests have been performed.

FIGURE 4.7: Left: Mica schistes outcrop from 12 to 15 meters depth, obtained from the borehole S3002 situated at the intersection between the Cabril biotitic gneisses and the Albariza mica schistes. Although not in the picture, the borehole presented several inclusions of biotite. Right: Interval between 22.6 to 25.55 meters depth from the borehole S3004.

the rock mass is less fractured, conductivities are relatively similar. Although the value of 1.3×10^{-6} m/s is higher by one order of magnitude, we should bear in mind that conductivities obtained under spherical and radial flow are significantly different in a heterogeneous media, which is, without a shadow of a doubt, the case here (see Figures 3.6 and 3.21 for the effects of variance in both radial and spherical flow).

Homogeneous behavior is obtained despite the fact that some of the outcrops reveal a preferential orientation of fractures. This challenges the results obtained in chapter 3, although the exact reason why, is not clear.

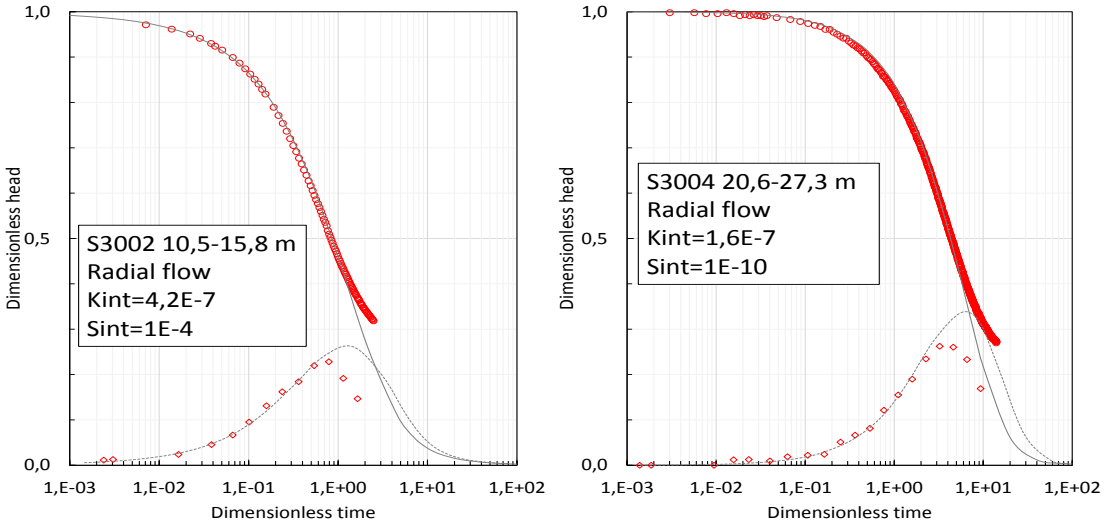

FIGURE 4.8: Examples of double permeability behavior in the Albariza schistes.

TABLE 4.1: Interpretation for the Albariza mica schistes

Borehole	$z_1[m]$	$z_2[m]$	K^{int} [m/sec]	Flow regime
S3002	5.5	10.8	1.6×10^{-7}	Radial
	10.5	15.8	1.6×10^{-8}	Radial
	16	21.4	1.3×10^{-6}	Spherical
S3003	17.5	22.8	1.8×10^{-7}	Radial
	22.5	27.3	2.8×10^{-9}	Radial
	27	32.3	3.2×10^{-9}	Radial
S3004	20.6	27.3	6.0×10^{-9}	Radial
	27	32.3	1.0×10^{-7}	Spherical
	32	37.3	1.9×10^{-8}	Radial
S3005	16.5	20.8	1.1×10^{-7}	Radial
	18.2	22.5	4.1×10^{-8}	Radial

4.3.3 Transition gneisses of El Cabril

The transition between the facies of Albariza and El Cabril consists of a series of migmatic gneisses, called the transition gneisses which have inclusions of several different minerals. Boreholes drilled at the surface of this formation are the S3000, S2001, S2002, S2004, S2005 and the S30. Furthermore at the intersections with the meta arkoses the S2003 in depth is also in contact with this formation and slug tests are available.

The conductivity values obtained in this formation are synthetized in Table 4.2. Such values are remarkably consistent for all the intervals, being of arround 10^{-7} m/s. The exception is the S30 which presents interpreted conductivities two orders of magnitude higher than the rest. This, toghether with the fact that data was well fitted to type curves gives confidence on the interpretation.

FIGURE 4.9: Left: Outcrop from the borehole S2001, interval from 15.4 to 17.8 meters depth, showing the plausibility of the double behavior assumption. Right: interval from 36 to 38.4 meters depth showing that the rock mass is preferentially fractured horizontally and that the anomalous behavior should come from a discrepancy between the transmissivities of each fracture.

TABLE 4.2: Interpretation for the Cabril transition gneises

Borehole	$z_1[m]$	$z_2[m]$	K^{int} [m/sec]	Flow regime
S2001	14.5	19.9	(1) 1.0×10^{-5}	Radial
	14.5	19.9	(2) 3.6×10^{-7}	Radial
	26.5	30.9	(1) 2.8×10^{-6}	Radial
	26.5	30.9	(2) 3.6×10^{-7}	Radial
	33.2	38.2	2.4×10^{-7}	Radial
S2002	20.5	25.3	1.6×10^{-7}	Spherical
	25.5	30.3	3.3×10^{-7}	Spherical
	35	40	1.3×10^{-7}	Radial
S2004	16.5	21.5	2.4×10^{-7}	Spherical
	20.5	25.4	1.9×10^{-7}	Spherical
	28	31	7.5×10^{-7}	Spherical
S2005	20.5	25.4	1.6×10^{-7}	Spherical
	26	30.9	5.6×10^{-7}	Radial
	33	38	6.0×10^{-8}	Spherical
S30	18	23	1.4×10^{-5}	Spherical
	23	28	4.1×10^{-6}	Spherical
S3000	22	27	3.7×10^{-8}	Radial
	27	32	1.8×10^{-6}	Spherical
	32	37	1.7×10^{-7}	Spherical
S3001	14	18.8	1.1×10^{-7}	Radial
	21.5	26.8	9.4×10^{-7}	Radial
S32	26	30	1.1×10^{-6}	Radial

Most of the intervals that resulted in homogeneous drawdown curves showed spherical flow regime. Radial flow is often combined with a strong indication of double medium, as it is observed for instance in the borehole S2001. The match in this case for the high permeability zone is achieved by fitting the derivative curve to the type curve, both for intervals 14 to 19 and 16 to 31, and justifies by itself the computation of the derivative plot. The inclusions of different minerals, that causes double porosity curves, have a thickness of 1 meter in the first interval and 50 cm in the second. The conductivity estimates were done by considering the whole interval of 5 meters in both cases, which reduces the representativeness of the values. These were of approximately one order of magnitude higher. It is interesting to note that both curves, from intervals 14.5 to 26.5 meters, did converge towards the same asymptote with a conductivity value of 3.6×10^{-7} m/s, this is shown in Figure 4.10 which represents the raw data obtained at these intervals.

The other non-homogeneous curves do not provide enough information to derive two permeability values. This is especially the case in the S32, which has a curve that presents a satisfactory match with the type curve of radial flow until it starts to diverge at $t_D = 20$, since this is a relatively advanced time compared to the other bi-modal

curves, and because we do not have data that justifies a change of permeability, we cannot distinguish it from a boundary condition.

Another interesting behavior is that of the interval between 21.5 and 26.8 meters depth of the borehole S3001, whose curve fairly follows a storage of 10^{-9} at the beginning and then at $t_D = 3$ starts to decrease until it reaches the curve of a storage 10^{-4}. Although it is true that at this depth exists an inclusion of a thin layer of biotite, this would cause a change of conductivity in an analogous manner as in the S2001 and thus is not a good conjecture. A priori we do not have enough information to explain this behavior, although there are some possible explanations. First a skin effect could result in a similar curve, although it seems unlikely that the estimated conductivity would be biased towards a much higher value from the other estimates of the formation. The other possibility could be a hydro-mechanical interaction, but the pressures at which slug tests operates are unlikely to alter significantly the test at a depth of 25 meters. On top of that, it looks as though this is a behavior more related to the geological conditions. Recall that the S3001 is drilled at the frontier with a meta arkoses layer and that precisely at this formation, the same behavior was obtained for most of the tests, especially at the S40, and therefore whatever the cause of this behavior, is closely related to the material.

Spherical flow was the typical regime obtained in this formation, indicating a considerable density of fractures in vertical direction. It is worth seeing that despite the different dimensionality of flow, conductivity estimates are almost independent of it, while in a heterogeneous media we would expect that estimates from spherical flow would be higher in the average. An exception is the S30, showing a conductivity higher than 10^{-5} m/s, a value that under radial flow was only obtained for the high permeability inclusion in the first interval of the S2001. It is interesting also the fact that the

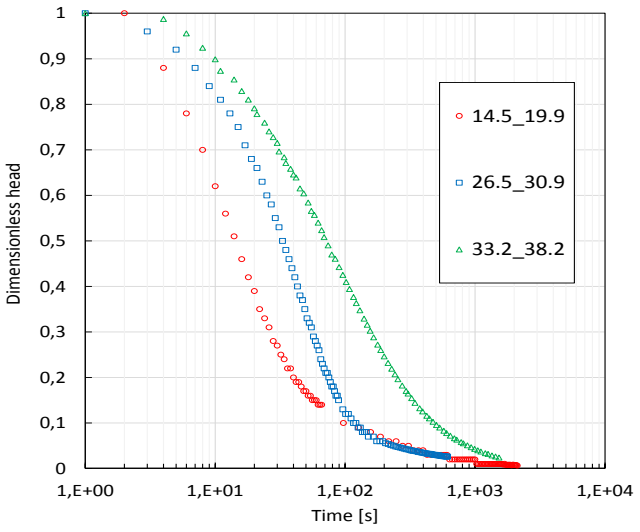

FIGURE 4.10: Measured data from the three intervals of the S2001.

estimates do not seem to be related to the depth at which these were obtained. This has been already mentioned in most field reports e.g. [55].

4.3.4 Meta arkoses of El Cabril

The transition gneisses at a local scale are alternated with feldespatic gneisses with a yellowish color. These are the so called meta arkoses of El Cabril and are present in a relatively thin layers, around 20 meters thickness with an almost vertical dip. They present a preferential fracture direction also in vertical.

Although few boreholes are present in which slug tests have been performed, these contain data from the deepest intervals in which these have been realized. Therefore, we have information on 12 intervals with a wide range of depths. In figure 4.6 we can situate these boreholes that are the S29, S40 and the S2003. In addition some boreholes already mentioned in the previous section are dilled near to this formation and, they could give related information on the interaction between the gneisses of transition and the meta arkoses, in particular the S3001, which presented a similar behavior to that of some tests that are going to be discussed herein. The results of type curve match are summarized in Table 4.3.

From our interpretation, this formation yielded the highest average of conductivities of all three examined. It is also in this formation that most of the slug tests resulted in anomalous curves. Anomalous behavior is essentially in the form of a "double type curve" match in radial flow with a single conductivity value (unlike for instance the S2001).

This is the case for intervals from 25 to 44 meters depth of the S40. Conductivity estimates are similar for estimations form 20 to 30 meters depth, varying around 2×10^{-7} m/s. In addition, the three curves corresponding to the interval between 25 to 44 meters, behave quite similarly, reaching the second type curve at values of dimensionless head

FIGURE 4.11: Outcrop from the borehole S2003. Left: interval from 26.4 to 28.3 meters depth, showing the plausibility of the anisotropy assumption. Right: interval from 33.6 to 36 meters depth showing the inclusion that may be responsible for the double permeability behavior

TABLE 4.3: Interpretation for the meta arkoses of El Cabril

Borehole	$z_1[m]$	$z_2[m]$	K^{int} [m/sec]	Flow regime
S40	20	25	7.5×10^{-6}	Spherical
	25	30	7.5×10^{-6}	Radial
	30	35	8.2×10^{-7}	Radial
	34	39	9.0×10^{-7}	Radial
	39	44	$(1)7.5 \times 10^{-7}$	Radial
	39	44	$(2)1.1 \times 10^{-7}$	Radial
S2003	26.4	31.3	2.4×10^{-7}	Radial
	30	34.8	1.7×10^{-6}	Spherical
S29	30	35	4.5×10^{-7}	Radial
	35	40	1.1×10^{-7}	Spherical
	44	49	2.5×10^{-6}	Spherical
	53	58	2.5×10^{-6}	Spherical
	58	63	2.2×10^{-6}	Spherical

of around 0.02. Exceptionally, two different matches were possible for the last interval between 39 to 44 meters depth, the first for mid times and the second yielding a fairly slope of 1 to 1 in a log log plot, thus indicating radial flow. We believe that this is an indication of a stationary structure, though it is that very structure the one that proves to be uncertain since we have no reasonable conjecture that can be applied based on the available information, besides the fact that flow is basically two dimensional except for the shallow interval. No data from the outcrop is available for that borehole.

If we observe the location of the S40 we can also assume that the double match is a consequence of its situation, just in between of two intersections with the gneisses of transition. It is very likely, given the vertical structure of the site, that this is the case for the depths at which slug tests have been performed. Therefore the curves obtained could be the result of the interaction between the meta arkoses and the transition gneisses, although if we were to accept this hypothesis we would have to be keen regarding a higher permeability for the gneisses than for the meta arkoses, which from our general results would be anomalous.

The results form the two intervals at the S2003 proved to be very interesting. From 26.4 to 31.3 meters depth the drawdown curve does not follow the usual first period of well bore storage in which the drawdown is relatively slow, but it follows a trajectory that remains to those obtained in chapter three for anisotropic fields of conductivity. It follows that period a noisy straight line with a slope in a log log plot of 1 to 1 indicating radial flow and a match that allows to derive a value of conductivity which seems to be consistent with the other tests. The other interval presented a double permeability behavior but in that case it does not allow a good match during early times to derive a set of two permeabilities. Furthermore late time data is also noisy and, although it

was matched to a spherical flow curve, does not provide confidence on it, and instead of spherical flow the late time data could indicate the presence of a constant head boundary as shown in [34].

The slug performed at the interval between 30 and 35 meters depth at the S29 also presented the same behavior of double type curve with an estimate of conductivity fairly similar to those of the S40. The remaining intervals, up to 63 meters depth, yielded spherical flow regime, the most interesting being that of the interval between 44 to 49 meters depth, which resulted in a double permeability curve that, even surprisingly, for both early and late time matches the same type curve, adding another mystery in the dynamics of the slug test. We could try to explain that by recalling that spherical type curves are strongly similar for small storage coefficients. It is therefore possible that the corresponding type curve for late time is not exactly the same as that for early time. Unfortunately data precision at this levels is probably not good enough to distinguish one curve from another and the derivative curve has lost all information (from our point of view) once the transition period between the two permeability modes starts. Nevertheless the estimated conductivity should be quite precise.

4.4 Synthesis and comparison with previous results

In general the division between geological formations proves to yield a consistent trend in the resulting drawdown curves, and resulting in similar estimates of conductivity for each zone. It is worth to remark that the "double type curve" behavior has been obtained exclusively for the meta arkoses (with the exception of the S3001). The transition gneisses resulted in most intervals on spherical flow showing a considerable importance of vertical conductivity in this formation.

In Figure 4.12 we show an histogram of the obtained conductivities. This shows clearly that the least permeable formation is the Albariza, as already mentioned in early reports [55] and that the most permeable are the meta arkoses of El Cabril. The transition gneisses as their name indicates are in the middle between the Albariza schistes and the meta arkoses. Since we have obtained double permeability behavior in some of the tests, we expect that for a higher number of tests we would obtain an histogram showing a bi modal distribution, especially for the gneisses of El Cabril as an effect of the several thin inclusions. Unfortunately our data is not enough to yield significant statistical parameters, but it shows a typical trend of log normal distribution of conductivities. On top of that, given the already mentioned similar behavior of the curves, the assumption of stationarity could be met for each different formation.

The double permeability behavior that has been obtained from some of the tests could be an effect of the fractal geometry of the fracture network observed at El Cabril. For this cases it is certainly better a double porosity model such as that presented in

[26]. It could be the case that if the slug test could sample a larger volume at a higher precision for small drawdowns (of the order of less than 10^{-4} we probably would obtain even triple behavior.

The interpretation that we have done here has yielded quite different results from the first analysis that were performed. Figure 4.13 shows the dispersion between the estimates of previous field reports [2–4] over the same tests interpreted herein. The interpretation, as already mentioned, was done by using the code MariaJ-IV [14], we strongly believe that the adjusted curves computed by the software are not representative of the actual hydrodynamic behavior of the rock mass. Although there exists a clear trend between both studies, our interpretation results in a significant increase of conductivity of around one order of magnitude, which is quite significant.

The calibration code relies on a generalized radial flow model, developed by Barker [6]. Nevertheless we note that the expression that he derived for slug tests it does not seem to be adequate and it fails to represent the actual behavior of the slug test. It rather seems that this solution is only valid for the Pulse test, which is a particular class of a slug test in which the water stored at the wellbore is pressurized and the evolving pressure is monitored [11]. This is usually used in the cases for which slug test would need too much time to yield significant drawdown.

We show in Figures 4.14 and 4.15 a comparison between our curve match and the adjustment achieved by the MariaJ-IV in previous analysis. Figure 4.14 represents two examples of homogeneous behavior observed in our interpretations, it is seen that neither for radial flow nor for spherical flow the adjustment is as good as it is by using the standard solutions from literature. Heterogeneous behavior, such as that shown in the S2001 is more difficult to assess, as depicted in Figure 4.15. In that case we benefit

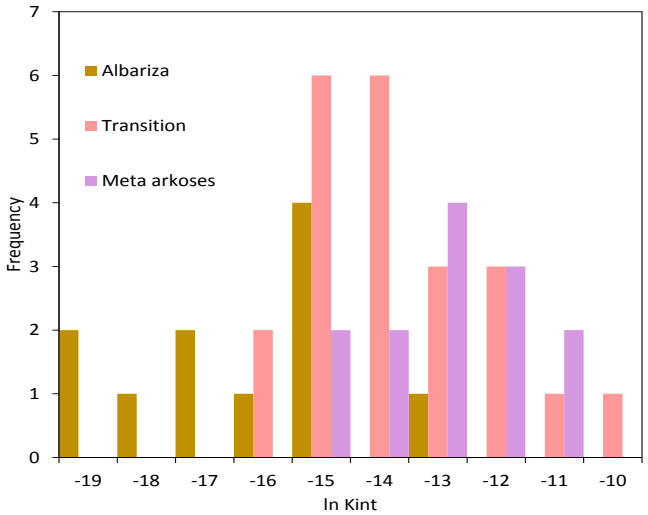

FIGURE 4.12: Histogram of the natural logarithm of interpreted hydraulic conductivities.

from our observations of the results from the Monte Carlo simulations which proved that although the field is heterogeneous, a late time approximation in a log log slope will yield a value of conductivity more or less approximated to the geometric mean. Furthermore, in some cases it is possible to infer two values of conductivities using a match to the first period curve as it is the case for the S2001. The curve derived in that case by the regression code adjusts the first period and thus one would think that the value is representative of a first mode of permeability. However we must note that this was achieved by reducing the wellbore storage. Despite the fact that it is true that low wellbore storage values results in a significant drop at early times, the same happens for double permeability systems and also because of heterogeneities, and therefore the derived parameters using this assumption must be viewed with sceptism.

All of the above does not exempt our analysis from being unbiased. Indeed from our Monte Carlo simulations we have concluded that slug test estimates in heterogeneous media are mostly biased towards the high permeability values, especially for spherical flow and as long as skin effect is not present and thus fracture connectivity exists. Similar results where obtained already by Barker & Black [7] who derived an analytical solution for a slug test that intercepts various horizontal fractures of different conductivities, showing that the equivalent conductivity in these cases is the arithmetic mean of the fracture system. Since skin effect could only be the case for some tests at the meta arkoses, and still these yielded the highest transmissivity values, we believe that our interpretation is representative of the high conductivity fractures.

Anisotropy is a well known feature of the site. Unfortunately from single well testing it is not possible to estimate the principal directions of hydraulic conductivity. An assumption on anisotropy must be made as well for the determination of the shape of

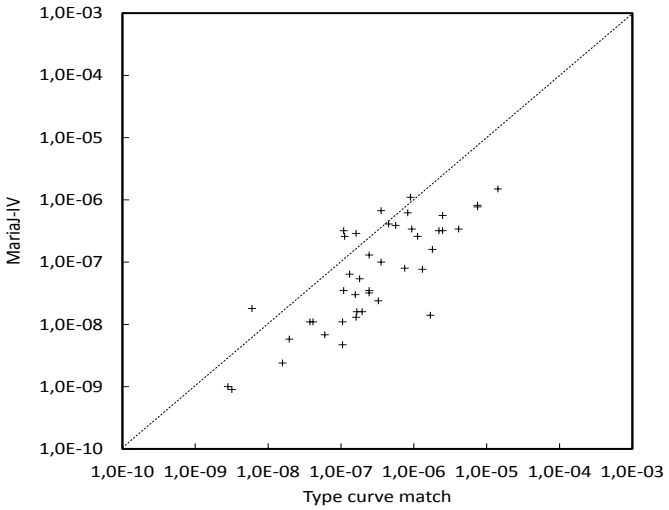

FIGURE 4.13: Comparison between estimated values by the calibration code MariaJ-IV and the estimates by type curve match in the present work

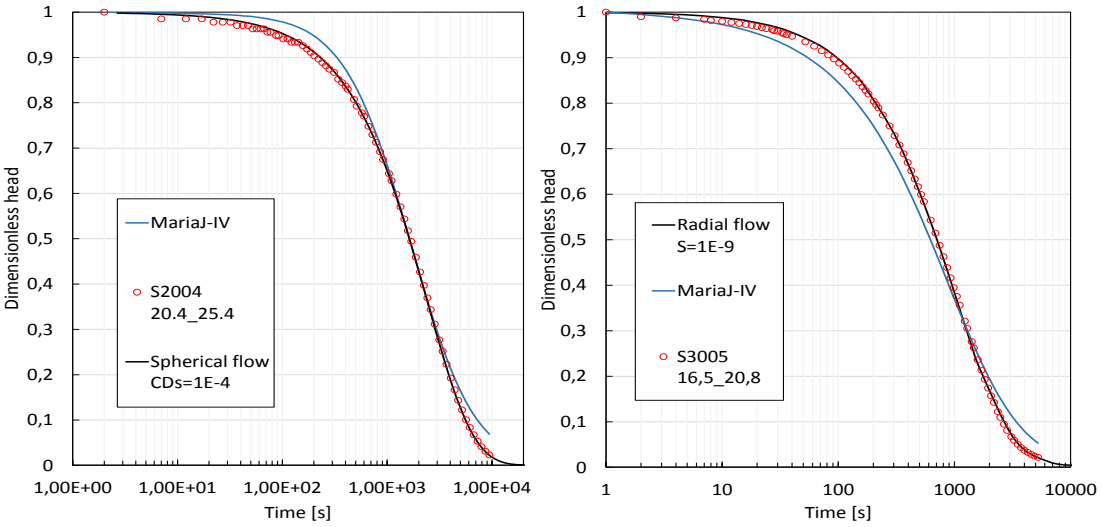

FIGURE 4.14: Adjustment to the drawdown curve by using the MariaJ-IV and type curve match in homogeneous responses. Left: Radial flow. Right: Spherical flow.

support volume. The fractured rock mass of the site has yielded low values of storativity which translates into a relatively large volume of sampled media. If we assume a storativity of $S = 10^{-6}$ which seems to be a reasonable value, we can estimate the support volume from Figure 2.4. Since wellbore radius are of around 0.05 meters, our support volume would have a radius around $5 \times 10^3 \times 0.05 = 250$ m for radial flow. This relation holds provided that dimensionless head at the wellbore has been monitored until at least $h_D = 0.05$.

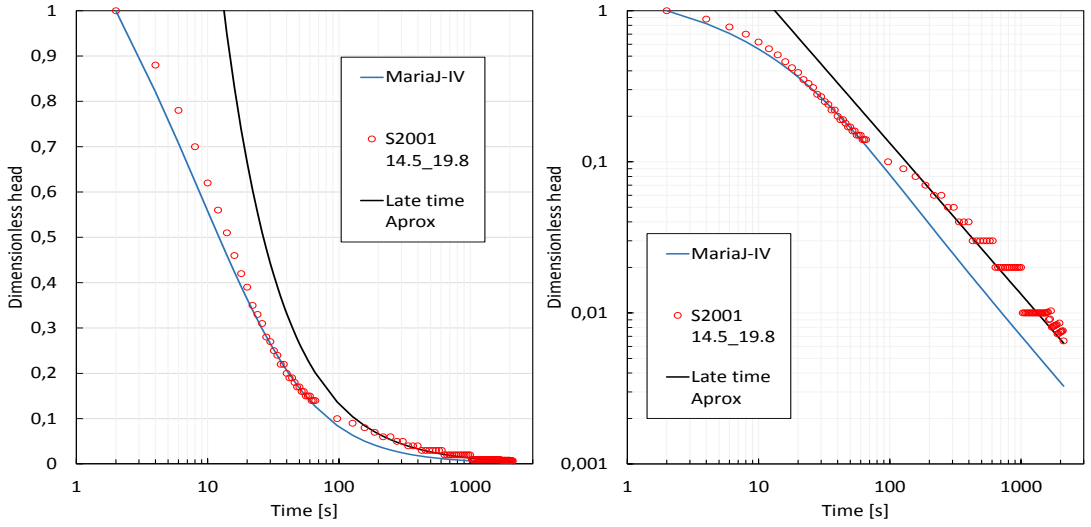

FIGURE 4.15: Comparison between the adjustment by the calibration code MariaJ-IV and the fit by type curve match to an heterogeneous behavor response.

4.5 Discussion of results

The geology of El Cabril is characterized by a significant degree of heterogeneity in a fractal and anisotropic way. This results in a complex hydrogeological behavior that requires analysis of hydraulic testing to be carried out with the help of complementary data. Our interpretation of slug tests, separated between formations, has proved to be consistent for each of the geological facies considered. These are characterized by differences of up to four orders of magnitude within each other.

The Albariza formation, as already reported in [55] has yielded the lowest values of hydraulic conductivity, with values lower of 10^{-8} m/s. The slug tests have resulted in homogeneous behavior and most of them revealing two dimensional flow, which implies a low connectivity in the vertical direction, as it was mentioned in field reports [4]. Geometric average of the interpreted values for hydraulic conductivity is around 10^{-8} m/s.

Most of slug tests have been performed at the transition gneisses, as the name of the rock indicates, several inclusions of different minerals corresponding to either the meta arkoses and the schistes such as biotite and pegmatite are present. Some of the heterogeneous behavior is most likely due to this inclusions. Some of the heterogeneous responses allow to derive two different conductivity values, although we must note that, as observed in the results of chapter three, the values are not exactly equivalent to the respective averages of both media, responding to two values that are rather situated in within. It is to expect that a more extended field testing would yield a well-defined bimodal histogram of log permeabilities. The geometric average conductivity obtained from these tests is around 10^{-7} m/s. Spherical flow was obtained in several of the tests. It is observed also that when an interval yields spherical flow the upper and lower interval also yields spherical flow and the conductivity estimates are very similar. Vertical conductivity in such cases shall not be neglected.

It is probably the meta arkoses the formation that happens to be the most interesting. None of the tests has resulted in a typical homogeneous radial flow behavior that would be well interpreted using the CBP model. Conversely, spherical flow homogeneous behavior has been obtained in most of them. Radial flow has resulted in either a double curve match, or a bimodal behavior. In addition a probable anisotropic behavior has been interpreted form the S2003 at a depth of 26-31 meters, recognizing a behavior similar to that of the Monte Carlo simulations. The same borehole presents a double permeability behavior that unlike others commented herein does not allow to derive two different conductivities. The double curve match has been observed at the S40 and S29, which are worth mentioning that are drilled at a significant distance between each other (with the gneisses of transition between them). The exact cause of this behavior should be worth examining as it could reveal important features of the hydrogeological behavior

of this formation. Spherical flow has been obtained at a depth of more than 50 meters. An interesting fact lies in that the storativity should be much less than 10^{-10} to obtain the precise match. To make an idea of the amount of storage reduction that should be made one can observe the trend of type curves of Figure 2.3, where it can be seen that the curves collapse rapidly for storage values of less than 10^{-4}.

It remains to assess the representativeness of the interpreted values for parallel flow in ordinary groundwater dynamics. From chapter three we have deduced some relationships between the ratio of interpreted conductivity and geometric average with respect to the variance of the $Y(\mathbf{x})$ field, though for geostatistical fields that in principle are not the best representation of a fractured porous media. Nevertheless it has allowed us to obtain a slight idea of how much could we expect the interpreted conductivities to differ from parallel flow. Another important issue is the determination of the actual directions of the hydraulic conductivity tensor, which from single well testing does not seem possible to obtain.

We have performed our interpretation by using solely two sets of type curves: radial and spherical. Nevertheless we have been able to describe and to evaluate most of the tests performed without major problems. More advanced models such as the KGS, developed and described in [33] could also be of interest as in principle it can fit both radial and spherical flow, but, of course, with the definition of more parameters. The double permeability behavior can also be analyzed with the double porosity model described in [26], it remains to make a comparison between the conductivities estimated here for such cases and the actual ones that would be derived from the analytical model.

Chapter 5

Conclusions

Our work has been focused on the interpretation and the usefulness of the derived parameters from slug tests in heterogeneous formations. To this aim we have made a set of numerical simulations in synthetic heterogeneous fields generated by a geostatistical simulator. Simulations of slug tests in fields with different statistical structures have been performed in order to understand the averaging process and the drawdown behavior of such tests. This has yield the following major results:

1. When we compare the drawdown curve that would be obtained in a homogeneous reservoir with a hydraulic conductivity equivalent to the geometric average of the heterogeneous field, we observe that late time curves obtained from that heterogeneous field are, for most of the cases, approximations to the homogeneous field. This is well observed in a log log plot.

2. Bimodal fields usually provided two different matches for middle and late times. The conductivities obtained from either matches are in within of the averages of both conductivity modes as defined in the histogram of small scale conductivities.

3. For all of the simulations in radial flow, the shape of the drawdown curve for early and middle time was significantly affected with respect to the homogeneous behavior. Therefore the determination of the storage parameter, which has already been questioned by most authors, is no longer possible by means of type curve match. This is especially the case for anisotropic media, where the slope of the drawdown curve tends to approximate a straight line as anisotropy increases. Nevertheless we have not studied the ability of double porosity models to match the observed behavior.

4. Radial flow interpretation by late time match yielded in general hydraulic conductivities smaller than the geometric mean. In particular, this is the case when the correlation length is increased both for anisotropic and isotropic fields. It remains to discuss whether this is also the case for fractured media.

5. On the contrary, our simulations of spherical flow in heterogeneous media, with layers that are not correlated in depth, yielded homogeneous behavior but, with an

interpreted conductivity significantly higher than the geometric average and proportional to the log-variance of hydraulic conductivity values. This is a point that should be taken into account when one evaluates the representativeness of the interpreted parameter for parallel flow.

6. The use of the head derivative with respect to the logarithm of time is a useful tool to achieve a good match with slug test data. We find that when both drawdown and the log-derivative are plotted in a log log plot we obtain two main advantages. First, initial head measurement is never in agreement with the actual head assumed by the analytical model, therefore the derivative plot is an unbiased indicator of the behavior for early time and on top of that it is amplified by the log log plot. Second, late time data, which from our set of numerical analysis is representative of a fair average of the formation is better recognized in a log log plot. Thus the use of both curves simultaneously constitutes a good way of performing type curve match.

7. Late time data in log log plots not only is representative of the average permeability but also of the flow dimension. This is of outmost importance since type curve match to a wrong set of type curves might results in differences of around three times the actual ones. The loss of information when assuming a certain flow dimension is also important. Unfortunately in tight formations usually late time data is difficult to achieve due to time constrains and, on top of that, little precision from the instruments is expected for dimensionless drawdown of less than 1%.

8. The storage coefficient is an important parameter regarding the analysis of slug tests, basically because it is the one controlling the extend of perturbation and measurement. This has been well documented by several authors in previous studies. Unfortunately, as we have noted, the estimates of this parameter with the same slug test are not reliable and thus we have to base our assumptions from other sources. Although the approximate suport volume can be well defined by only the storage coefficient, the actual media covered by such volume depends on flow geometry and anisotropy and thus a reliable hypothesis is difficult to make.

Regarding the field study of the slug tests performed at the heterogeneous fractured site of El Cabril we draw the following general conclusions:

9. As we have mentioned in several occasions during the manuscript, a basic geostatistical approach is not the best representation of a fractured media. Indeed from our field data of El Cabril, only few examples have yield similar behavior to those obtained in the Monte Carlo simulations. Among them we have observed an anisotropic behavior and several bi modal curves. Nevertheless there is one effect that has not been simulated by the numerical models and this is the one that we have called double type curve match. This has been obtained in slug tests performed at the meta arkoses and the cause of it is not clear except for the fact that it happens under radial flow and that all of them have yielded very similar interpreted conductivities, even in different boreholes.

10. Most of drawdown curves yielded homogeneous behavior. This does not mean that the media is uniform, but that the well test can be modeled by an equivalent homogeneous behavior. As we have noted from our numerical study, homogeneous behavior from heterogeneous field results in interpreted conductivities that are significantly different from that of the equivalent conductivity for parallel flow (the geometric average in the case of a multi-Gaussian field). Furthermore, anisotropy complicates matters when we try to relate the interpreted value with the equivalent for parallel flow.

11. Our interpretation using two sets of type curves, radial and spherical, has proved to be equally, or in some cases more reliable than an automatic calibration code based on a general flow model. Our methodology also allows to derive extra information such as double permeability behavior and the actual flow dimensionality, which is of interest for numerical models.

12. As a general conclusion, based on both the numerical and the field study, we share the opinion of Karasaki et al [34] regarding the need of complementary data to determine representative parameters from slug tests. This is especially the case for highly heterogeneous media. Indeed by separating our tests based on the geological formation at which were performed, we have obtained some interesting data, of the behavior of each formation. The existence of vertical fractures has helped in those cases in which spherical flow was suspected but confused with boundary effects and the same with the existence of horizontal fractures and the expected radial flow. Double permeability is proved by the existence of inclusions and so on. Thus it is important to verify our model with complementary data.

Appendix A

Type curve match of slug tests

A.1 Mica schistes of Albariza

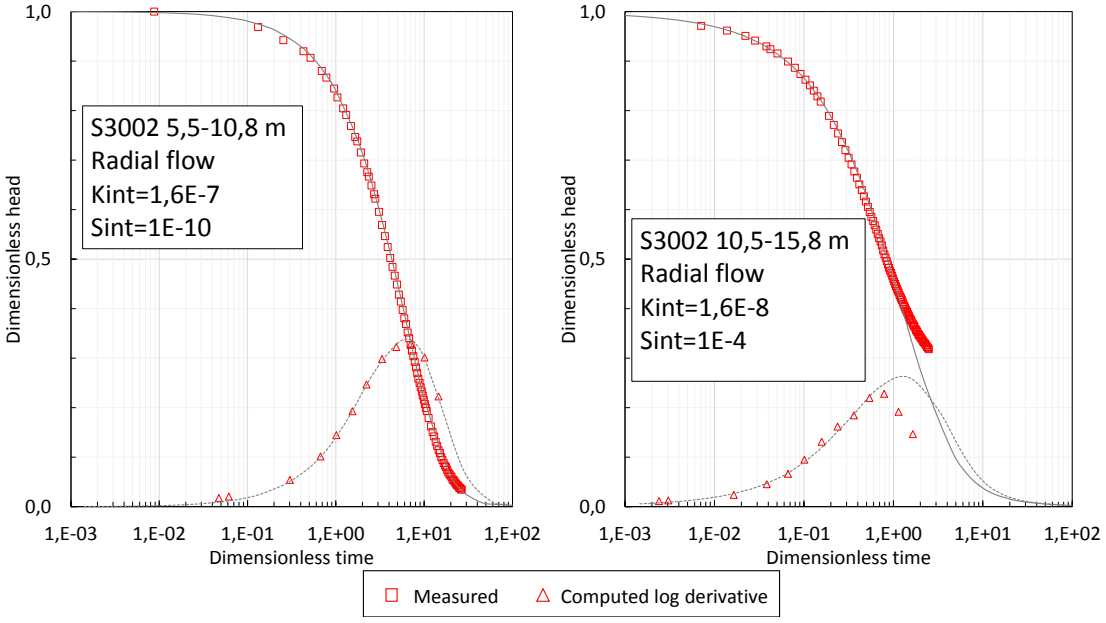

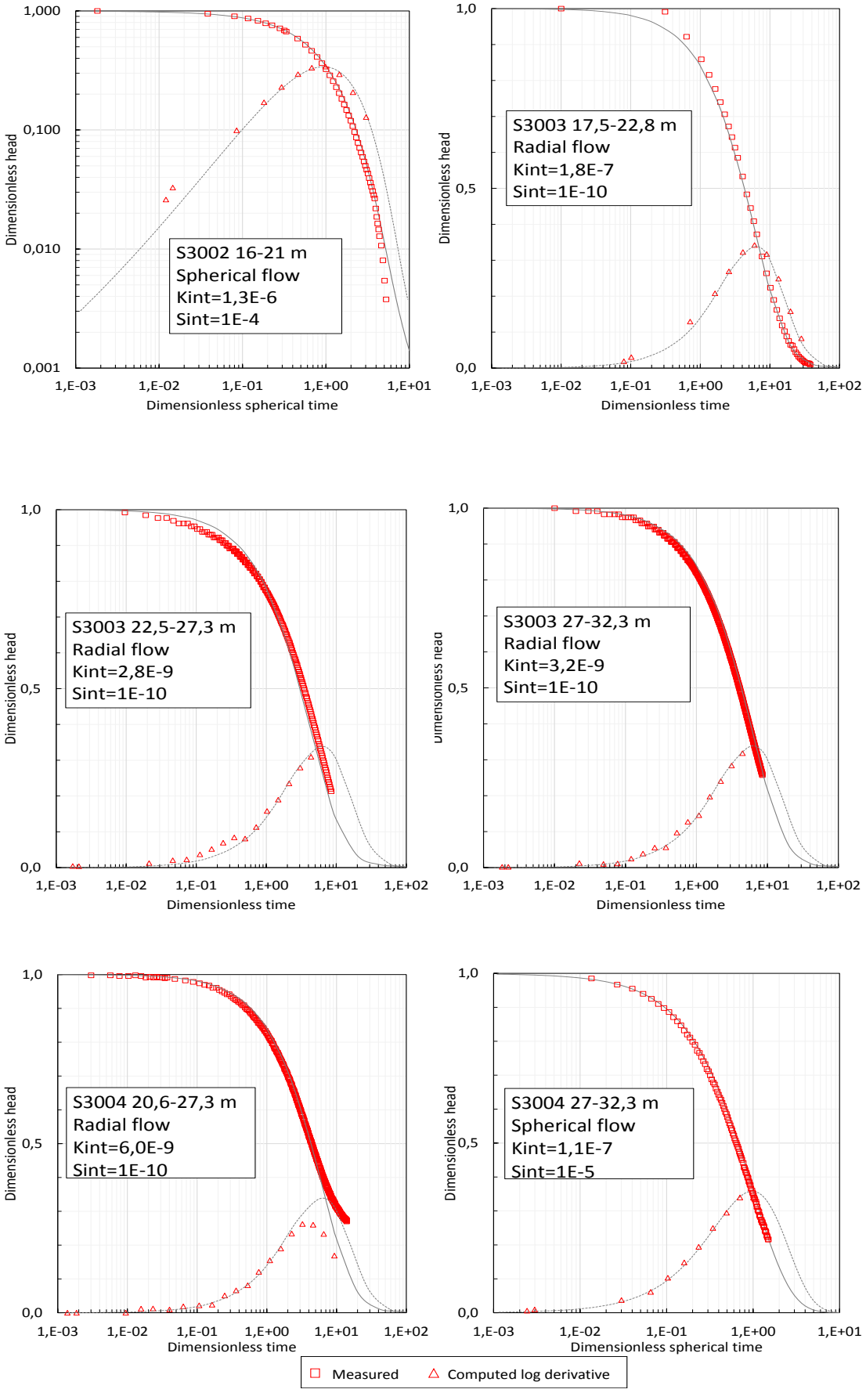
S3002 16-21 m
Spherical flow
Kint=1,3E-6
Sint=1E-4
Dimensionless head
Dimensionless spherical time
S3003 17,5-22,8 m
Radial flow
Kint=1,8E-7
Sint=1E-10
Dimensionless time
S3003 22,5-27,3 m
Radial flow
Kint=2,8E-9
Sint=1E-10
S3003 27-32,3 m
Radial flow
Kint=3,2E-9
Sint=1E-10
S3004 20,6-27,3 m
Radial flow
Kint=6,0E-9
Sint=1E-10
S3004 27-32,3 m
Spherical flow
Kint=1,1E-7
Sint=1E-5
Measured
Computed log derivative

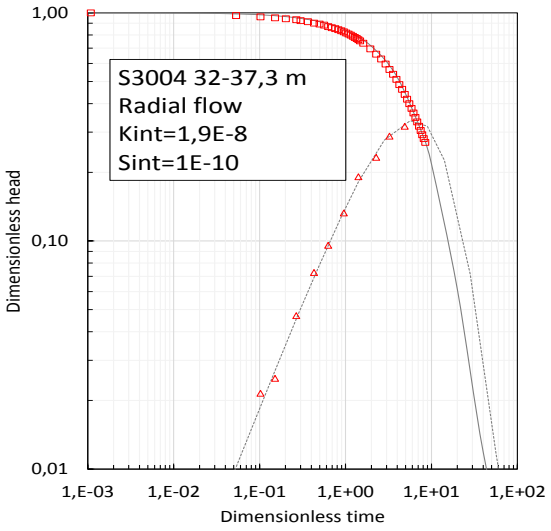
S3004 32-37,3 m
Radial flow
Kint=1,9E-8
Sint=1E-10
Dimensionless head
1,00
0,10
0,01
1,E-03
1,E-02
1,E-01
1,E+00
1,E+01
1,E+02
Dimensionless time

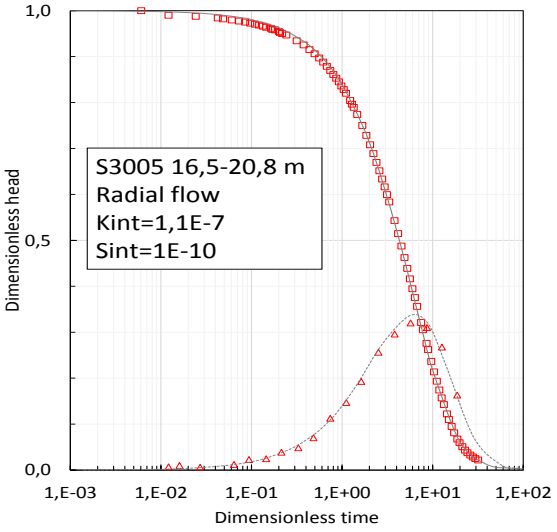
S3005 16,5-20,8 m
Radial flow
Kint=1,1E-7
Sint=1E-10
Dimensionless head
1,0
0,5
0,0
1,E-03
1,E-02
1,E-01
1,E+00
1,E+01
1,E+02
Dimensionless time

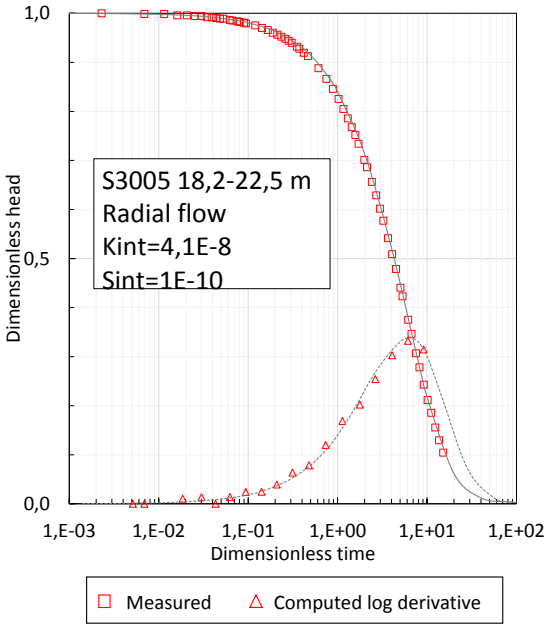
S3005 18,2-22,5 m
Radial flow
Kint=4,1E-8
Sint=1E-10
Dimensionless head
1,0
0,5
0,0
1,E-03
1,E-02
1,E-01
1,E+00
1,E+01
1,E+02
Dimensionless time
Measured
Computed log derivative

A.2 Transition gneises

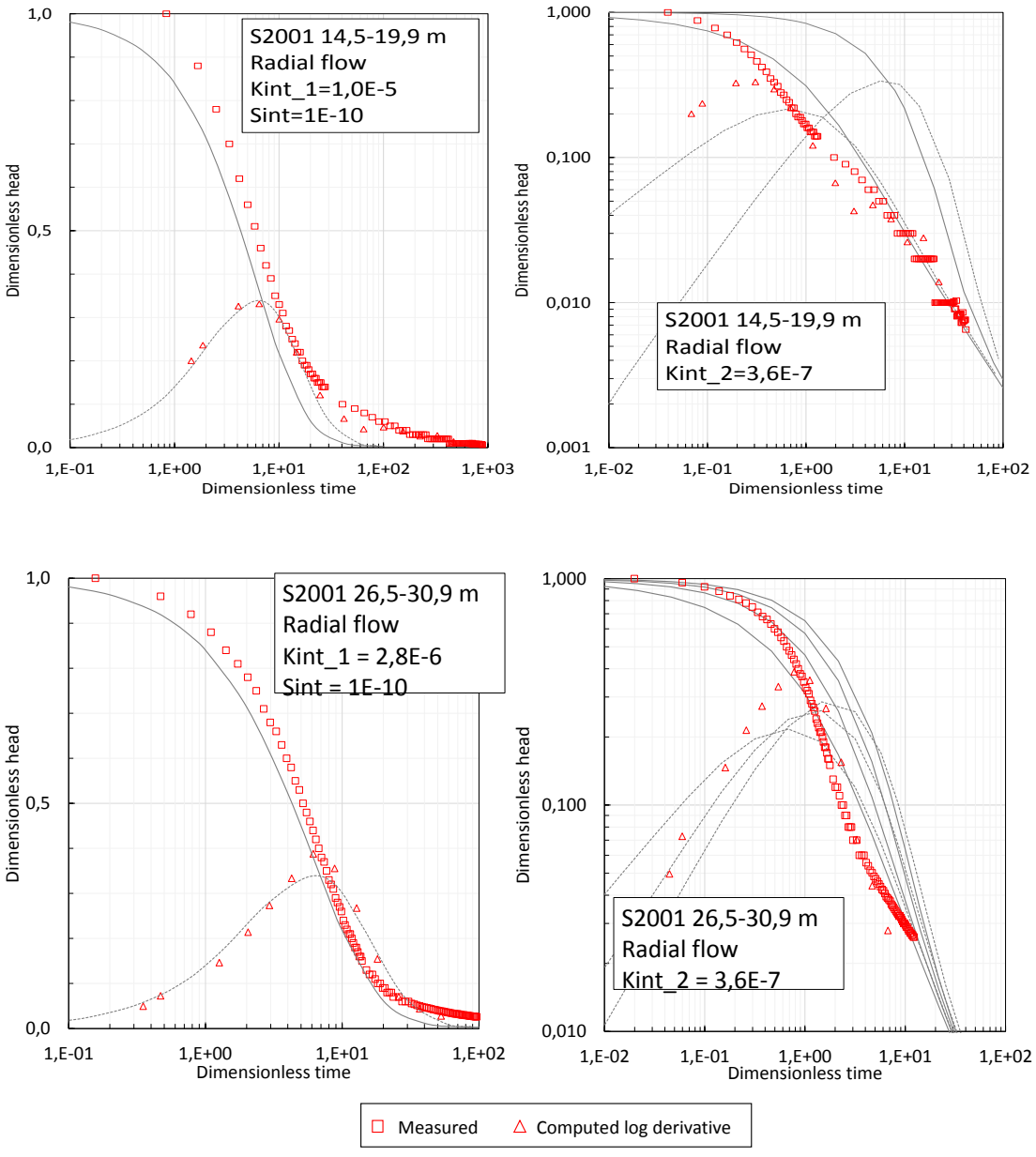

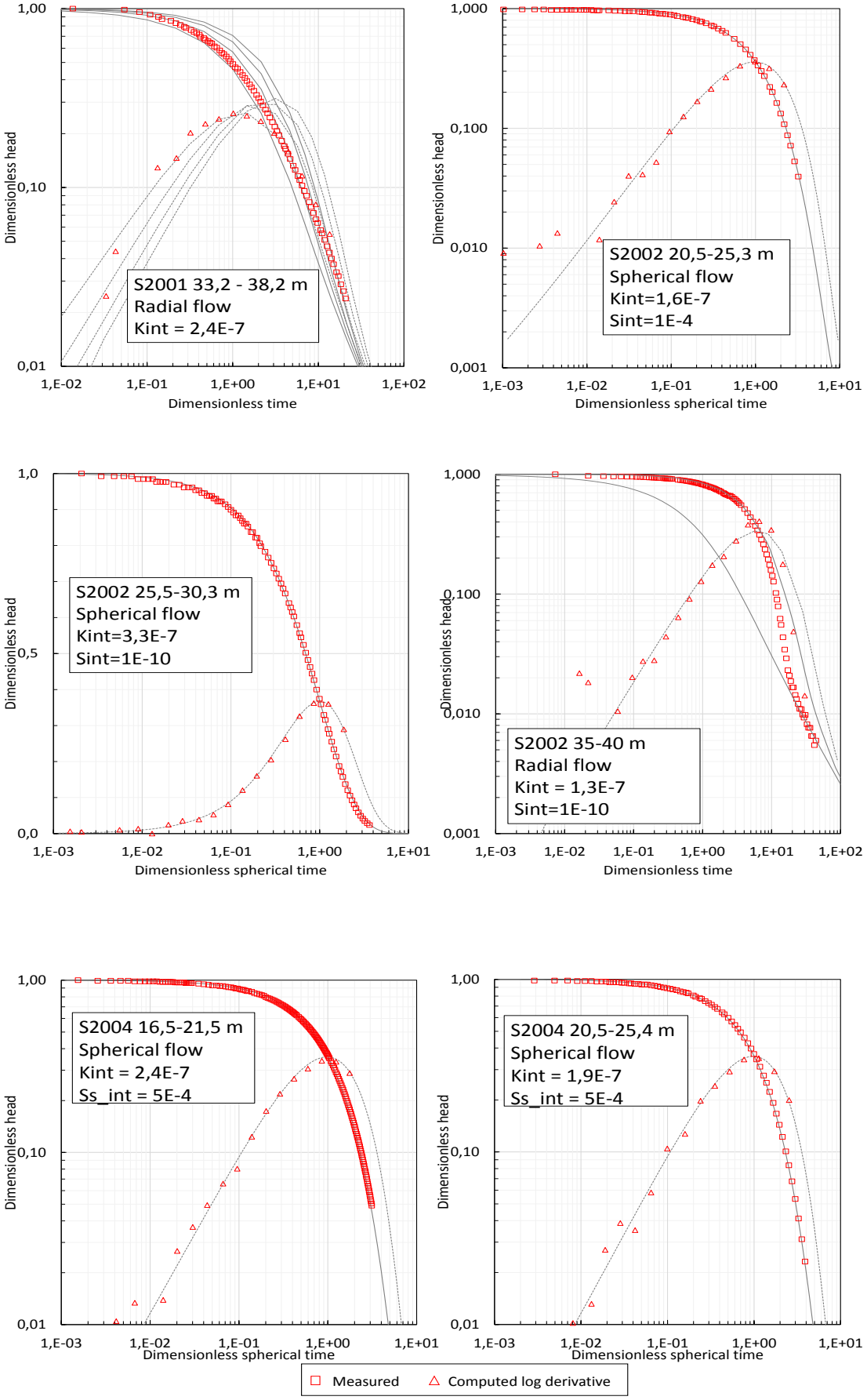
S2001 33,2 - 38,2 m
Radial flow
Kint = 2,4E-7
Dimensionless head
Dimensionless time
S2002 20,5-25,3 m
Spherical flow
Kint=1,6E-7
Sint=1E-4
Dimensionless spherical time
S2002 25,5-30,3 m
Spherical flow
Kint=3,3E-7
Sint=1E-10
S2002 35-40 m
Radial flow
Kint = 1,3E-7
Sint=1E-10
S2004 16,5-21,5 m
Spherical flow
Kint = 2,4E-7
Ss_int = 5E-4
S2004 20,5-25,4 m
Spherical flow
Kint = 1,9E-7
Ss_int = 5E-4
Measured
Computed log derivative

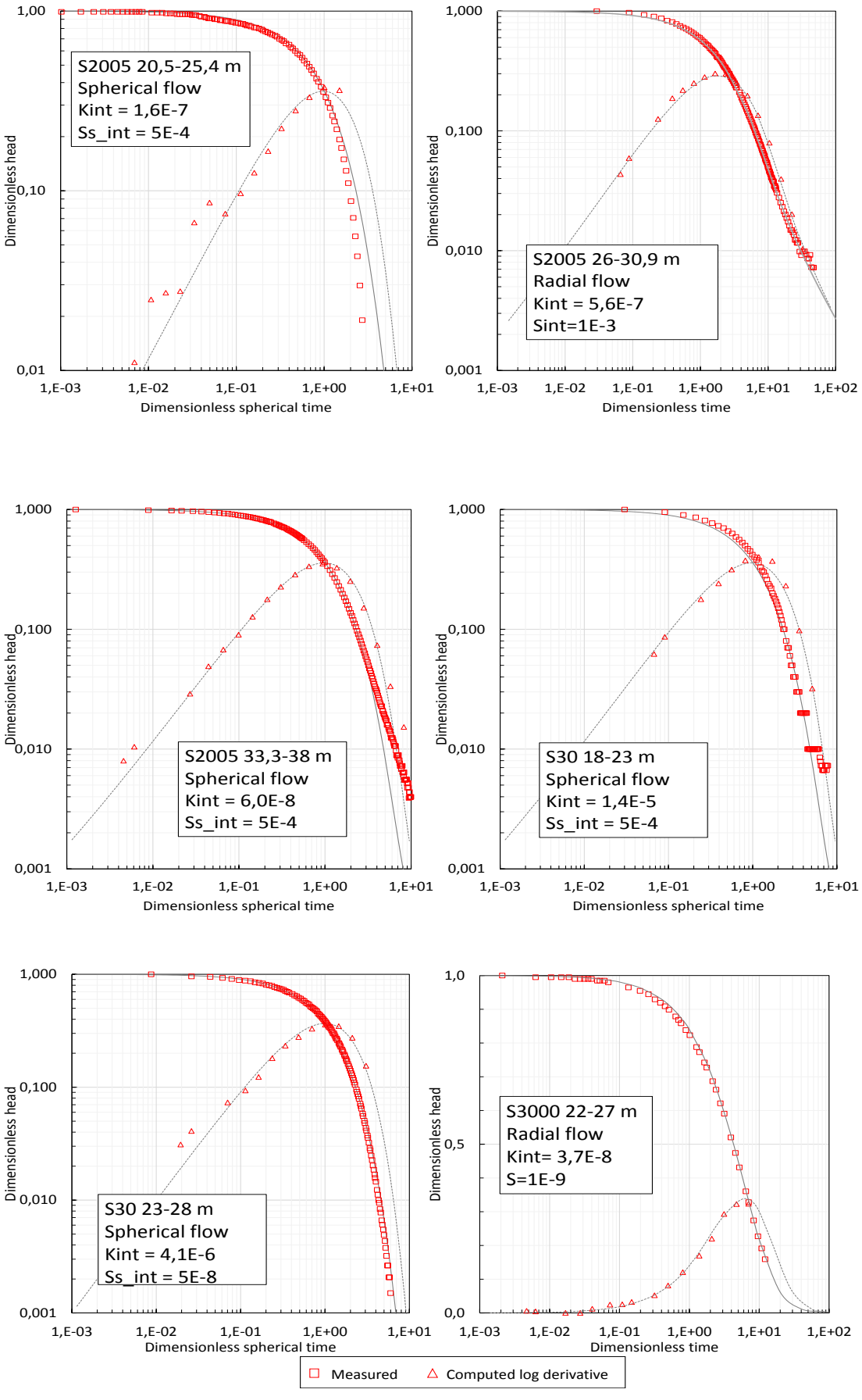
S2005 20,5-25,4 m
Spherical flow
Kint = 1,6E-7
Ss_int = 5E-4
Dimensionless head
Dimensionless spherical time
S2005 26-30,9 m
Radial flow
Kint = 5,6E-7
Sint=1E-3
Dimensionless time
S2005 33,3-38 m
Spherical flow
Kint = 6,0E-8
Ss_int = 5E-4
S30 18-23 m
Spherical flow
Kint = 1,4E-5
Ss_int = 5E-4
S30 23-28 m
Spherical flow
Kint = 4,1E-6
Ss_int = 5E-8
S3000 22-27 m
Radial flow
Kint= 3,7E-8
S=1E-9
Measured
Computed log derivative

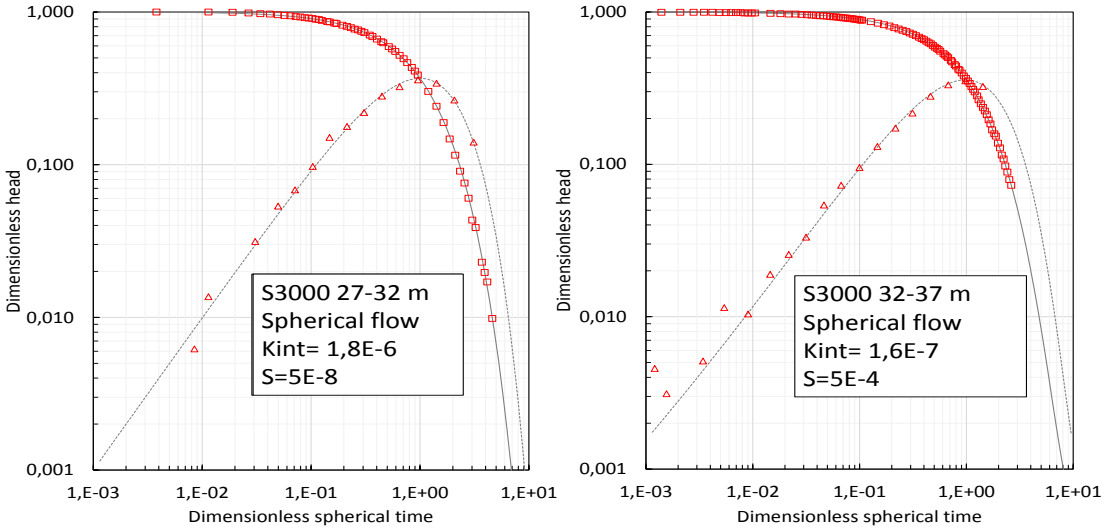
1,000
0,100
0,010
0,001
Dimensionless head
S3000 27-32 m
Spherical flow
Kint= 1,8E-6
S=5E-8
1,E-03
1,E-02
1,E-01
1,E+00
1,E+01
Dimensionless spherical time

1,000
0,100
0,010
0,001
Dimensionless head
S3000 32-37 m
Spherical flow
Kint= 1,6E-7
S=5E-4
1,E-03
1,E-02
1,E-01
1,E+00
1,E+01
Dimensionless spherical time

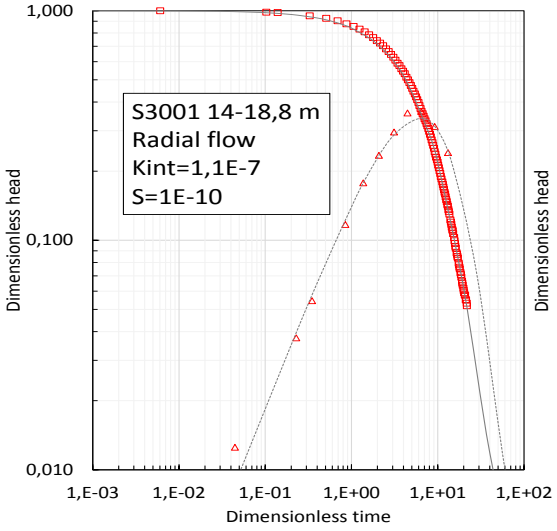
1,000
0,100
0,010
Dimensionless head
S3001 14-18,8 m
Radial flow
Kint=1,1E-7
S=1E-10
1,E-03
1,E-02
1,E-01
1,E+00
1,E+01
1,E+02
Dimensionless time

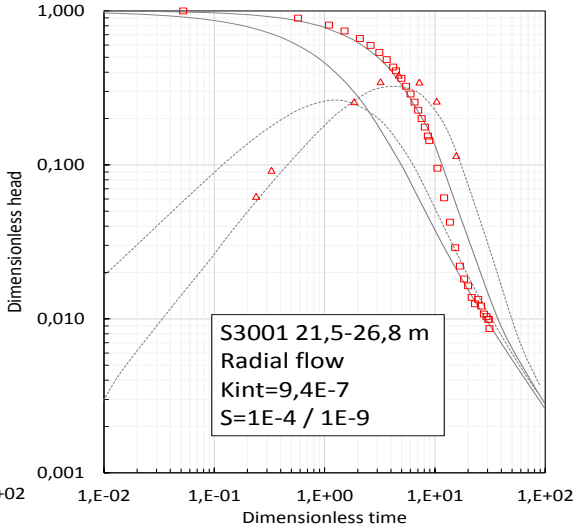
1,000
0,100
0,010
0,001
Dimensionless head
S3001 21,5-26,8 m
Radial flow
Kint=9,4E-7
S=1E-4 / 1E-9
1,E-02
1,E-01
1,E+00
1,E+01
1,E+02
Dimensionless time

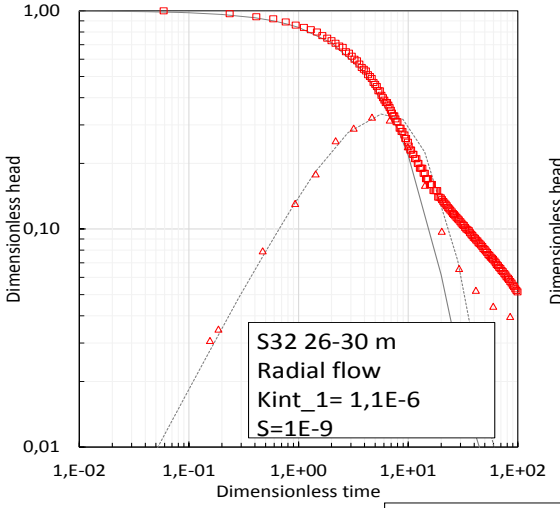
1,00
0,10
0,01
Dimensionless head
S32 26-30 m
Radial flow
Kint_1= 1,1E-6
S=1E-9
1,E-02
1,E-01
1,E+00
1,E+01
1,E+02
Dimensionless time

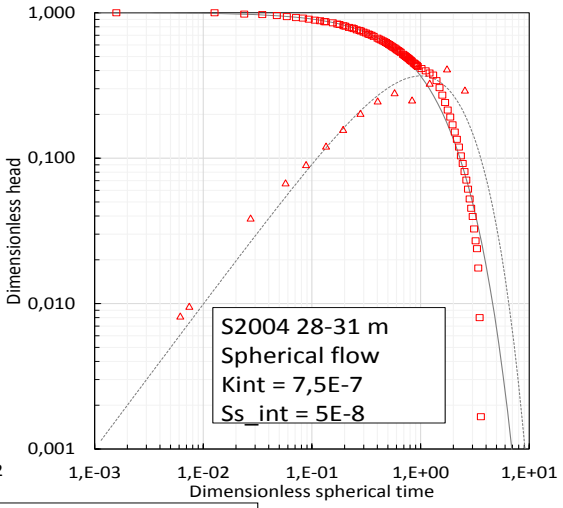
1,000
0,100
0,010
0,001
Dimensionless head
S2004 28-31 m
Spherical flow
Kint = 7,5E-7
Ss_int = 5E-8
1,E-03
1,E-02
1,E-01
1,E+00
1,E+01
Dimensionless spherical time


Measured
Computed log derivative

A.3 Meta arkoses of El Cabril

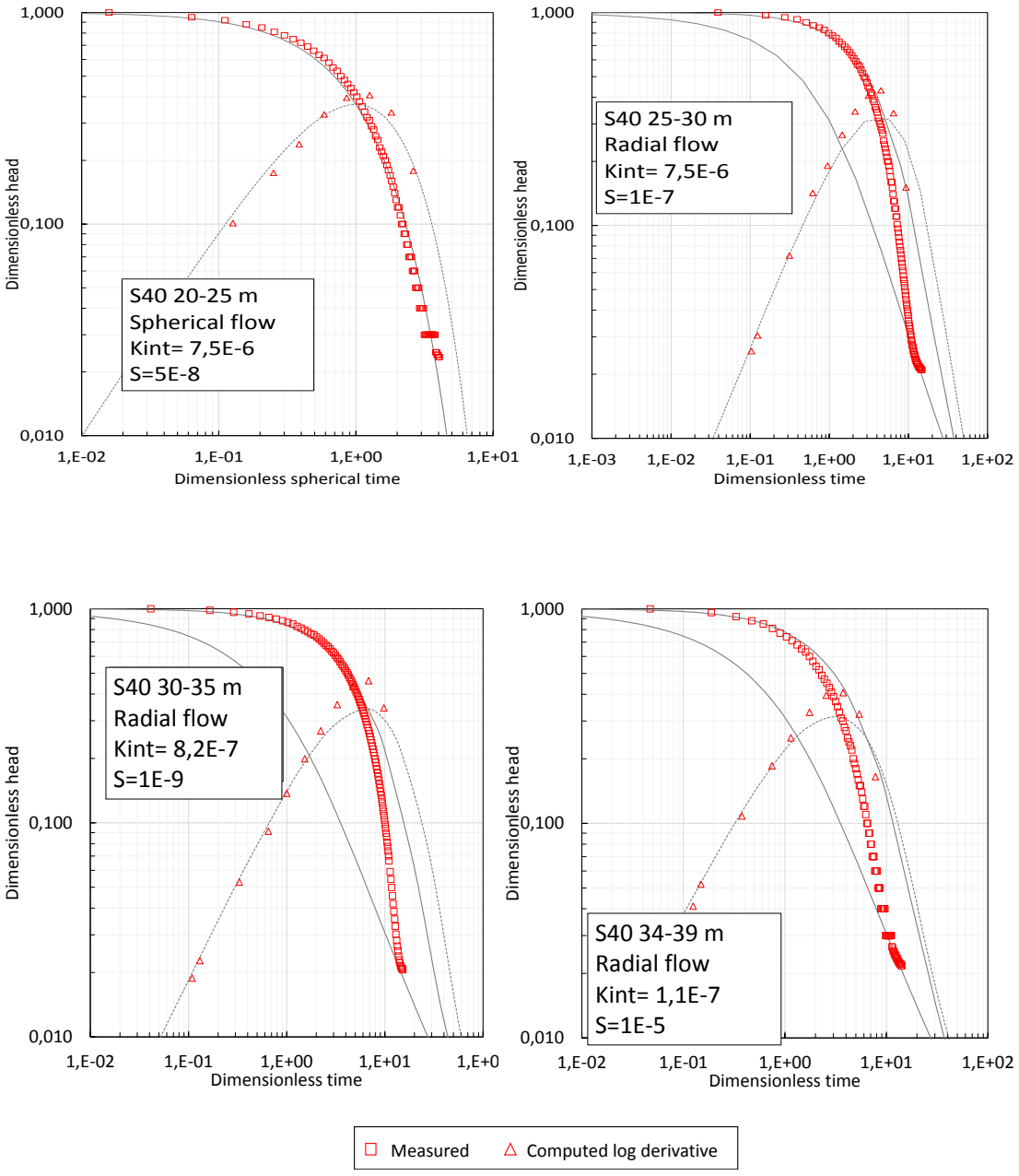

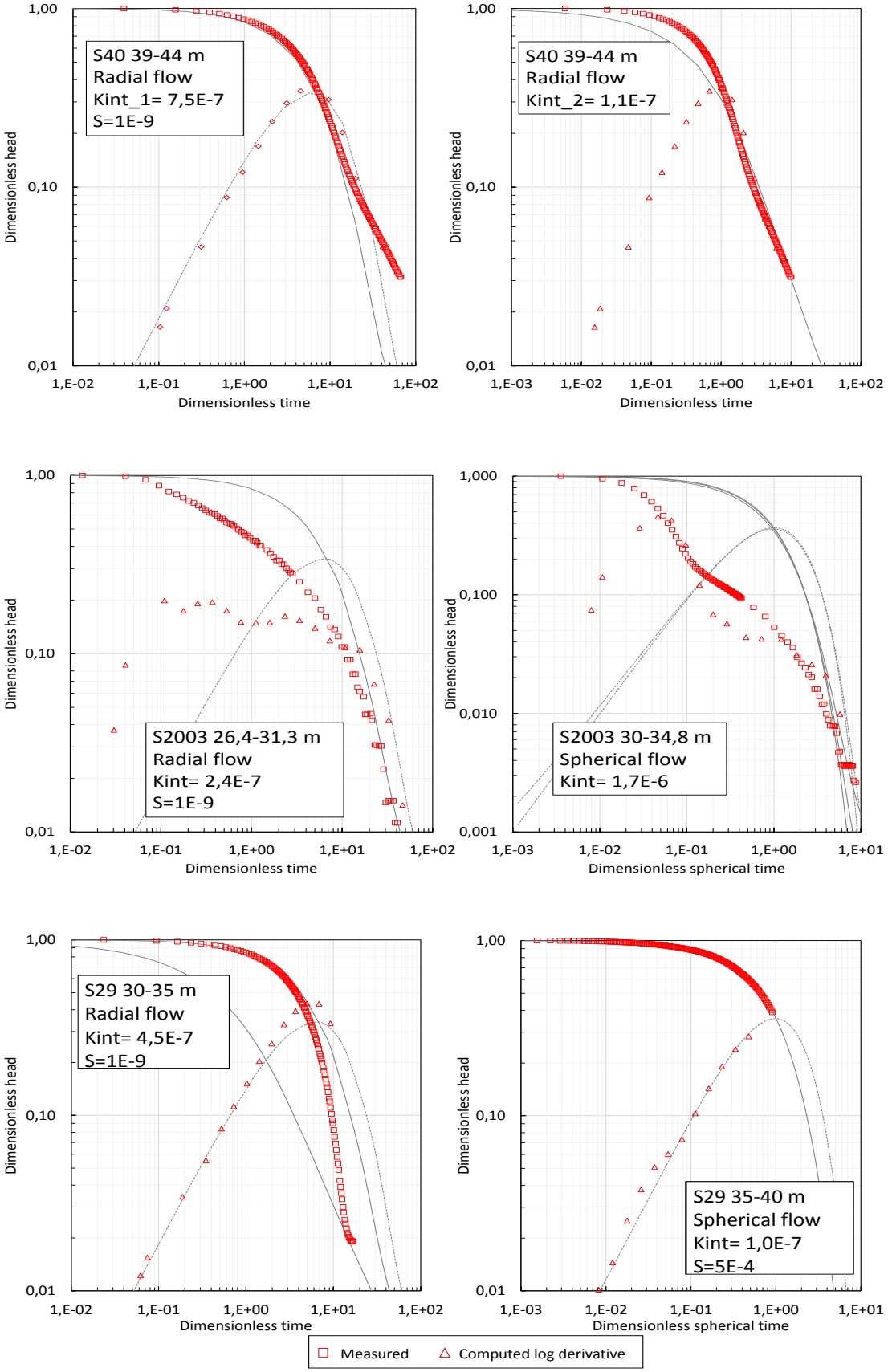
S40 39-44 m
Radial flow
Kint_1= 7,5E-7
S=1E-9
S40 39-44 m
Radial flow
Kint_2= 1,1E-7
S2003 26,4-31,3 m
Radial flow
Kint= 2,4E-7
S=1E-9
S2003 30-34,8 m
Spherical flow
Kint= 1,7E-6
S29 30-35 m
Radial flow
Kint= 4,5E-7
S=1E-9
S29 35-40 m
Spherical flow
Kint= 1,0E-7
S=5E-4
Dimensionless head
Dimensionless time
Dimensionless spherical time
Measured
Computed log derivative

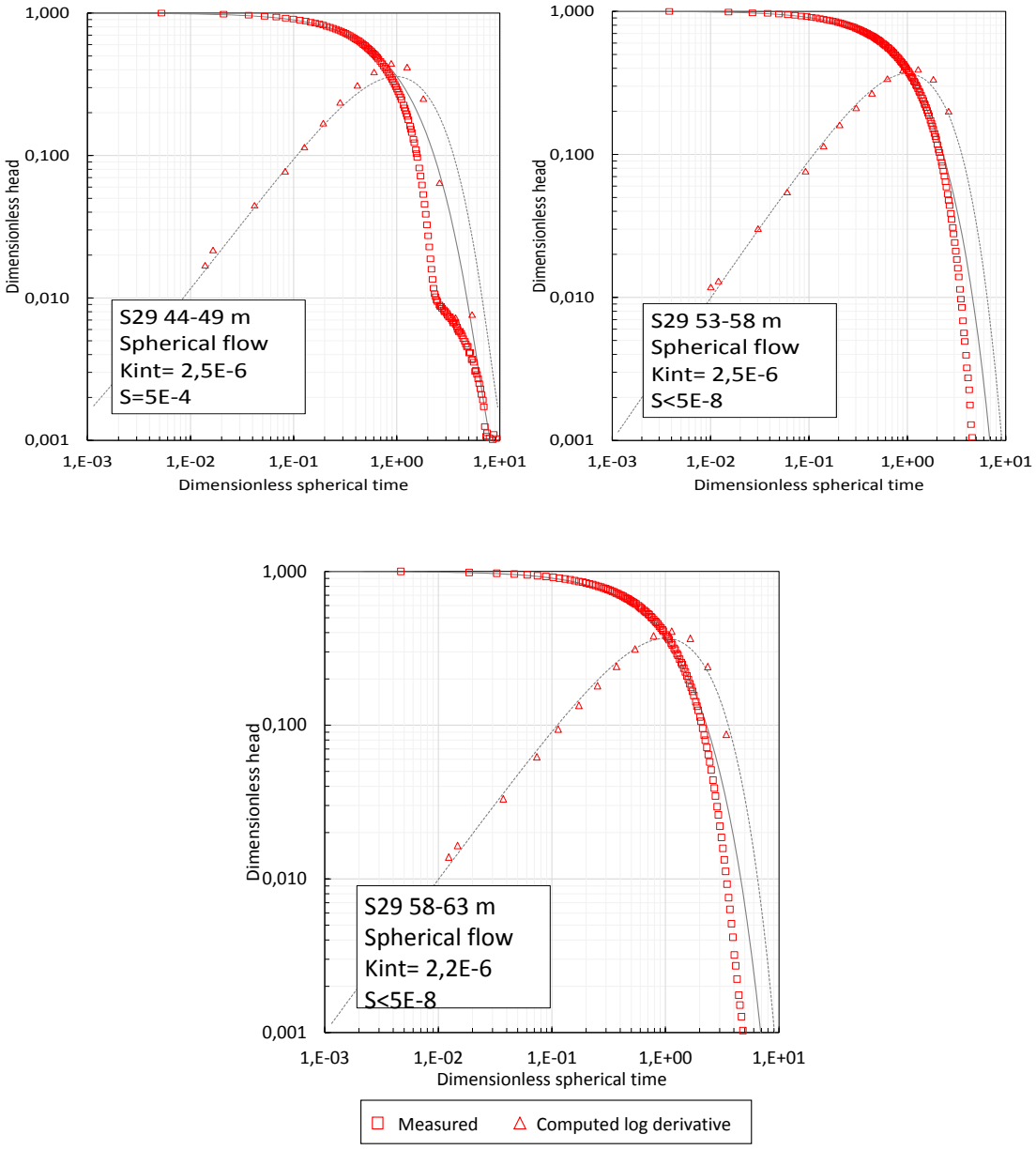
1,000
0,100
0,010
0,001
Dimensionless head
S29 44-49 m
Spherical flow
Kint= 2,5E-6
S=5E-4
1,E-03
1,E-02
1,E-01
1,E+00
1,E+01
Dimensionless spherical time
S29 53-58 m
Spherical flow
Kint= 2,5E-6
S<5E-8
S29 58-63 m
Spherical flow
Kint= 2,2E-6
S<5E-8
Measured
Computed log derivative

Bibliography

[1] R.G. Agarwal, G.C. Al-Hussainy, and H.J. Ramey. An investigation of wellbore storage and skin effect in unsteady liquid flow, i, analytical treatment. *Trans. AIME*, 249:279–290, 1970.

[2] AITEIM. Ensayos hidraulicos en el cabril fase iii, ensayos en sondeo unico en la zona sur para el futuro emplazamiento de la zona de rbma. *Technical Report, Enresa*, 2003.

[3] AITEIM. Ensayos hidraulicos en el cabril, ensayos en los sendeos serie 2000. *Technical Report, Enresa*, 2008.

[4] AITEIM. Campaa de testificacion hidrulica en los sondeos de la serie 3000 del c.a. el cabril. *Technical Report, Enresa*, 2012.

[5] F. Ballio and A. Guadagnini. Convergence assessment of numerical monte carlo simulations in groundwater hydrology. *Water Resources Research*, 40(4):n/a–n/a, 2004. W04603.

[6] J. A. Barker. A generalized radial flow model for hydraulic tests in fractured rock. *Water Resources Research*, 24(10):1796–1804, 1988.

[7] J.A. Barker and J. H. Black. Slug tests in fissured aquifers. *Water Resources Research*, 19(6):1558–1564, 1983.

[8] R. Beckie and C.F. Harvey. What does a slug test measure: An investigation of instrument response and the effects of heterogeneity. *Water Resources Research*, 38(12):26–1–26–14, 2002. 1290.

[9] D. Bourdet. A new set of type curves simplifies well test analysis. *World Oil*, 1983.

[10] H. Bouwer and R. C. Rice. A slug test for determining hydraulic conductivity of unconfined aquifers with completely or partially penetrating wells. *Water Resources Research*, 12(3):423–428, 1976.

[11] John D. Bredehoeft and Stavros S. Papadopulos. A method for determining the hydraulic properties of tight formations. *Water Resources Research*, 16(1):233–238, 1980.

[12] J.J. Butler and J. M. Healey. Relationship between pumping-test and slug-test parameters: Scale effect or artifact? *Ground Water*, 36(2):305–312, 1998.

[13] J.J. Butler, Carl D. McElwee, and W. Liu. Improving the quality of parameter estimates obtained from slug tests. *Ground Water*, 34(3):480–490, 1996.

[14] J.A. Carbonell, A. Perez-Paricio, and J. Carrera. Mariaj-iv: Programa de calibracin automtica de ensayos de bombeo. modelos analticos y numricos para medios 2d y 3d. *ETSECCPB,UPC*, 1997.

[15] C. Chakrabarty and C. Enachescu. Using the deconvolution approach for slug test analysis: Theory and application. *Ground Water*, 35(5):797–806, 1997.

[16] G. R. Chirlin. A critique of the hvorslev method for slug test analysis: The fully penetrating well. *Ground Water Monitoring and Remediation*, 9(2):130–138, 1989.

[17] H. H. Cooper and C. E. Jacob. A generalized graphical method for evaluating formation constants and summarizing well-field history. *Eos, Transactions American Geophysical Union*, 27(4):526–534, 1946.

[18] H.H. Cooper, J.D. Bredehoeft, and I.S. Papadopulos. Response of a finite-diameter well to an instantaneous charge of water. *Water Resources Research*, 3(1):263–269, 1967.

[19] CRN. Actualizacion de la informacion geologica del centro de almacenamiento de el cabril. *Technical Report ENRESA*, 2009.

[20] G. Dagan. Flow and transport in porous formations.463 pp. 1989.

[21] A. J. Desbarats. Spatial averaging of transmissivity in heterogeneous fields with flow toward a well. *Water Resources Research*, 28(3):757–767, 1992.

[22] A. J. Desbarats. Spatial averaging of hydraulic conductivity under radial flow conditions. *Mathematical Geology*, 26(1):1–21, 1994.

[23] D. E. Dougherty and D. K. Babu. Flow to a partially penetrating well in a double-porosity reservoir. *Water Resources Research*, 20(8):1116–1122, 1984.

[24] J.G. Ferris and D.B. Knowles. The slug test for estimating transmissibility. *U.S. Geological Survey*, 1954.

[25] L. W. Gelhar and C. L. Axness. Three-dimensional stochastic analysis of macrodispersion in aquifers. *Water Resources Research*, (42):1–29, 1983.

[26] A.S. Grader and H.J. Ramey. Slug-test analysis in double-porosity reservoirs. *SPE Formation Evaluation*, 1988.

[27] A.C. Gringarten. From straight lines to deconvolution: The evolution of the state of the art in well test analysis. *SPE Reservoir Evaluation and Engineering*, 11(01), 2008.

[28] D. Guyonnet, S. Mishra, and J. McCord. Evaluating the volume of porous medium investigated during slug tests. *Ground Water*, 31(4):627–633, 1993.

[29] T. M. Hansen and K. Mosegaard. Visim: Sequential simulation for linear inverse problems. *Computers and Geosciences*, 34(1):53 – 76, 2008.

[30] Arlen W. Harbaugh, Edward R Banta, Mary C. Hill, and Michael G. McDonald. Modflow-2000, the us geological survey modular ground-water model-user guide to modularization concepts and the ground-water flow process. *Open-file Report. U. S. Geological Survey*, page 134, 2000.

[31] M.J. Hvorslev. Time lag and soil permeability in ground-water observations. *U.S. Army Waterways Experiment Station*, 1951.

[32] Z. Hyder and J. J. Butler. Slug tests in unconfined formations: An assessment of the bouwer and rice technique. *Ground Water*, 33(1):16–22, 1995.

[33] Z. Hyder, J. J. Butler, C.D. McElwee, and W. Liu. Slug tests in partially penetrating wells. *Water Resources Research*, 30(11):2945–2957, 1994.

[34] K. Karasaki, J. C. S. Long, and P. A. Witherspoon. Analytical models of slug tests. *Water Resources Research*, 24(1):115–126, 1988.

[35] J. B. Keller. A theorem on the conductivity of a composite medium. *Journal of Mathematical Physics*, (5):548–549, 1964.

[36] C.D. McElwee, G.C. Bohling, and J.J. Butler. Sensitivity analysis of slug tests. part 1. the slugged well. *Journal of Hydrology*, 164(1):53 – 67, 1995.

[37] P.M. Meier, J. Carrera, and X. Sanchez-Vila. An evaluation of jacob's method for the interpretation of pumping tests in heterogeneous formations. *Water Resources Research*, 34(5):1011–1025, 1998.

[38] A. F. Moench and P. A. Hsieh. Comment on evaluation of slug tests in wells containing a finite-thickness skin by c. r. faust and j. w. mercer. *Water Resources Research*, 21(9):1459–1461, 1985.

[39] S. P. Neuman. Trends, prospects and challenges in quantifying flow and transport through fractured rocks. *Hydrogeology Journal*, 13(1):124–147, 2005.

[40] D.S. Oliver. The averaging process in permeability estimation from well-test data. *SPE Formation Evaluation*, (03), 1990.

[41] S.S. Papadopulos, J.D. Bredehoeft, and H.H. Cooper. On the analysis of slug test data. *Water Resources Research*, 9(4):1087–1089, 1973.

[42] A.M. M. Peres, M. Onur, and A.C. Reynolds. A new analysis procedure for determining aquifer properties from slug test data. *Water Resources Research*, 25(7):1591–1602, 1989.

[43] R. Raghavan. A review of applications to constrain pumping test responses to improve on geological description and uncertainty. *Reviews of Geophysics*, 42(4):n/a–n/a, 2004. RG4001.

[44] H. J. Ramey, R. G. Agarwal, and I. Martin. Analysis of "slug test" or dst flow period data. *Journal of Canadian Petroleum Technology*, 14(03), 1975.

[45] H.J. Ramey and R.G. Agarwal. Anulus unloading rates as influenced by wellbore storage and skin effect. *Society of Petroleum Engineers Journal*, 12:453–462, 1972.

[46] P. Renard, D. Glenz, and M. Mejias. Understanding diagnostic plots for well-test interpretation. *Hydrogeology Journal*, 17(3):589–600, 2009.

[47] Philippe Renard. The future of hydraulic tests. *Hydrogeology Journal*, 13(1):259–262, 2005.

[48] A. Sageev. Slug test analysis. *Water Resources Research*, 22(8):1323–1333, 1986.

[49] X. Sanchez-Vila. Radially convergent flow in heterogeneous porous media. *Water Resources Research*, 33(7):1633–1641, 1997.

[50] X. Sanchez-Vila, A. Guadagnini, and J. Carrera. Representative hydraulic conductivities in saturated groundwater flow. *Reviews of Geophysics*, 44(3):n/a–n/a, 2006. RG3002.

[51] X. Sanchez-Vila, P. M. Meier, and J. Carrera. Pumping tests in heterogeneous aquifers: An analytical study of what can be obtained from their interpretation using jacob's method. *Water Resources Research*, 35(4):943–952, 1999.

[52] A. M. Shapiro and P. A. Hsieh. How good are estimates of transmissivity from slug tests in fractured rock? *Ground Water*, 36(1):37–48, 1998.

[53] F. A. Spane and S. K. Wurstner. Deriv: A computer program for calculating pressure derivatives for use in hydraulic test analysis. *Ground Water*, 31(5):814–822, 1993.

[54] H. Sun. A semi-analytical solution for slug tests in an unconfined aquifer considering unsaturated flow. *Journal of Hydrology*, 532:29 – 36, 2016.

[55] UPC-UPM. Sintesis de estudios hidrogeologicos para la modelacion del flujo del agua subterranea en el entorno de las instalaciones de el cabril. *Technical Report*, 1994.